2008

# Dissolution of Biogenic Silica in Permeable Coastal Sands

Melissa K. Higgs

FLORIDA STATE UNIVERSITY

COLLEGE OF ARTS AND SCIENCES

# DISSOLUTION OF BIOGENIC SILICA IN PERMEABLE COASTAL SANDS

By

MELISSA K. HIGGS

A Thesis submitted to the
Department of Oceanography
in partial fulfillment of the
requirements for the degree of
Master of Science

Degree Awarded:
Fall Semester, 2008

The members of the Committee approve the Thesis of Melissa K. Higgs defended on October 20, 2008.

Markus Huettel
Professor Directing Thesis

Thorsten Dittmar
Outside Committee Member

Richard Iverson
Committee Member

Approved:

William Dewar, Chair, Oceanography

The Office of Graduate Studies has verified and approved the above named committee members.

This work is dedicated to my father who instilled his love of the ocean in me.

## TABLE OF CONTENTS

# LIST OF TABLES

# LIST OF FIGURES

## ABSTRACT

Riverine inputs, groundwater efflux, and terrestrial runoff enrich coastal waters with silica. Diatoms, which require silicic acid ($Si(OH)_4$) for frustule formation and cell growth, are therefore predominantly found in these waters. Less than half of the pelagic primary production is consumed in the shallow water column; the remaining fraction settles on the seafloor. However, large fractions of these shelf sediments are composed of permeable relict sands, which do not accumulate organic matter. As a result, the fate of the deposited diatoms and the biogenic silica ($bSiO_2$) is poorly understood, and little is known about the processes that control transport and decomposition of sedimented diatoms in permeable shelf beds. To determine the fate of these deposited diatoms, four study objectives were addressed. These objectives were:

I. To determine how diatoms are deposited on permeable sediments and how $Si(OH)_4$ is distributed in upper-sediment layers;
II. To determine how flushing of permeable sediments affects degradation and dissolution of diatoms embedded in the sands;
III. To determine fluxes of $Si(OH)_4$ from permeable sediments under different filtration conditions; and
IV. To assess $Si(OH)_4$ concentration ranges in the water and the pore water in the northern Gulf of Mexico in a time series to determine the coupling between water-column and pore-water concentrations.

In the laboratory, two flume experiments were conducted to address the first objective. The first experiment revealed that deposition of algal cells occurred at the bottom of sediment-ripple troughs and the upper slopes of the ripples, while the ripple crest was associated with a deposition minimum. The second experiment demonstrated that the highest $Si(OH)_4$ concentrations were found in the upwelling zone at the downstream slope of the ripple and the ripple crest (~100 μmol $Si(OH)_4$). The upwelling pore-water flows that carry $Si(OH)_4$ upwards focus near the ripple crest and dissolution of diatoms deposited in the ripple slopes add to the $Si(OH)_4$ concentration in this zone. Meanwhile, the lowest concentrations were seen in the downwelling zone (e.g., ripple troughs and lower flanks). Here flume water with relatively low $Si(OH)_4$ concentrations penetrated into the sediment.

To address the second objective, the dissolution of the frustules in the permeable sand was quantified in five column-reactor experiments that permitted sediment flushing at well-defined pore-water flow velocities. The column experiments showed that the $Si(OH)_4$ remobilization was higher in the pore space than in reaction columns that were filled with water only, suggesting that the dissolution of diatoms is more rapid in flushed sediments. The measured dissolution-rate constants ($k$) were 0.0144-0.0150 in columns with sediment versus 0.0070-0.0082 in columns with water only. This finding can be explained by the depression of the diffusive-boundary layer at the surface of the frustule when the diatoms are embedded in the sand.

Sediment-water flux measurements with in-situ chamber incubations addressed the third objective and revealed that advective pore-water exchange enhanced $Si(OH)_4$ flux up to a factor of six. Day and night fluxes differed due to the changes in $Si(OH)_4$ uptake during daytime. Fluxes of $Si(OH)_4$ were an order of magnitude higher in the sediments than in the water column at both the Gulf and the Bay sites.

To address the fourth objective, monthly field samples were taken on St. George Island at the two field sites. These samplings revealed peaks in benthic primary production in the summer months and maxima in water and sediment silica concentrations in the fall and winter months. However, when nutrients became depleted during summer, an increase in $Si(OH)_4$ concentrations was observed, suggesting that diatom growth was limited by other nutrients than $Si(OH)_4$.

The results of this study show that in permeable coastal sediments the dissolution of deposited diatom frustules and the release of the mobilized $Si(OH)_4$ from the sediment are enhanced by the advective-pore water flows caused by bottom flow-topography interaction and emphasize the importance of coastal permeable sediments in the cycling of marine silica.

# CHAPTER 1
# INTRODUCTION

## Diatoms and the Global Carbon Cycle

Diatoms—class Bacillariophyceae—comprise a significant fraction of coastal and open-ocean phytoplankton; consequently, these algae are primary contributors to the global carbon (C) cycle (Sarthou et al., 2005). They are responsible for up to 40-50% of total ocean primary production (Nelson et al., 1995; Tréguer et al., 1995; Van Cappellen et al., 2002; Sarthou et al., 2005; Truesdale et al., 2005), which underlines their importance in the global C cycle. Diatoms require silicic acid or silicate, $Si(OH)_4$, for the formation of their cell walls or frustules (Wischmeyer et al., 2003), so diatom productivity is controlled by the availability of $Si(OH)_4$ (Bidle and Azam, 2001). Thus, these algae also play a central role in the marine silica cycle (Tréguer et al., 1995; Yool and Tyrell, 2003).

Zooplankton feed on pelagic diatoms and excrete $Si(OH)_4$-rich waste materials as fast-sinking pellets (Yool and Tyrell, 2003). In shallow waters, where light penetrates to the bottom, sedimentary diatoms often maintain high benthic-primary production rates (Jahnke et al., 2000).

Under conditions of nutrient depletion, such as low $Si(OH)_4$ concentration, pelagic diatoms are unable to thrive, and they sink to deeper nutrient-rich waters (Smetacek, 1985; Engel et al., 2002; Yool and Tyrrell, 2003). During diatom blooms, the increasing phytoplankton population can exhaust nutrient supplies in the euphotic zone, causing the bloom to cease. As the bloom degrades, the diatoms sink through the water column, often forming aggregates as they fall, thereby increasing their sinking velocities (Sarthou et al., 2005). In the shelf environment, such aggregates may form thick fluff layers on the sediment surface. In open ocean environments, the heavy diatoms rapidly sink out for the upper water layers (Yool and Tyrell, 2003), so zooplankton and other grazers have less opportunity to feed on the algae. This sinking out of the surface layer moves "new" production from the surface ocean into deeper waters or to the sediment where a large fraction of the biogenic silica ($bSiO_2$) is remobilized (Dugdale et al., 1995, Ragueneau et al., 2000; Yool and Tyrell, 2003). However, the role of diatoms in the silica and C cycles is not yet fully understood (Dugdale et al., 1995; Ragueneau et al., 2000; Sarthou et al., 2005).

## Diatoms and the Marine Silica Cycle

Because of their large contribution to ocean primary production, diatoms link the global C cycle to the silica cycle (Tréguer et al., 1995; Ragueneau et al., 2000). Figure 1.1 shows a schematic of the biogeochemical cycle of silicon (Si) in the world ocean at a steady state. Understanding the processes controlling dissolution of $bSiO_2$, also known as opal, and spatial variations between $bSiO_2$ production and preservation, thus, is essential for assessing the global Si and C cycles (DeMaster, 1981; Shemesh et al., 1989; Rickert et al., 2002). In seawater, most dissolved Si exists as $Si(OH)_4$ (Tréguer et al., 1995), with the two predominant forms of marine $Si(OH)_4$ being $H_4SiO_4$ and $H_3SiO_4^-$ (Wischmeyer et al., 2003). Net $Si(OH)_4$ input into the world's oceans comes from three main sources. (1) Sedimentary and crystalline rocks exposed to weathering release $Si(OH)_4$, which is transported by rivers, groundwater, and surface run-off into coastal waters. (2) Eolian erosion of deserts and other terrestrial environments suspends siliceous debris in the atmosphere. These particles are often deposited into the surface ocean. The sinking of this fine material releases $Si(OH)_4$ to the water through dissolution. (3) Submarine basalt weathering, the result of hydrothermal high-temperature reactions at midocean ridges and low-temperature alteration of the basalts of the oceanic crust, $Si(OH)_4$ releases to the ocean waters (Tréguer et al., 1995).

Diatoms, radiolarians, silicoflagellates, and siliceous sponges take up $Si(OH)_4$ to form shells and structural elements (Tréguer et al., 1995; DeMaster, 2002). Diatoms form exoskeletons of amorphous silica or opal. $BSiO_2$ is primarily produced by planktonic organisms living in the surface ocean. In the coastal waters of the continental shelf, diatoms are more abundant because of their ability to outcompete radiolarians and silicoflagellates. These algae are key producers of $bSiO_2$ (Tréguer et al., 1995; Ragueneau et al. 2000; Fujii and Chai, 2005). The estimated global rate of $bSiO_2$ production in surface waters is $2.0–2.8 \times 10^{14}$ moles Si $yr^{-1}$ or 1.5–2.1 mmol Si $m^{-2}d^{-1}$ (Tréguer et al., 1995; Ragueneau et al., 2000).

Dissolution of $bSiO_2$ has an important role in diatom production, vertical export production, and the marine silica cycle (Fujii and Chai, 2005). Between 10 and 100% of the mass of $bSiO_2$ produced is immediately remobilized and recycled in the upper 100 m of the water column (Tréguer et al., 1995; Van Cappellen et al., 2002). The remaining, undissolved

$bSiO_2$ rapidly sinks, and dissolution continues as the debris settle through the water column. After the $bSiO_2$ particles reach the seafloor, they are incorporated into the sediment and their continued dissolution leads to the build-up in $Si(OH)_4$ concentration in the pore water (Van Cappellen et al., 2002). Diffusion, pore-water flows, and biological activities release the $Si(OH)_4$ back into the water column, and only 3% of $bSiO_2$ is buried and lost in the sediments (Tréguer et al., 1995; Van Cappellen et al., 2002). However, in highly productive zones, e.g., upwelling regions or the Antarctic $Si(OH)_4$ belt, sediments can contain a large fraction of opal, which led to the suggestion that sediment $bSiO_2$ content can be used as a productivity indicator (Ragueneau et al., 2000).

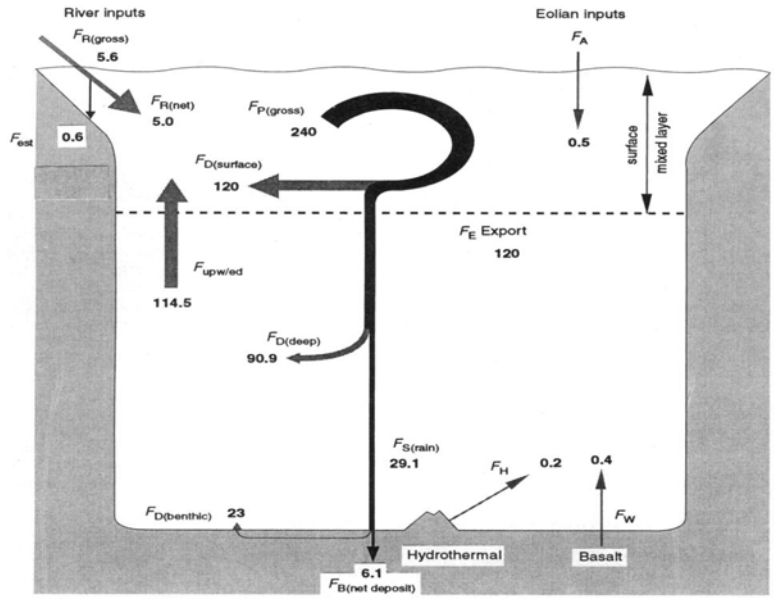


Figure 1.1. Biogeochemical cycle of Si in the world ocean at steady state: A possible balance that is in reasonable agreement with the individual range of each flux ($F$). Gray arrows, fluxes of $Si(OH)_4$ (dissolved silica); black arrows, fluxes of particulate $bSiO_2$. All fluxes are in teramoles of Si per year. Abbreviations are as follows: River fluxes: gross inputs, $F_{R(gross)}$, and net inputs, $F_{R(net)}$; eolian inputs, $F_A$; seafloor weathering inputs, $F_w$; hydrothermal inputs, $F_H$; net deposit of $bSiO_2$ in estuaries, $F_{est}$; net deposit of $bSiO_2$ in coastal and abyssal sediments, $F_B$; $bSiO_2$ gross production, $F_{P(gross)}$; flux of $Si(OH)_4$ recycled in the surface reservoir, $F_{D(surface)}$; flux of $bSiO_2$ exported toward the deep reservoir, $F_E$; flux of $Si(OH)_4$ recycled in the deep reservoir, $F_{D(deep)}$; and at the sediment-water interface, $F_{D(benthic)}$; flux of $bSiO_2$ that reaches the sediment-water interface, $F_{S(rain)}$; and flux of $Si(OH)_4$ transferred from the deep reservoir to the surface mixed layer, $F_{upw/ed}$. From Tréguer et al., 1995.

## Dissolution of $BSiO_2$

The ocean is undersaturated with respect to $bSiO_2$. Thus, dissolution of diatom frustules starts in the water column when the silica skeleton of decaying algae is exposed to undersaturated seawater, and this process occurs at all depths. At the sediment surface and within the sediment, dissolution continues until pore water becomes saturated or the $bSiO_2$ particle surfaces are chemically altered preventing further dissolution (Nelson et al., 1995).

The specific dissolution rate of opal in seawater ($V_{dis}$) can be calculated using the equation $V_{dis}=k\,([Si(OH_4)]_{sat} - [Si(OH)_4]_{amb})\,A_{sp.}$, where $V_{dis}$ is expressed in $h^{-1}$, $k$ is the first-order rate constant (cm $h^{-1}$), $[Si(OH_4)]_{sat}$ is the solubility of opal (mol $cm^{-3}$), $[Si(OH)_4]_{amb}$ is the ambient $Si(OH)_4$ concentration (mol $cm^{-3}$), and $A_{sp}$ is the specific surface area of the opal present expressed in $cm^2\ mol^{-1}$ (Ragueneau et al., 2000).

Numerous variables affect $bSiO_2$ dissolution on both regional and local scales. (1) $BSiO_2$ dissolution is a temperature-dependent process (Nelson et al., 1995). With each 15°C increase in temperature, the specific dissolution rate (dissolution rate per unit mass of $bSiO_2$) increases by almost an order of magnitude (Nelson et al., 1995). Rates of dissolution at 8 to 30ºC vary from 0.2 to 0.002 $d^{-1}$ (Kamatani, 1982). Therefore, opal accumulates in productive regions where surface waters are cold. (2) Incorporation of trace elements, e.g., aluminum, beryllium, iron, gallium, gadolinium, and yitrium, within the opaline matrix can lead to a large decrease in solubility of the opal (Nelson et al., 1995; Ragueneau et al., 2000). These metals are capable of forming insoluble hydroxides, and may bind to hydroxyl groups on the surface of hydrated amorphous silica (Nelson et al., 1995). Aluminum (Al) has been particularly well-studied as it relates to $bSiO_2$ dissolution. As the Al/Si ratio of silica increases, the dissolution rate and equilibrium solubility of diatom silica decrease (Nelson et al., 1995; Dixit et al., 2001; Van Cappellen et al., 2002). If aluminosilicates or detrital materials form on the silica surface, this can decrease the solubility of $bSiO_2$ in sediment samples (Rickert et al., 2002). In detrital-rich sediments, the relatively high levels of soluble Al (III) may induce the precipitation of authigenic aluminosilicates (Dixit et al., 2001). (3) During the later stages of a diatom bloom, the cells tend to aggregate (Nelson et al., 1995). As a result, they are rapidly transported to the seafloor, thereby minimizing the exposure time of the frustules to undersaturated waters. Aggregate formation also decreases the surface area of opal exposed to seawater during sinking and burial

(Nelson et al., 1995). In consequence, the solubility of $bSiO_2$ fragments may be 10-15% higher than the solubility of fresh diatom assemblages (Dixit et al., 2001). (4) Grazing can enhance dissolution by physically or chemically changing the frustule. The dissolution of $bSiO_2$ may also be affected when it is in the form of fecal pellets. In some organisms, their pellets are covered with an organic membrane, which makes it harder for dissolution to occur because of a decreased exchange of the silica to ambient water (Nelson et al., 1995). In areas of high microbial activity, bacteria play a pivotal role in frustule degradation. The diatom frustule is covered by a three-layered organic coating that consists of a polysaccharide, a lipid, and a protein layer (Hecky et al., 1973). Using bacterial ectoprotease, bacteria colonize and enzymatically degrade the organic matrix of diatom frustules leading to increased silica dissolution (Bidle and Azam, 1999; Bidle and Azam, 2001). (5) The dissolution rate and the apparent solubility of $bSiO_2$ are dependent on the pH and electrolyte composition of the aqueous medium, specific surface area, impurity content, and aging of the silica (Kamatani and Riley, 1979; Van Cappellen and Qiu, 1997b; Dixit et al., 2001; Rickert et al, 2002; Van Cappellen et al., 2002). For example, there is a strong dependency of $bSiO_2$ dissolution rate on pH. A pronounced minimum dissolution rate exists between pH of 4 and 6 (Canfield et al., 2005). (6) Specific dissolution rate varies from species to species as a result of variability in specific surface areas, morphology and structure of the frustules, and in the growth of organic and inorganic coatings (Ragueneau et al., 2000). (7) Pressure variations can also affect the solubility of silica because silica solubility is pressure dependent (Dixit et al., 2001; Van Cappellen et al., 2002).

## Diatoms and Permeable Shelf Beds

Diatoms flourish in the nutrient-rich waters of the continental shelves, which are one of the most productive oceanic environments. Permeable sediments predominantly cover this region (Riggs et al., 1996), but only elementary knowledge of organic-matter decomposition in these sands exists.

Tides, density gradients, winds, and waves create boundary-layer flows along the shelf bed (Huettel et al., 1996). As these bottom currents encounter sediment topography, they are deflected (Huettel et al., 1996; Huettel and Rusch, 2000). This deflection creates horizontal pressure gradients where pressure increases at the slopes of sediment topography opposing the

flow. Decreased pressure occurs in areas where flow velocity increases as it travels over the structure (Huettel and Gust, 1992; Huettel et al., 1996). In permeable coastal sands (permeabilities exceeding $10^{-12}$ $m^2$), these pressure gradients allow water to move with ease through the interstitial spaces, resulting in the transfer of substances between the upper sediment layers and the water column (Huettel and Rusch, 2000). As sediment permeability increases, advective solute exchange rates also increase.

Permeable sands trap individual phytoplankton cells and short diatom chains in the interstitial space, so the deposited cells and other organic material are not resuspended by bottom currents and waves. High shear forces in the turbulent boundary layer can destroy aggregates of organic matter (Huettel and Rusch, 2000), and the resulting smaller particles can be carried into the porous bed.

The permeable shelf sand beds, thus, act as filters that accumulate $bSiO_2$ from the water column. In addition, benthic diatoms add $bSiO_2$ to the sediment. In the permeable bed, the $bSiO_2$ is exposed to pore-water flows that may maintain a large difference between $[Si(OH_4)]_{sat}$ and $[Si(OH)_4]_{amb}$ suggesting that the dissolution rate in these sediments can exceed those recorded for diffusion-dominated deposits.

So far, the processes controlling $bSiO_2$ deposition in the shallow shelf and the recycling of the $bSiO_2$ in permeable sediment have not been investigated and are poorly understood. This study investigates diatom deposition, dissolution, and $Si(OH)_4$ dynamics in permeable sediments in the northern Gulf of Mexico.

## Study-Site Description

Apalachicola Bay is a bar-built estuary located in the northern Gulf of Mexico, off the northwest coast of Florida. The Apalachicola River, which is part of the Apalachicola-Chattahoochee-Flint (ACF) River Basin (Figure 1.2), flows into the Gulf of Mexico at Apalachicola Bay. Two field sites on St. George Island, located on the Florida-Panhandle coast, were chosen (Figure 1.3). The first is located on the Gulf of Mexico side of the island. The site is exposed to constant wind and wave action, so sediments are frequently resuspended. The surf action creates mixing and more habitats for aerobic bacteria, thereby increasing the rate of organic-matter decomposition and subsequent release of nutrients from the sediments into the water column. The second field site is located on the Apalachicola Bay side of the island.

Sediments at this site are exposed to less wave action but experience higher organic-matter deposition. As a result, higher concentrations of organic matter are found in these sediments.


Figure 1.2. Apalachicola-Chattahoochee-Flint (ACF) Basin.

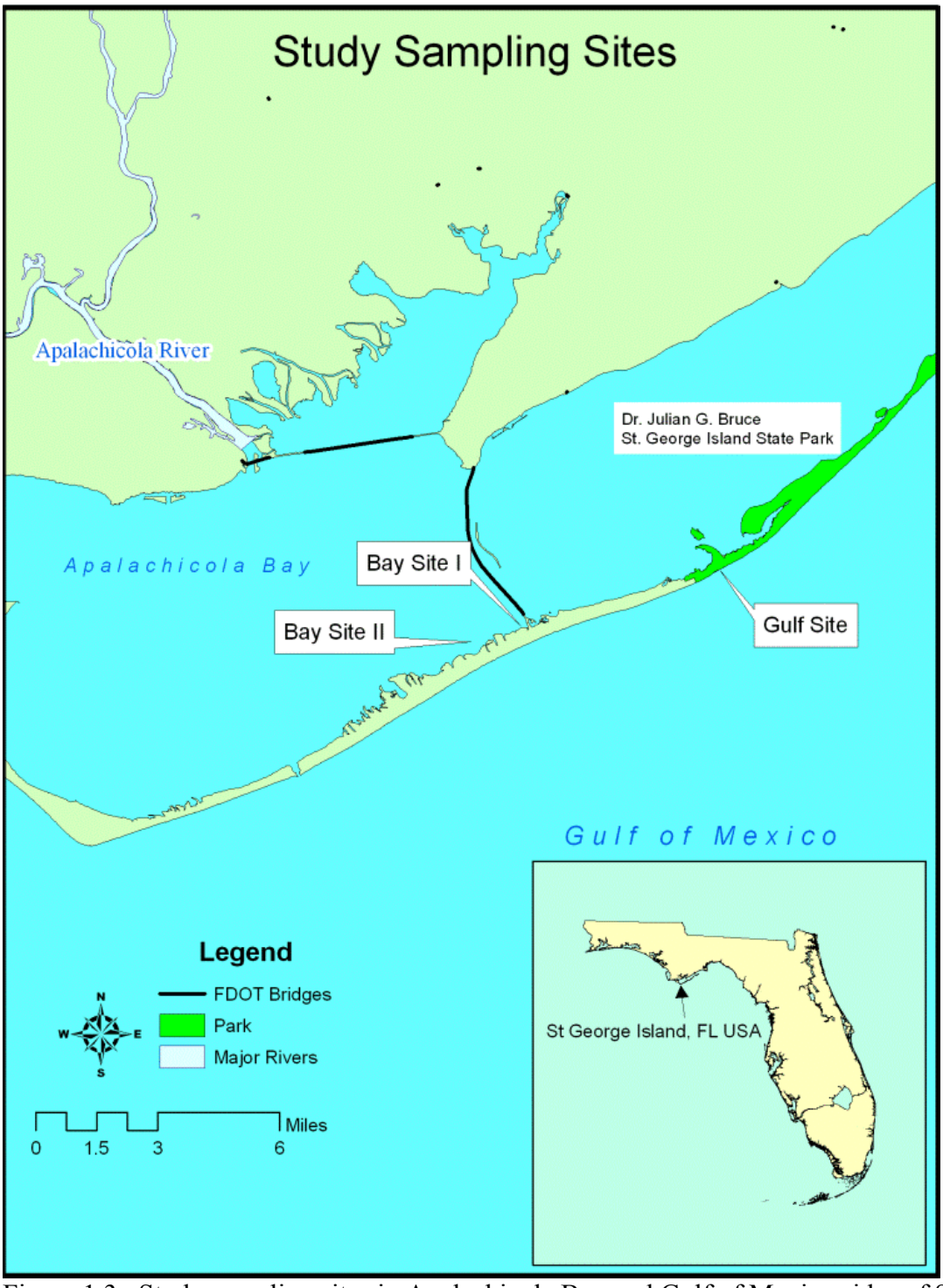


Figure 1.3. Study sampling sites in Apalachicola Bay and Gulf of Mexico sides of St. George Island, Florida, USA.

## Research Objectives

The objectives of the research presented in the following chapters are as follows:

I. To determine how diatoms are deposited on permeable sediments and how $Si(OH)_4$ is distributed in upper-sediment layers;

II. To determine how flushing of permeable sediments affects degradation and dissolution of diatoms embedded in the sands;

III. To determine fluxes of $Si(OH)_4$ from permeable sediments under different filtration conditions; and

IV. To assess $Si(OH)_4$ concentration ranges in the water and the pore water in the northern Gulf of Mexico in a time series and to determine the coupling between water-column and pore-water concentrations.

These objectives were addressed in laboratory-flume experiments (objective I), column-reactor experiments (objective II), in-situ flux chamber measurements (objective III), and with time series measurements in the northern Gulf of Mexico (objective IV).

## Working Hypotheses

Based on the above objectives, the following working hypotheses were tested:

I. When "heavy" diatoms are deposited on a rippled sandy surface, the $bSiO_2$ is not distributed evenly but instead accumulates in the slopes and troughs of sediment ripples. $Si(OH)_4$ that results from the dissolution of the accumulated material is transported by the advective water flows into the surface layer of the permeable bed;

II. Flushing of the pore space with bottom water maintains relatively low $Si(OH)_4$ concentrations in the pore water and thin diffusive-boundary layers around embedded $Si(OH)_4$ particles, thereby promoting dissolution. Diatom dissolution in percolated sediment thus is faster than in stagnant water;

III. Bottom flows and associated flushing of the upper sediment layer enhance $Si(OH)_4$ release from the permeable sediment, thereby accelerating recycling of the $Si(OH)_4$; and

IV. $Si(OH)_4$ concentrations in the shallow near-shore waters are strongly influenced by the sedimentary $Si(OH)_4$ recycling.

## Chapters

The results of this study are reported in four chapters:

- CHAPTER 2 addresses the deposition and the distribution of $bSiO_2$ in permeable sediment investigated in laboratory flumes;
- CHAPTER 3 reports the results from the laboratory column-reactor experiments investigating the dissolution of $bSiO_2$ in water and in percolated sand columns;
- CHAPTER 4 reports the results from laboratory and in-situ flux studies addressing the release of $Si(OH)_4$ from flushed permeable sediment;
- CHAPTER 5 reports the results from the nutrient time series measurements conducted in the northern Gulf of Mexico that investigated concentration ranges, temporal dynamics, and sediment-water exchange of the $bSiO_2$.

# CHAPTER 2
# DEPOSITION AND DISTRIBUTION OF $BSiO_2$ INVESTIGATED IN LABORATORY FLUMES

## Algal-Cell Deposition Experiment

### Introduction

In the shallow-shelf, deposition of phytoplankton is one of the main sources of organic matter (Jørgensen, 1996). Diatoms often comprise a large fraction of these settling algae. The shallow shelf sediments are typically sandy with permeabilities ($k$) exceeding $10^{-12}m^2$ ($k = K\mu/\rho g$, where $K$ is hydraulic conductivity, $\mu$ is dynamic viscosity, $\rho$ is density, and $g$ is gravity). As a result, pore-water flows are capable of transporting dissolved and particulate matter through the interstitial spaces (Huettel et al., 1998). This pressure-driven advective pore-water flow is generated when bottom currents interact with sediment topography (Huettel et al., 1996), such as sediment ripples (Precht and Huettel, 2004).

In the shallow coastal zone, the sandy beds are often covered by sediment ripples generated by waves and bottom currents, and the interaction between these ripples and boundary flows causes filtration, which may result in uneven uptake of particulate matter. Such uneven distribution of sedimented diatoms may affect the local fluxes of $Si(OH)_4$ into and out of the bed. Thus, the question arises, what is the fate of these deposited cells when settling onto a rippled surface influenced by wave-orbital motion? This question was addressed with an experiment in a wave flume at Florida State University (FSU). The experiment was designed to assess the effect of surface gravity waves and ensuing oscillating boundary flows on the distribution pattern of settling planktonic algal cells in a permeable rippled sand bed. The working hypothesis was that the algae would not settle evenly but would accumulate in depressed areas and zones where water flow into the sediment is highest.

### Methods

**Experimental set-up.** For this experiment, conducted in November 2004, the FSU Geophysical Fluid Dynamics Institute's (GFDI) recirculating flume (610-cm length, 31-cm width, 30-cm

height, 567.3-$cm^3$ water volume) was used (Figure 2.1). An 8-cm thick layer of organic-free, clean glass-bead sand (200–300 μm grain size) was placed in the flume, and water depth in the flume was adjusted to 30 cm. During an initial period (10 min), a wave paddle generated waves of 10-cm amplitude and 1.2-Hz frequency that resulted in ripple formation on the sediment surface (0.5-cm wave amplitude, 7-cm wavelength). The wave paddle was then adjusted to reduce the wave size (2.5-cm amplitude, 0.6-Hz frequency). The wave-orbital motion created an oscillating flow at the sediment-water interface; however, this flow was not strong enough to cause movement or erosion of the sand ripples. A suspension of dead, intact phytoplankton cells, obtained from Reed Mariculture, including *Thalassiosira weissflogii, Pavlova*, and *Nannochloropsis*, was added to the water to yield a final concentration of $2.64 \times 10^8$ cells $l^{-1}$ in the water column.

Figure 2.1. GFDI flume, picture courtesy of Dr. Markus Huettel.

**Sampling procedure.** At the end of the experimental period (24 h), the water was partially drained from the wave tank, and the sediment surface was photographed for subsequent image analysis. Three pictures covering 12 cm x 12 cm of the rippled surface were digitized, and sediment cores (2-cm diameter, 5-cm length) were taken for chlorophyll analysis.

**Sample analysis.** The digitized photographs of the sediment surface were analyzed using the software program, ImageJ 1.37 V, a program developed at the National Institutes of Health (NIH). The colors of the pictures were separated into their red, blue, and green components, and the intensity of the reflected green light at 500 to 550 nm, the wavelength (λ) of maximum reflectance for this phytoplankton assemblage, was calibrated with the chlorophyll concentrations assessed in the sediment cores according to the procedure of Parsons et al. (1984).

## Nutrient-Distribution Experiment

### Introduction

The interaction between sediment-surface topography and boundary-layer flow results in a specific pattern of pore water upwelling and downwelling zones in permeable sediments. The question arises, how do these pore-water flows affect the distribution of $Si(OH)_4$ released from diatoms that settled onto the surface of a permeable bed? Therefore, an experiment was conducted in the summer of 2006 in order to assess the distribution of $Si(OH)_4$ in permeable sands exposed to unidirectional boundary-layer flow after the deposition of an algal bloom at the sediment surface with biogenic topography. The working hypothesis for this experiment was that the $Si(OH)_4$ distribution within the upper sediment layers would be controlled by the advective pore-water flows.

### Methods

**Experimental set-up.** For this experiment, a laboratory recirculating flume (Figure 2.2) was set up at the FSU Coastal and Marine Laboratory. Sediment (210-µm mean grain size, 34% porosity, $1.7 \times 10^{-11}$ $m^2$ permeability) was collected from the Gulf of Mexico field site and placed in the flume, while maintaining the original biogeochemical layering (flume: 200-cm long, 30-cm wide, and 40-cm high; sediment-core dimensions: 60-cm long, 20-cm wide, and 20-cm deep; water column height above the sediment: 8 cm). Three sediment mounds (8-cm diameter, 1-cm height), mimicking biogenic topography, were created on the sediment surface keeping maximum distance between mounds. The flume was filled with unfiltered natural seawater that contained phytoplankton from the Gulf of Mexico field site. The mounds were exposed to constant, unidirectional flow with a velocity of 20 cm $s^{-1}$ at 7 cm above the bed and a shear stress at the sediment-water interface of approximately 0.8 cm $s^{-1}$. Each week 1 L of live *Rhodomonas* algal culture, approximately $2x10^5$ cells $l^{-1}$, was added to the flume in order to feed the benthic community. The *Rhodomonas* algae were cultured and maintained by Dr. Nancy Marcus's laboratory. Using a set of fluorescent lamps controlled by a timer, a 12 h light/dark cycle was maintained in the flume. During the 59-d duration of the experiment, benthic diatoms grew on the sediment, which produced a brown coloration of the surface.

Figure 2.2. Nutrient-distribution experiment at FSU Coastal and Marine Laboratory**.**

**Sampling procedure.** At the end of the experiment, 24 sediment cores (8-cm diameter, 1-cm length) were taken along transects (four cores per transect, two parallel transects/mound) crossing the three mounds in flow direction. Nine additional cores of the same dimensions were taken in areas not affected by the pressure gradients caused by mound-flow interaction, and another four cores of the same dimensions were taken for permeability and porosity measurements.

**Sample analysis.** The cores for nutrient analysis were sectioned at 1-cm depth intervals from which pore water was extracted by centrifugation. The pore-water samples were weighed and diluted to a final volume of 50.0 ml with B-pure water and analyzed spectrophotometrically for dissolved inorganic silicate ($Si(OH)_4$) according to the methods of Grasshoff et al. (1983). Cores for permeability determination were attached to a constant head permeability meter and measured according to the procedures described in Klute and Dirksen (1986). The $Si(OH)_4$ data were plotted two dimensionally using the Surfer program in order to view the areas of upwelling and downwelling and differences in $Si(OH)_4$ concentrations.

## Results

### Algal Cell-Deposition Experiment

The deposition of the planktonic algae on the permeable sediment was not uniform. Instead, it was characterized by alternating bands of enhanced and decreased deposition paralleling the sediment ripples (Figure 2.3). Although the deposition of algae showed relatively

strong variability between the three analyzed areas, a general pattern emerged. Enhanced deposition was recorded at the bottom of the ripple troughs and on the upper slopes of the ripples, and the ripple crest was associated with a deposition minimum. The highest concentrations of chlorophyll were found in the depositional areas. The average highest concentrations averaged over the three analyzed areas (0.72± 0.61 µg $cm^{-2}$) exceeded the averaged lowest concentrations (0.40± 0.53 µg $cm^{-2}$) approximately two-fold (factor 1.8).

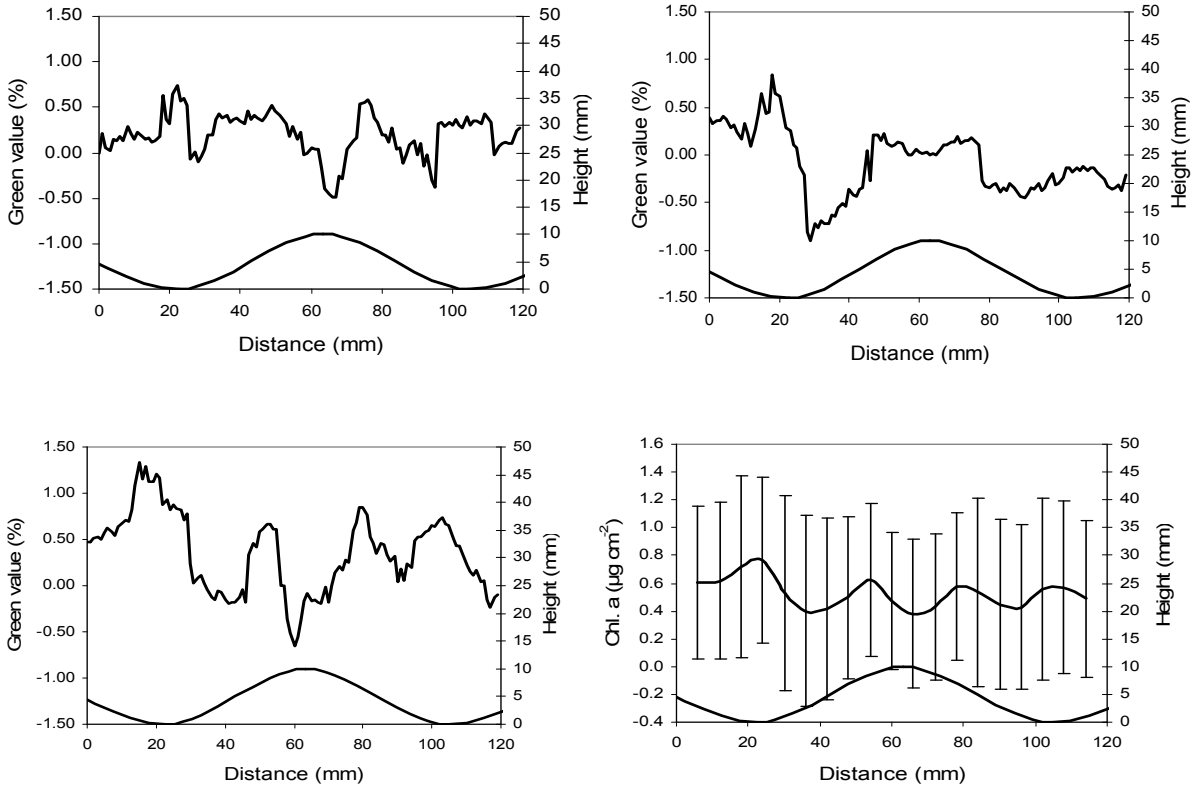


Figure 2.3. Results of GFDI Experiment. First three panes (left to right): Relative intensity of the green light (jagged line, 500-550 nm), reflected by the algae measured at three different locations in the flume along ripples. The smooth line in the lower section of the panes shows the cross section of the ripple relative to the green reflection. Measurements in each pane cover a square sediment surface area of 12 x 12 cm. Lower pane in right-hand side: average of the three upper panes with standard deviation.

**Nutrient-Distribution Experiment**

Despite the relatively long duration of this experiment (59 d), the $Si(OH)_4$ was unevenly distributed in the pore water of the sediment core. The two-dimensional plots depicting the distribution of $Si(OH)_4$ under the three mounds revealed two major zones of high concentration. The first zone was under the downstream slope of the mounds, and the second zone was in the anoxic subsurface layers of the sediment (>2cm) (Figure 2.4). As shown in the averaged plot, the $Si(OH)_4$ distributions measured below the three mounds show a zone of upwelling of the $Si(OH)_4$-rich pore water that connects the deeper layers and the zone under the downstream slope of the mound. The lowest $Si(OH)_4$ concentrations were measured upstream and downstream of the mound. This concentration distribution pattern agrees with the pore-water flow pattern that is associated with the interaction of the flume flows with the mounds on the sediment surface. In the areas upstream and downstream of the mounds, flume water with low concentrations of $Si(OH)_4$ was forced into the sediment, while under the downstream slope of the mounds pore-water streamlines converged and pore water from deeper, $Si(OH)_4$-rich sediment layers was drawn to the surface (Figure 2.4).

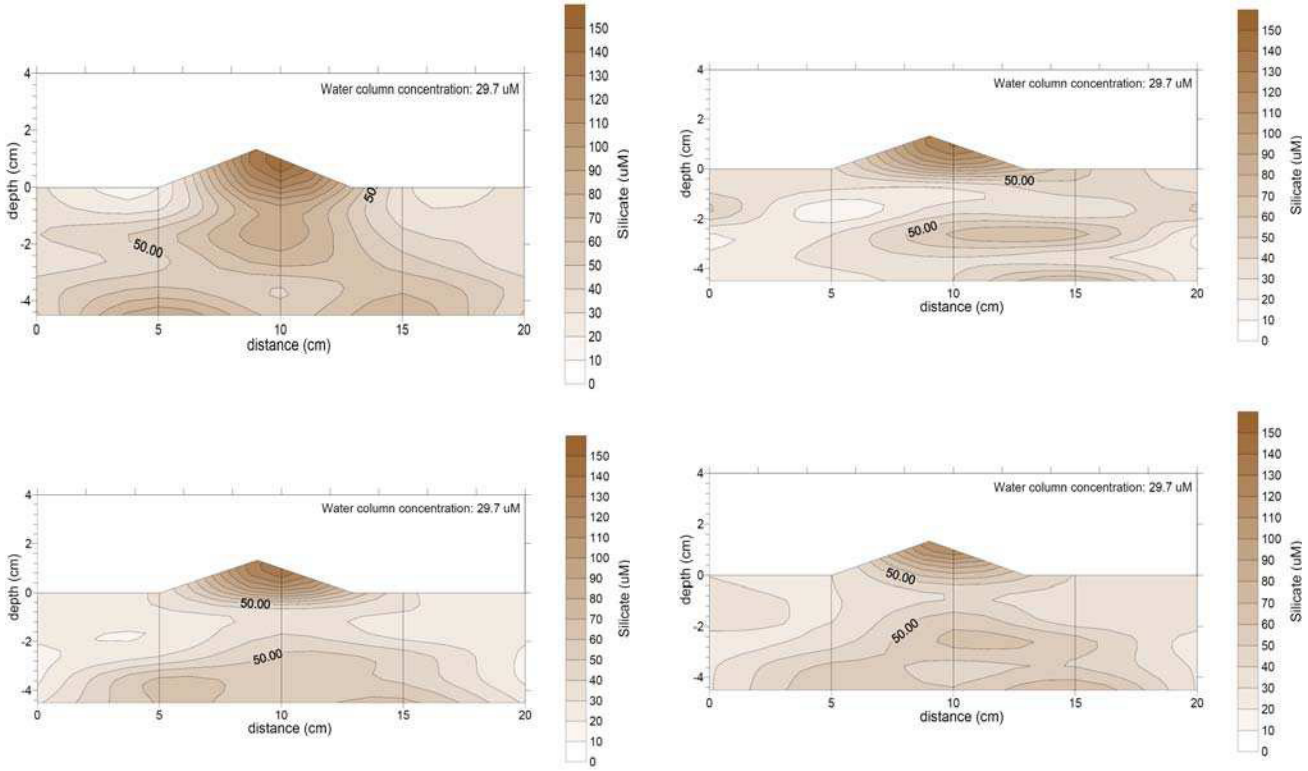


Figure 2.4. Nutrient-distribution experiment results. $Si(OH)_4$ distribution in the flume core under the three mounds after 59 d.

## Discussion

### Diatoms and Permeable Shelf Beds

Shallow coastal areas are typically high energy environments; therefore, the transfer of matter into the permeable bed is controlled by advective pore-water flows and lateral sediment transport (Huettel et al., 2003). When unidirectional or oscillating boundary layer flows interact with sediment topography, small lateral pressure gradients of 1-3 Pa $cm^{-1}$ are formed. These pressure gradients drive interfacial advective flows (Huettel and Gust, 1992).

When water depth is less than half the wavelength of surface gravity waves, as it was in the algal cell-deposition experiment, oscillating boundary flows are created at the sediment-water interface by orbital motion (Precht and Huettel, 2003). These oscillating flows drive pore water into and out of permeable shelf beds (Precht and Huettel, 2003; Pilditch and Miller, 2006). In the algal cell-deposition experiment, the regular striped pattern of organic-matter distribution revealed the filtration of cells into ripple slopes, with maximum deposition of the cells in the ripple troughs and slopes where water intruded into the sediment because of this oscillating flow. These findings confirmed the working hypothesis that algae would not settle evenly but would accumulate in depressed areas and zones where water flow into the sediment is highest. Precht and Huettel (2003) also saw similar results when they performed a wave-tank experiment with tracer dyes, and they observed gradients generated by the interaction of oscillating boundary flows and sediment ripples. The pressure gradients produced a pore-water flow field with a regular pattern of both intrusion and release zones that moved with ripple migration (Precht and Huettel, 2004). Shum's (1992) model calculations also yielded similar findings. Pilditch and Miller (2006) also found that 3.5 times as many diatoms were deposited in ripples troughs in comparison to ripple crests.

These uneven, yet predictable, depositional patterns have physical, geochemical, and biological consequences. Where organic particles such as diatoms accumulate, sediment pores may become clogged, which reduces advective pore water flow and filtration. The wave-induced transport processes may affect the biogeochemical zonation in sandy, permeable sediments (Huettel et al., 1998; Precht and Huettel, 2004) due to the uneven distribution of pore-water transport, electron acceptors, and nutrients (Shum, 1993). Combined, the physical and geochemical effects may, in turn, affect the biology. Sedimentary organisms may depend on

organic matter (e.g., heterotrophs), inorganic nutrients (e.g., autotrophs), and dissolved gases (e.g., oxygen and carbon dioxide). An uneven distribution of these substances may cause an uneven distribution of sedimentary organisms as was the finding of Danovaro et al. (2001).

Oscillating flows can cause sediment ripples to migrate, which in turn affects the resuspension and burial of organic particles. Jenness and Duineveld (1985) observed that high levels of chlorophyll were buried in the sediment to a depth of 5 cm and later resuspended during each tidal cycle. Based on laboratory experiments, they concluded that this finding was related to the formation and migration of sediment ripples that moved over organic particles that accumulated in the ripple troughs.

Although strong bottom currents can resuspend deposited organic matter, these currents can also cause permeable sediments to act as traps for single phytoplankton cells and short diatom chains by preventing the resuspension of these cells and driving them further into the sediment. This occurrence can increase mineralization as well as the recycling of organic matter and $Si(OH)_4$ in these sediments (Ehrenhauss and Huettel, 2004).

Advective transport processes driven by unidirectional flows are better understood than those driven by oscillating currents (Precht and Huettel, 2004). However, pore-water advection caused by unidirectional flows and oscillating flows can be of the same order of magnitude (Huettel and Precht, 2004). Unidirectional flow in the marine environment can be caused by wind-driven currents, tides, density gradients, and geostrophic currents. Unlike oscillating flows, unidirectional flows cause upwelling of fluid under the downstream slope of sediment ripples (Figure 2.5; Huettel and Gust, 1992; Huettel et al., 1996). This upwelling pattern is also shown in the results of the flume experiment that addresses $Si(OH)_4$ distribution in a sandy bed with topography. This experiment supported the working hypothesis that the $Si(OH)_4$ distribution within the upper sediment layers is largely controlled by the advective pore-water flows associated with the topography.

In the surface ocean, $bSiO_2$ dissolution takes place at a much faster rate than in deeper ocean waters (Van Cappellen et al., 2002). Because permeable sediments are constantly flushed at rapid rates, this flushing can prevent the build-up of $Si(OH)_4$ in the pore water and lead to higher degrees of undersaturation in these waters (Ehrenhauss and Huettel, 2004). Rickert et al. (2002) found that in silica-depleted waters, the dissolution rate of opal is increased; therefore, advection may promote higher dissolution rates in permeable shelf sediments. This increased

rate of dissolution may also lead to higher levels of remobilized $Si(OH)_4$ back into the water column from the sediment.

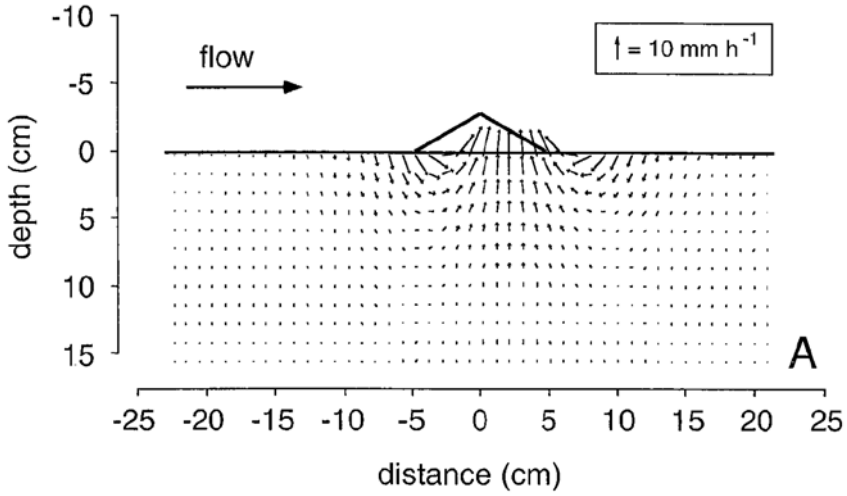


Figure 2.5. Unidirectional flow schematic. This plot from Huettel et al. (1996) shows the pore-water flow vectors under a mound built on permeable sediment for similar settings as used in this flume experiment.

**$Si(OH)_4$ Distribution**

Advective flows create uneven depositional patterns. As a result, $Si(OH)_4$ can be unevenly distributed in the sediment, which affects the $Si(OH)_4$ fluxes as well as benthic diatom growth. After deposition on the seafloor, dissolution of $Si(OH)_4$ continues at the sediment surface (Van Cappellen et al., 2002). However, the sediment surface is not a stagnant environment as it is constantly affected by boundary-layer flows as well as other natural elements. As sediment ripples reconfigure, these deposited diatoms can be buried deeper in the sediment (Pilditch and Miller, 2006). Therefore, $Si(OH)_4$ concentrations in the sediment may be higher in areas where more diatoms are buried deeper in the sand. In some cases, dissolution can lead to a build up of $Si(OH)_4$ concentrations in the pore water in the first 5-20 cm below the sediment-water interface (Hurd, 1973; McManus et al., 1995; Van Cappellen et al., 2002). In turn, these concentration gradients drive the $Si(OH)_4$ from the sediment back into the water column. Advective solute exchange rates also play a role as they prevent the accumulation of $Si(OH)_4$ near the dissolving frustules and in the pore water. This constant flushing allows for the efficient cycling of $Si(OH)_4$ back into the water column. Ehrenhauss and Huettel (2004) found that 95 to 101 μmol $Si(OH)_4$ $m^{-2}d^{-1}$ can be released. Benthic diatoms located in areas of high

$Si(OH)_4$ concentrations will thrive on these $Si(OH)_4$-rich conditions. Because of the overall dynamic nature of these sediments, frequent $Si(OH)_4$ influxes are likely to reach these benthic communities.

Diatom deposition in a smooth bed differs from deposition in a rippled sand bed. Depending on where the algae are deposited, different processes control their fates. Huettel and Rusch (2000) demonstrated that depositional flux due to advective transport on rippled sandy beds was larger by a factor of nine when compared to the smooth sediment control. Penetration depth of the unicellular algae used in their experiment increased up to a factor of seven when compared to the smooth sediment control. Similar findings were presented in Huettel et al. (1996). In this study, the researchers found that ripple topography (0.8-2.8 cm high) increased interfacial particle (1 μm) flux by a factor of 2.3 when compared to the smooth sediment control. Pilditch and Miller's (2006) work also agrees with these findings. They found that ripples increased total diatom deposition and spatial variability in chlorophyll a in comparison to the flat bed. Diatoms settled uniformly on the sediment surface in their flat bed. These findings suggest that without the sediment ripples diatoms simply create layers on the sediment surface. As these layers increase in size and depth, they can provide organisms living on the surface with an ample food source. In both instances, diatom deposition provides resources to the sediment community.

Diatom deposition (e.g., following a diatom bloom in the shelf) has many effects on the sedimentary organisms. Most coastal bloom diatoms are characterized by their small size, spiny exteriors, thin frustules, and chain-forming tendencies (Smetacek, 1985). The presence of spines and the tendency to form chains may both be ways to combat grazing (Ehrenhauss and Huettel, 2004). In particular, these features may be designed to protect the thin frustule, which may be more likely to dissolve than a thicker frustule. These features may also reduce benthic filtration (Ehrenhauss and Huettel, 2004). These diatoms may then sit on the sediment surface rather than be drawn into the sediment with the advective pore-water flows. The benthic organisms on the surface may benefit from this food source.

In other instances, the deposited diatoms may also provide food sources to organisms living deeper in the sediment. As diatom blooms degrade, the cells often form aggregates. These aggregates of living organisms form large particles of marine snow that can reach several centimeters in diameter (Smetacek, 1985; Brzezinski et al., 1997). Brzezinski et al. (1997)

conducted a study of marine snow from coastal waters off central California. Within the aggregates, they measured $Si(OH)_4$ concentrations of approximately ten fold greater on average than those in the surrounding seawater. This high nutrient environment decreases the likelihood of nutrient limitation within the aggregate. When the snow finally settles on the seafloor, a new source of nutrients exists for the benthic community. In permeable sediments, these aggregates may be driven into sediments stimulating the microbial community.

Distribution of these deposited diatoms also depends on the permeability of the sediments. In muddy, cohesive sediments, diffusion is the major transport mechanism. This process is slow over large distances. Meanwhile, in permeable sediments, advective transport processes increase with increasing permeability (Huettel and Rusch, 2000).

# CHAPTER 3
# DIATOM DISSOLUTION-RATE MEASUREMENTS IN WATER AND PERCOLATED MARINE SANDS

## Dissolution-Rate Experiments

### Introduction

From the experiments conducted in Chapter 2, one can conclude that diatoms accumulate in ripple troughs and upper slopes of sediment ripples and penetrate into the upper-sediment layer. It is also known that diatoms degrade in water and in sediments. The question arises whether the filtration of diatoms into permeable beds affects degradation and dissolution rate of the diatom frustules. In this chapter, experiments were conducted to determine if pore-water flow and the presence of the organic coating covering the $Si(OH)_4$ frustules affects the dissolution rate. The working hypotheses were that pore-water flows enhance the dissolution rate and that the frustules dissolve faster after the organic coating is decomposed. When organic coating is removed, flow velocity controls dissolution rate (assuming undersaturated water). Secondly, it was investigated whether the diatom degradation rates in water and sediment differ. The working hypothesis was that diatoms degrade faster in percolated permeable sediment due to higher microbial activities that accelerate the removal of the organic coating and due to the higher flow velocities near the diatom surface.

### Methods

In order to calculate the maximum dissolution rate of $bSiO_2$ in seawater, two dissolution-rate experiments were conducted. These experiments were designed to complement the reaction-rate experiments in the percolation columns.

#### Dissolution-Rate Experiment I

**Experimental set-up.** Three opaque, plastic bottles (v = 250 ml) were filled with exactly 90.0 ml of artificial seawater (S = 32 ppt) each. To the first bottle, a concentration of $10^9$ cells $l^{-1}$ of dead, cultured *Thalassiosira weissflogii*, obtained from Reed Mariculture, was added (same amount added to columns in reaction-rate experiment I). To the second bottle, twice the amount of cells was added, and to the third bottle, 2.47 times the amount of cells. The experimental set-

up is shown in Table 3.1. The bottles were placed on a shaker and continuously agitated throughout the experiment.

**Experimental settings.** This experiment, conducted in summer 2006, ran for 1437.25 h (59 d, 21 h, 15 min) at a temperature of 23± 0.1°C.

**Sampling procedure.** Periodic samplings for $Si(OH)_4$ or dissolved inorganic silicate (DIS) were taken. Table 3.2 shows the collection dates and times of the samples. Prior to sampling, the bottles were inverted several times to mix any potential concentration gradient in the bottle. Exactly 5.0 ml of fluid were removed with a pipette from each of the bottles and placed in an individual 50-ml centrifuge tube. To maintain a constant volume, 5.0 ml of $Si(OH)_4$-free artificial seawater (S = 32 ppt) were added after sampling.

**Sample analysis.** Samples were filtered through 0.45-µm syringe filters, and the fluid was analyzed spectrophotometrically for $Si(OH)_4$ or DIS according to Grasshoff et al. (1983).

**Data analysis.** The $Si(OH)_4$ concentration was calculated using a calibration line, and the change in concentration over time (h) was plotted. From the concentration change, $k_{diss}$, the dissolution rate constant, was calculated per Truesdale et al. (2005) according to the following equations:

The common classification of dissolution behavior in batch reactors, like the bottles and columns used for the experiments in this chapter, uses plots of $\ln\{(C_\infty-C_t)/C_\infty\}$ versus time (t), where $C_\infty$ and $C_t$ are the dissolved $Si(OH)_4$ concentration at times infinity ($\infty$) and t, respectively (e.g., Kamatani et al., 1980; Kamatani, 1982; Hubbard and Riley, 1984; Trégeur et al., 1989). When the $Si(OH)_4$ concentration ($C_t$) is an increasing exponential function from 0 to $C_\infty$,

$$C_t = C_\infty(1-e^{-kt})$$

K is the dissolution rate constant, *k*. Taking the difference, $C_\infty-C_t$, rotates the graph and shows it as a decreasing exponential function between $C_\infty$ and 0. This plot can be normalized by dividing the concentration difference ($C_\infty-C_t$) by the final concentration $C_\infty$. The $\{(C_\infty-C_t)/C_\infty\}$ plot thus runs between 1 and 0. By using the logarithms, a straight line with negative gradient results, starting from 0 (ln = 1) and continuing into negative values {ln (<1)}, as time increases. Dissolution experiments with different rate constants produce a fan of straight lines, radiating

from the origin and the gradient of these lines is solely dependent upon the dissolution rate constant, *k*. With $C_t$ described by the exponential function $C_t = C_\infty (1-e^{-kt})$,

$\{(C_\infty - C_t)/C_\infty\} = \{C_\infty - C_\infty (1-e^{-kt})\}/C_\infty$

$\{C_\infty - C_\infty(1- e^{-kt})\}/C_\infty = C_\infty (e^{-kt})/C_\infty$

$C_\infty (e^{-kt})/C_\infty = (e^{-kt})$

By using the natural logarithms, the dissolution rate constant, *k*, can be directly derived from the resulting linear plot:

$\ln(C_\infty - C_t)/C_\infty = \ln (e^{-kt}) = -k_t$

This approach can be applied to simple and to sum of exponential dissolutions even when exponential dissolutions run to different $C_\infty$ values, e.g., if slightly different amounts of the same silica were used in the batch incubations like in the experiments presented in this chapter. However, if the *k* values are expected to be different over time, e.g., because different sources of $Si(OH)_4$ are present in the batch experiment (as in the sediment cores used in the reaction-rate experiments), the plot $\ln(C_\infty - C_t)/C_\infty$ may produce curves with two or more distinct linear portions reflecting different *k* values dominating throughout a certain period of the experiment (e.g., faster initial dissolution of fresh diatom frustules followed by slower dissolution of sedimentary opal that was altered by binding clay).

In the column-reactor experiments, the researcher observed such a behavior with $\ln(C_\infty - C_t)/C_\infty$ plots showing two linear sections with different slopes (i.e., k values). These functions can be expressed as:

$\ln(C_\infty - C_t)/C_\infty = \{(A_\infty/(A_\infty+B_\infty)*e^{-kat})+(B_\infty/(A_\infty+B_\infty)*e^{-kbt})\}$

**Dissolution-Rate Experiment II**

**Experimental set-up.** Six opaque, plastic bottles (v = 250 ml) were filled with exactly 90.0 ml of artificial seawater (S = 32 ppt). To each of two bottles, dead, cultured *T. weissflogii*, obtained from Reed Mariculture, were added resulting in a final concentration of $10^6$ cells $l^{-1}$. To each of

the next two bottles, algae were added to produce a final concentration of $10^7$ cells $l^{-1}$. In the remaining two bottles, cell concentration was adjusted to $10^8$ cells $l^{-1}$. The experimental set-up is shown in Table 3.1. One bottle containing each concentration was placed on a shaker (~0.1 cm $h^{-1}$), and the other bottles were placed on the lab bench (no stirring).

**Experimental settings.** This experiment, conducted in summer and early fall 2006, ran for 645.83 h (26 d, 21 h, 50 min). The experiment ran at a temperature of 23± 0.1°C.

**Sampling procedure.** Periodic samples for $Si(OH)_4$ or DIS were taken. Table 3.3 shows the collection dates and times of the samples. To mix the fluid and to remove the diffusive layer, each of the stagnant bottles—those placed on the lab bench—were inverted twice prior to sampling. The same sampling procedures from the first experiment were followed in this experiment.

**Sample analysis.** Samples were analyzed following the same procedures used in the first experiment.

**Data analysis.** $Si(OH)_4$ concentration was calculated following the same procedure used in the first experiment.

Table 3.1. Experimental set-up of dissolution-rate experiments I and II.

| Bottle Experiment I | | |
|---|---|---|
| Bottle | Treatment | Diatoms Added (cells $l^{-1}$) |
| 1 | Shaken | $10^6$ |
| 2 | Shaken | $2 \times 10^6$ |
| 3 | Shaken | $2.47 \times 10^6$ |
| Bottle Experiment II | | |
| Bottle | Treatment | Diatoms Added (cells $l^{-1}$) |
| 1A | Shaken | $10^6$ |
| 1B | Stagnant | $10^6$ |
| 2A | Shaken | $10^7$ |
| 2B | Stagnant | $10^7$ |
| 3A | Shaken | $10^8$ |
| 3B | Stagnant | $10^8$ |

Table 3.2. Sampling schedule for dissolution-rate experiment I.

| Sampling | Collection Date | Time | Time (h) |
|---|---|---|---|
| 0 | 7/8/2006 | 1715 | 0 |
| 1 | 7/9/2006 | 1315 | 20.00 |
| 2 | 7/10/2006 | 1315 | 44.00 |
| 3 | 7/11/2006 | 1315 | 68.00 |
| 4 | 7/12/2006 | 1315 | 92.00 |
| 5 | 7/17/2006 | 1315 | 212.00 |
| 6 | 7/22/2006 | 1315 | 332.00 |
| 7 | 7/31/2006 | 1615 | 551.00 |
| 8 | 8/7/2006 | 1600 | 718.75 |
| 9 | 8/10/2006 | 1640 | 791.42 |
| 10 | 8/12/2006 | 1515 | 838.00 |
| 11 | 8/14/2006 | 1800 | 888.75 |
| 12 | 8/18/2006 | 2215 | 989.00 |
| 13 | 8/21/2006 | 1800 | 1056.75 |
| 14 | 8/24/2006 | 1915 | 1130.00 |
| 15 | 8/29/2006 | 1115 | 1242.00 |
| 16 | 9/6/2006 | 1430 | 1437.25 |

Table 3.3. Sampling schedule for dissolution-rate experiment II.

| Sampling | Collection Date | Time | Time (h) |
|---|---|---|---|
| 0 | 8/10/2006 | 1640 | 0 |
| 1 | 8/12/2006 | 1515 | 46.58 |
| 2 | 8/14/2006 | 1800 | 50.75 |
| 3 | 8/18/2006 | 2215 | 100.25 |
| 4 | 8/21/2006 | 1800 | 67.75 |
| 5 | 8/24/2006 | 1915 | 73.25 |
| 6 | 8/29/2006 | 1115 | 112.00 |
| 7 | 9/6/2006 | 1430 | 195.25 |

## Reaction-Rate Experiments

### Introduction

These experiments were conducted to determine the rate of $bSiO_2$ dissolution in percolated permeable sands under controlled laboratory settings (e.g., constant salinity (S) and temperature). The main research objective of these experiments was to determine how flushing of permeable sediment facilitates degradation of diatoms embedded in the sands. Four reaction-rate experiments, also referred to as column experiments, and one coil experiment were conducted. All of the experiments were run at S = 32 and a temperature of 23± 0.1°C. Table 3.4 shows the experimental set-up, and Figure 3.1 shows a schematic of these column-reactor experiments.

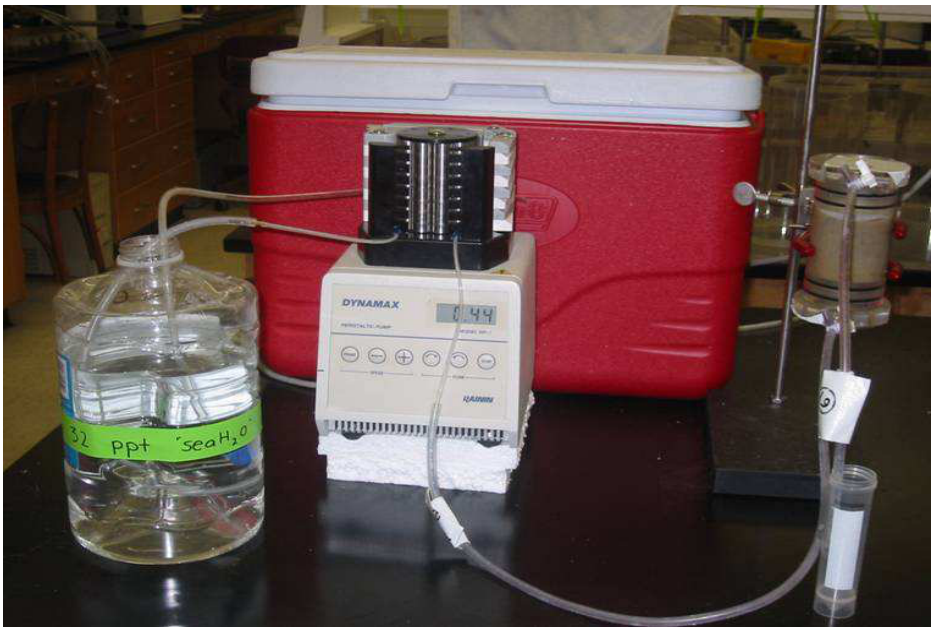

Figure 3.1. Experimental set-up of column-reactor experiments.

Table 3.4. Experimental set-up of column-reactor experiments I, II, III, and IV.

| Column No. | Sediment Characteristics | Treatment (Diatom Cells $l^{-1}$ Pore Water) | Flushing Rate (ml $h^{-1}$ $cm^{-2}$) |
|---|---|---|---|
| Experiment I | | | |
| 1 | Live | 0 | 2 |
| 2 | Sterile | 0 | 2 |
| 3 | Live | $10^9$ | 2 |
| 4 | Sterile | $10^9$ | 2 |
| Experiment II | | | |
| 1 | Live | 0 | 1 |
| 2 | Live | $10^7$ | 1 |
| 3 | Live | $10^6$ | 1 |
| 4 | Live | $10^8$ | 1 |
| 5 | Live | 0 | 2 |
| 6 | Live | $10^6$ | 2 |
| 7 | Live | $10^7$ | 2 |
| 8 | Live | $10^8$ | 2 |
| Experiment III | | | |
| 1 | Opal-Free, Live | 0 | 1 |
| 2 | Opal-Free, Live | 0 | 1 |
| 3 | Opal-Free, Live | $10^{10}$ | 1 |
| 4 | Opal-Free, Live | $10^{10}$ | 1 |
| 5 | Opal-Free, Live | 0 | 2 |
| 6 | Opal-Free, Live | 0 | 2 |
| 7 | Opal-Free, Live | $10^{10}$ | 2 |
| 8 | Opal-Free, Live | $10^{10}$ | 2 |

Table 3.4. Continued

| Experiment IV | | | |
|---|---|---|---|
| Column No. | Sediment Characteristics | Treatment (Diatom Cells $l^{-1}$ Pore Water) | Flushing Rate (ml $h^{-1}$ $cm^{-2}$) |
| 1 | Opal-Free, Live | 0 | 1 |
| 2 | Opal-Free, Live | 0 | 1 |
| 3 | Opal-Free, Live | $10^{10}$ | 1 |
| 4 | Opal-Free, Live | $10^{10}$ | 1 |
| 5 | Opal-Free, Live | 0 | 2 |
| 6 | Opal-Free, Live | 0 | 2 |
| 7 | Opal-Free, Live | $10^{10}$ | 2 |
| 8 | Opal-Free, Live | $10^{10}$ | 2 |

Column experiment I (reaction-rate experiment I) tested the difference in diatom dissolution between sterilized and natural sediments. This experiment was conducted to determine if diatom dissolution was affected by bacteria that colonize the sediments. Column experiment II (reaction-rate experiment II) was conducted to determine the difference in dissolution rates between various concentrations of diatoms in natural sediment as well as to determine if flushing rate affected diatom dissolution in the natural sediment. Column experiment III (reaction-rate experiment III) was conducted to test whether the organic coating surrounding the frustule enhances degradation of diatoms embedded in opal-free sediment. Column experiment IV (reaction-rate experiment IV) was conducted to test whether the flushing rate affected the dissolution rate of fresh, dead diatoms in opal-free sediments. Coil experiment I (reaction-rate experiment V) was conducted to determine whether the flushing rate affected the dissolution of opal in water.

## Methods

### Reaction-Rate Experiment I

**Sediment preparation.** Permeable sediment was collected from the Gulf of Mexico field site on St. George Island. To remove shell debris and macrofauna, the sediment was sieved through

1.55-mm mesh. A portion of the sieved sediment was wrapped in Al foil and combusted overnight in a muffle furnace at 500°C. Both the sterile and the live sediments were washed in artificial (S = 32 ppt) seawater.

**Diatom preparation.** A cell count was performed on the *Thalassiosira weissflogii* 1200™ stock, obtained from Reed Mariculture, with the Coulter Z2 AccuComp program in Dr. Nancy Marcus's laboratory. This cell count was used to determine the required amount of diatom stock to be added to the sediment for the experiment. The diatoms were mixed into the sediments resulting in a final pore water concentration of $10^9$ cells $l^{-1}$.

**Experimental set-up.** This experiment was conducted in June 2006. Before the experiment began, the polycarbonate percolation columns (10-cm OD, v = 250 ml), plastic tubing, stopcocks, and lids were placed in a 1% HCl bath and allowed to sit overnight in order to remove any substances that could interfere with the experiment. The sterilized and natural sediments with added diatoms were then filled into the column reactors. Sediment was added to each of the columns carefully to avoid creating air bubbles or pockets, which could affect the experiment, and equal amounts of sediment were added to columns. Once the diatoms were added and mixed into the sediments in the columns, and before the actual experiment was begun, three 1.0-$cm^3$ portions of sediment from each of the columns were placed in individual 50-ml plastic centrifuge tubes. TSi analysis of the sediments was conducted according to the methods of Grasshoff et al. (1983) in order to determine the amount of $bSiO_2$ in the columns. This same analysis was also to be conducted at the end of the experiment; however, for this particular experiment, no final samples were taken. A thin Teflon frit was used on both sides of the sediment to avoid flushing diatoms and sediment out of the columns. Inflow and outflow tubing were Nalgene® 180 PVC tubing with 3.175 mm ID x 6.35 mm OD x 1.5875 mm wall, and the pump tubing for the peristaltic pump was PVC 3.18 mm 14" black/white tubing. The columns were wrapped with Al foil to prevent potential diatom growth due to light exposure and placed in a cooler with artificial seawater (S = 32 ppt) to keep the temperature constant. The peristaltic pump was set at a throughput of 50 ml $h^{-1}$, resulting in a fluid-front velocity of 5 cm $h^{-1}$ in the columns, which is a conservative pore-water velocity for sediment with the measured permeability in coastal settings (Huettel and Gust, 1992; Reimers et al., 2004). This setting was equivalent to roughly an output of 2 ml $h^{-1}$ $cm^{-2}$ when related to the cross-sectional area of the column. The columns were flushed for at least 1 h before two cell counts were performed on the samples collected at the

outflow in order to assess retention of cells in the column. These counts revealed that only negligible numbers of cells were initially flushed from the columns.

**Sampling procedure.** Samples were taken at least once daily over the duration of the experiment (504.53 h or 21 d, 0.53 h, 32 min). When samples were taken, the water was collected from the outflow of each column in a 50-ml centrifuge tube for 0.5 h. The pH was measured for several of the samples.

**Sample analysis.** Prior to analysis, the samples were each individually filtered through 0.45 μm syringe filters to remove debris and particulate $bSiO_2$, and $Si(OH)_4$ analysis was conducted in triplicates according to the methods of Grasshoff et al. (1983).

**Data analysis.** After calculating $Si(OH)_4$ concentration using a calibration line, the change in concentration over time was plotted. From the concentration change, the $k_{diss}$, dissolution rate constant, was calculated according to Truesdale et al. (2005). With the $k_{diss}$, the dissolution over time was calculated and compared with the measured data.

**Reaction-Rate Experiment II**

**Sediment preparation.** Sediment was cleaned and sieved as it was for the first experiment. However, for this experiment, the sediment was not combusted.

**Diatom preparation.** This step was carried out as it was for the first experiment. Dead, fresh *Thalassiosira weissflogii*, obtained from Reed Mariculture, were added to six of the columns. Diatoms were added to the sediment with 3.0 ml of artificial seawater (S = 32 ppt) and mixed thoroughly into the sediment.

**Experimental set-up.** The percolation columns were cleaned, and the experiment was set up the same way as it was in the first experiment. The pump tubing for the peristaltic pump was PVC 3.18 mm 14" black/white tubing and PVC 1.651 mm ID tubing. The columns were run with a fluid-front velocity of either 2.5 or 5 cm $h^{-1}$.

**Sampling procedure.** The experiment ran for 694.867 h (28 d, 22 h, 53 min). Water was collected from each of the outflows of the columns daily. For this experiment, the sampling period was 1 h.

**Sample and data analysis.** These steps were conducted as they were in the first experiment.

**Reaction-Rate Experiment III**

**Sediment preparation.** Sediment was collected and sieved as it was in the previous experiments. To minimize the natural background concentration of $bSiO_2$, the sediment was mixed with an oxidizing reagent (mixture of $K_2S_2O_8$, $H_3BO_3$, and 0.375 NaOH), as used for the total Si analysis, and placed in an autoclave for a 1-h cycle at 121°C. The samples were then allowed to sit in the oxidizing reagent overnight. The following day, the sediment was rinsed with artificial seawater (S=32 ppt), and it was then filled in the columns. The columns were flushed overnight with artificial seawater (S=32 ppt), and a sample was taken from the outflow of each column in order to assess the $Si(OH)_4$ background concentration. The samples were filtered through 0.20-µm syringe filters and analyzed for DIS (dissolved inorganic silicate) according to Grasshoff et al. (1983). The columns were then disassembled, and the sediment was placed in a bucket containing natural 5.0-µm filtered seawater that contained bacteria but no diatoms as verified through inspection with a microscope. A bubble stone was placed in the bucket, and the bucket was covered with aluminum foil to prevent any potential algal growth. This step was done to reintroduce natural bacteria back into the sediment. The sediment sat in the bucket for 3 d, and it was then placed back in the columns and flushed thoroughly with artificial seawater (S = 32 ppt).

**Diatom preparation.** Diatom frustules, without their natural organic coating, were added to the treatment columns. In order to remove this coating, the diatoms were digested according to the following procedure: 50 ml of dead, fresh *T. weissflogii*, obtained from Reed Mariculture, were digested in 50 ml of concentrated nitric acid ($HNO_3$) for 1 h at 100°C followed by digestion in hydrogen peroxide ($H_2O_2$) for another 1 h at 100°C. The fluid was allowed to cool to room temperature, and it was centrifuged at 3500 rpm for 5 min three times. In between each centrifugation, the pellet was rinsed with B-pure water. Digested cells were finally inspected under a microscope for cleanliness.

**Experimental set-up.** The experiment was set up as the first two experiments were.

**Sampling procedure.** The third experiment ran for 311.0833 h (12 d, 23 h, 5 min). Over the course of the experiment, water was collected from each of the columns at the outflow point at various intervals. The sampling period (1 h) was timed, and the exact volume collected in each 50-ml plastic centrifuge tube was measured.

**Sample and data analysis.** Prior to analysis, the samples were filtered through 0.20-µm syringe filters in order to remove debris and $Si(OH)_4$ particles from the samples. All other steps were the same as those followed in the previous two experiments.

**Reaction-Rate Experiment IV**

This experiment repeated reaction-rate experiment III except that untreated diatoms—washed but not digested—were used. The experimental set-up, sediment cleaning, and procedures were the same as in the third experiment. This experiment ran for 313.8 h (13 d, 1 h, 48 min). Sampling and data analysis were the same as in the previous experiment.

**Reaction-Rate Experiment V**

**Purpose.** This experiment was essentially a column experiment without sand. It measured the dissolution of $bSiO_2$ in a volume of flowing water corresponding to the volume of pore water in the sediment cores. This experiment was conducted to test the dissolution of cleaned diatom frustules in water flow rather than in sediment in order to assess whether the dissolution within the sediment was faster compared to dissolution in the water or at the sediment surface. The diatom frustules were acid cleaned using the same procedure as was used in the third column experiment.

**Experimental set-up.** Water-filled tubing coils were used that had the same volume as the pore-water volume in the sediment columns. The lengths of the tubing, 6.35 mm ID x 12.7 mm OD x 0.3175 mm wall, for the coils were cut to match the pore-water volume in the sediment. Flushing rate in the coils was set to the same values as for the third and fourth column experiments. The exact amount of diatoms as was added to the experimental columns in the third column experiment was added to the experimental coils. The diatoms were added with the appropriate amount of artificial seawater (S = 32 ppt), and the tubing was closed and coiled in order to enhance mixing within the tubing. To prevent flushing of diatoms from the coils, gauze was used to plug the ends of the tubing, and 0.20-µm syringe filters were placed at the inflow and outflow of each coil. Artificial seawater (S = 32 ppt) was percolated continuously through each of the coils with a peristaltic pump. The experimental set-up can be seen in Table 3.5. The coil treatments matched those of the columns from the third column experiment. Figure 3.2 shows the layout.

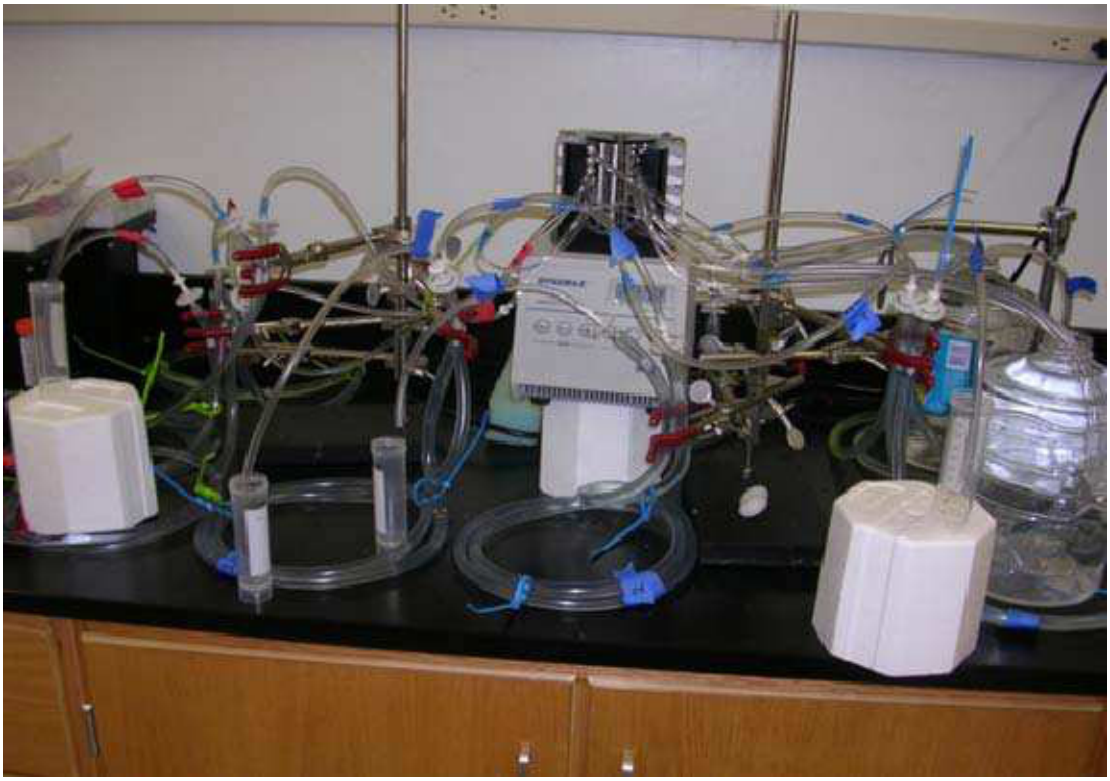

Figure 3.2. Experimental set-up of coil experiment.

Table 3.5. Experimental set –up of coil experiment.

| Coil Experiment I | | |
|---|---|---|
| Coil No. | Treatment (Diatom Cells $l^{-1}$ Pore Water) | Flushing Rate (ml $h^{-1}$ $cm^{-2}$) |
| 1 | 0 | 1 |
| 2 | 0 | 1 |
| 3 | $10^{10}$ | 1 |
| 4 | $10^{10}$ | 1 |
| 5 | 0 | 2 |
| 6 | 0 | 2 |
| 7 | $10^{10}$ | 2 |
| 8 | $10^{10}$ | 2 |

**Sampling procedure.** The same sampling protocol was carried out as it was in the third and the fourth experiments. Water was collected at the outflows in 50-ml centrifuge tubes.

**Sample and data analysis.** The samples were filtered through 0.20-µm syringe filters and analyzed for DIS according to Grasshoff et al. (1983). The data analysis proceeded as described in the previous experiments.

## Results

### Dissolution-Rate Experiments

**Dissolution-rate experiment I.** As the diatom concentration increased, the initial dissolution reaction rate constant did not change significantly and amounted to 0.0062 for bottle 1, 0.0059 for bottle 2, and 0.0066 for bottle 3 (Table 3.6 and Figure 3.3).

**Dissolution-rate experiment II.** For the shaken and stagnant conditions, no significant change in the initial dissolution reaction rate was observed for any of the concentrations (Figure 3.4).

For both bottle experiments, the dissolution rates were not significantly different. The standard deviation among them is 0.001, and the mean value is 0.0096. For the rate constants, all of these values were similar (Table 3.6). The rate constants ranged from 0.0034 to 0.0056, so they were in the same order of magnitude.

Table 3.6. Rate constants and $r^2$ values for bottle experiments I and II.

| Bottle Experiment I | | Treatment (Diatom Cells $l^{-1}$ Water) | Mixing | Dissolution Rate Constant, *k* | $r^2$ |
|---|---|---|---|---|---|
| | Seawater | 1.00E+10 | Shaken | 0.0062 | 0.8157 |
| | Seawater | 2.00E+10 | Shaken | 0.0059 | 0.2562 |
| | Seawater | 2.47E+10 | Shaken | 0.0066 | 0.7354 |
| Bottle Experiment II | | | | | |
| | Seawater | 1.00E+06 | Stagnant | 0.0050 | 0.7419 |
| | Seawater | 1.00E+07 | Stagnant | 0.0042 | 0.8123 |
| | Seawater | 1.00E+08 | Stagnant | 0.0052 | 0.7515 |
| | | | | | |
| | Seawater | 1.00E+06 | Shaken | 0.0056 | 0.7212 |
| | Seawater | 1.00E+07 | Shaken | 0.0034 | 0.8604 |
| | Seawater | 1.00E+08 | Shaken | 0.0053 | 0.7354 |

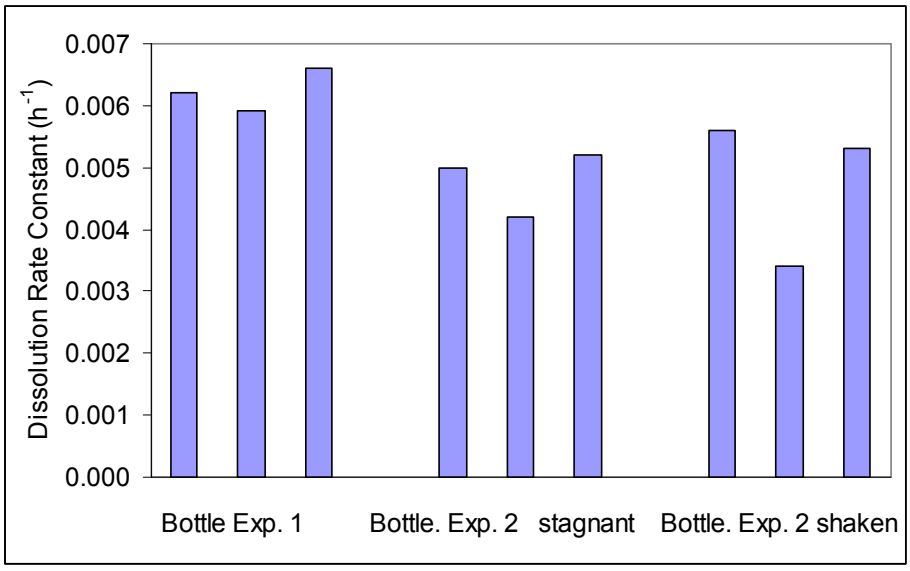


Figure 3.3. Bottle experiments I and II, diatom dissolution in seawater only. The dissolution rate constants were derived from the slope of ln{(Cz-Ct)/Cz}.

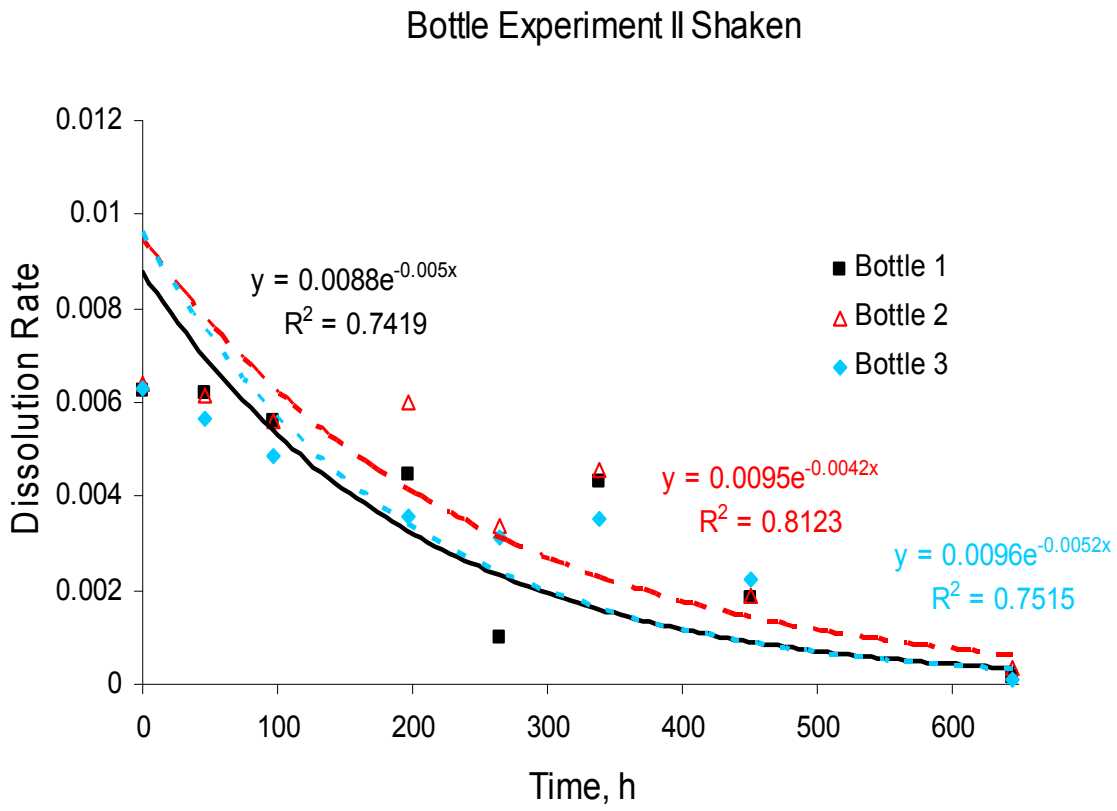


Figure 3.4. Bottle experiment II dissolution rate over time in shaken and stagnant bottles.

Figure 3.4. Continued.

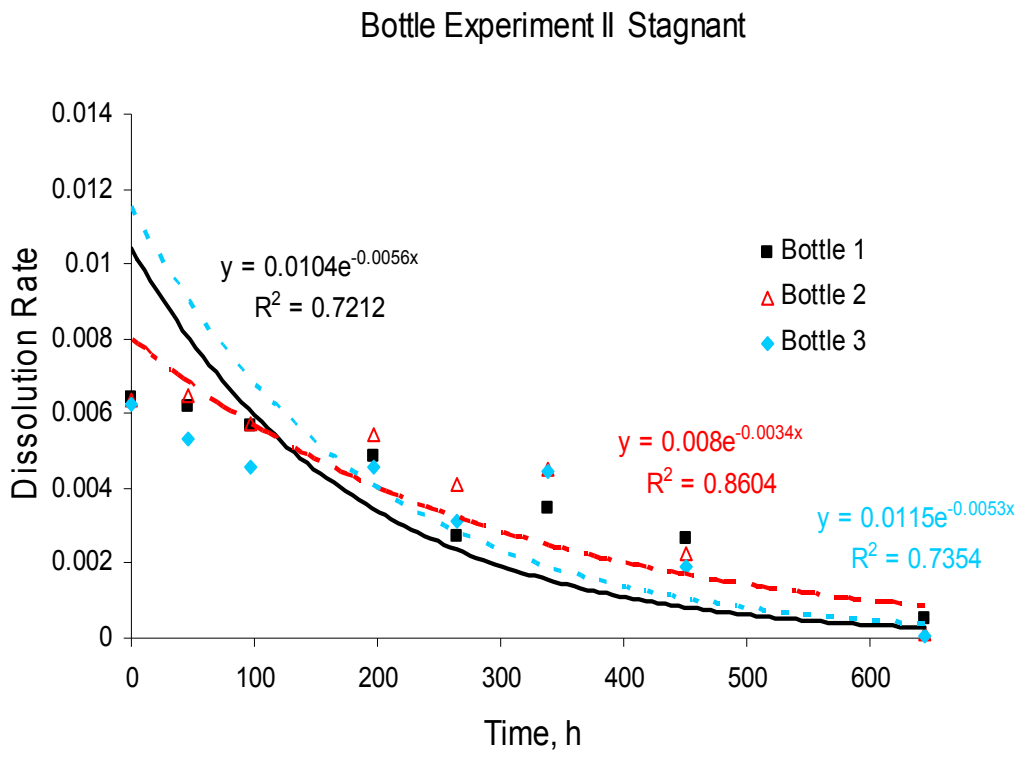


**Reaction-Rate Experiments**

**Reaction-rate experiment I.** In both the live and the sterile columns, no difference was found between the rate of $Si(OH)_4$ released over time in the control versus the experimental. Rate constants were higher in the columns that received diatoms. The rate constants in the controls were 0.0028 and 0.0027, and the rate constants in both the live and the sterile experimental columns was 0.0041 (Table 3.7 and Figure 3.5). There was no significant difference between the rate constants in the controls versus the experimental columns. These rate constants were in the same magnitude as the dissolution-rate experiments I and II.

Table 3.7. Column experiment I dissolution rate constants and $r^2$ values.

| Column Experiment I | | | | | |
|---|---|---|---|---|---|
| Initial Rates | | | | | |
| Column | Characteristics | (Diatom Cells $l^{-1}$ Pore Water) | (ml $h^{-1}$ $cm^{-2}$) | *k* | $r^2$ |
| 1 | Live | 0 | 2 | 0.0028 | 0.9862 |
| 2 | Sterile | 0 | 2 | 0.0027 | 0.9785 |
| 3 | Live | 1.00E+09 | 2 | 0.0041 | 0.9585 |
| 4 | Sterile | 1.00E+09 | 2 | 0.0041 | 0.9568 |

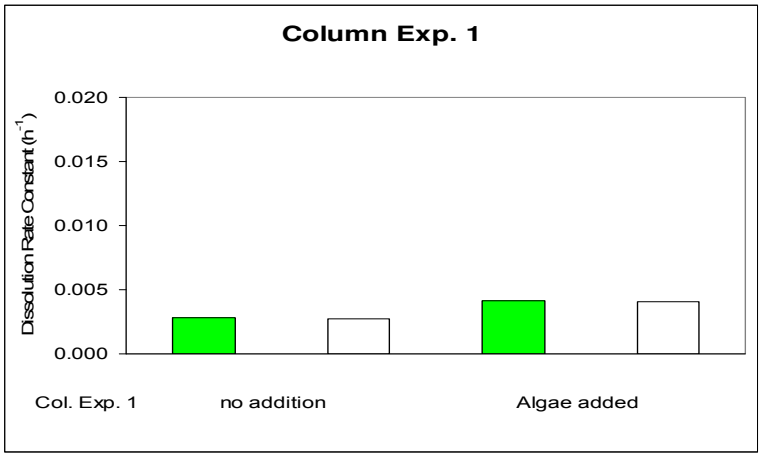


Figure 3.5. Column experiment I: initial and final dissolution rate constants. Dissolution rate constant as determined from the slope of the regression line of ln{(Cz-Ct)/Cz}.

**Reaction-rate experiment II.** Rate constants varied between the initial and the final phases of the experiment. All calculated rate constants were relatively low because large volumes of $Si(OH)_4$ were mobilized in the live columns during the experiment, which masked the effect of the diatom addition. The dissolution rate constant during the final phase of the experiment differed from that in the initial phase. Initial rate constants in the columns with faster pore-water flow were slightly higher than in the columns with slower flow, though they were not significantly different. The final rate constants for all of the columns at all of the flow rates were similar (Table 3.8 and Figure 3.6).

Table 3.8. Column experiment II dissolution rate constants and $r^2$ values.

| Column Experiment II | | | | | |
|---|---|---|---|---|---|
| Initial Rates | Sediment | | | | |
| Column | Characteristics | (Diatom Cells $l^{-1}$ Pore Water) | (ml $h^{-1}$ $cm^{-2}$) | *k* | $r^2$ |
| 1 | Live | 0 | 1 | 0.0010 | 0.9992 |
| 2 | Live | 1.00E+06 | 1 | 0.0010 | 0.9976 |
| 3 | Live | 1.00E+07 | 1 | 0.0015 | 0.9953 |
| 4 | Live | 1.00E+08 | 1 | 0.0015 | 0.9921 |
| | | | | | |
| 5 | Live | 0 | 2 | 0.0034 | 0.9931 |
| 6 | Live | 1.00E+06 | 2 | 0.0036 | 0.9955 |
| Initial Rates Column | Sediment Characteristics | (Diatom Cells $l^{-1}$ Pore Water) | (ml $h^{-1}$ $cm^{-2}$) | *k* | $r^2$ |
| 7 | Live | 1.00E+07 | 2 | 0.0038 | 0.9924 |
| 8 | Live | 1.00E+08 | 2 | 0.0038 | 0.9958 |
| Final Rates | | | | | |
| 1 | Live | 0 | 1 | 0.0020 | 0.9437 |
| 2 | Live | 1.00E+06 | 1 | 0.0020 | 0.9215 |
| 3 | Live | 1.00E+07 | 1 | 0.0020 | 0.9383 |
| 4 | Live | 1.00E+08 | 1 | 0.0020 | 0.9764 |
| | | | | | |
| 5 | Live | 0 | 2 | 0.0019 | 0.9818 |
| 6 | Live | 1.00E+06 | 2 | 0.0020 | 0.9428 |
| 7 | Live | 1.00E+07 | 2 | 0.0020 | 0.9366 |
| 8 | Live | 1.00E+08 | 2 | 0.0019 | 0.9331 |

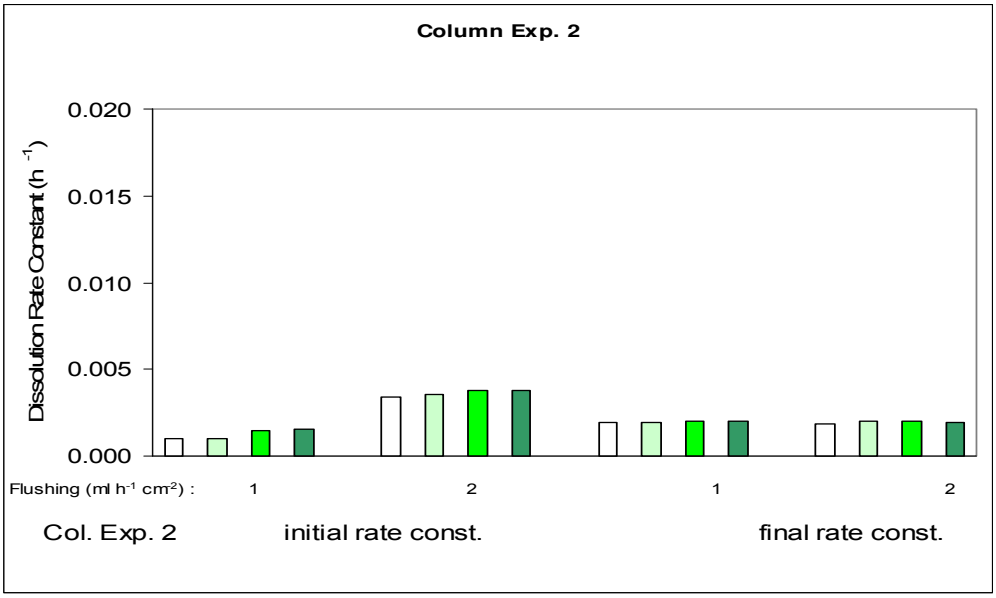


Figure 3.6. Column experiment II $Si(OH)_4$ concentration over time. Dissolution rate constants determined from the slope of the regression line of $\ln\{(Cz-Ct)/(Cz)\}$.

**Reaction-rate experiment III.** In both flow regimes—2.5 cm $h^{-1}$ and 5.0 cm $h^{-1}$—the dissolution rate constants of the experimental columns was significantly ($\alpha = 0.05$) greater than the dissolution rate constants of the control columns (Table 3.9 and Figure 3.7 and 3.8). The dissolution rate constants for the experimental columns were not significantly different (i.e., 0.0144 and 0.0150 for the 2.5 cm $h^{-1}$ and 0.00147 and 0.0149 for the 5.0 cm $h^{-1}$). In the experimental columns, the dissolution rate constants at both velocities were higher than the rates of either bottle-dissolution experiment. Flushing velocity had no significant effect. Opal was removed from all columns prior to the experiment; however, some opal was still present as indicated by the rate constants recorded in the control columns. Two different dissolution rate constants were observed in the amended columns with the change occurring after approximately 100 h.

Table 3.9. Column experiment III dissolution rate over time. Column experiment dissolution rate constants and $r^2$ values.

| Column Experiment III | | | | | |
|---|---|---|---|---|---|
| Initial Rates | Sediment Characteristics | (Diatom Cells $l^{-1}$ Pore Water) | Flow Rate (ml $h^{-1}$ $cm^{-2}$) | *k* | $r^2$ |
| Column No. | | | | | |
| 1 | Opal-Free, Live | 0 | 1 | 0.0054 | 0.9903 |
| 2 | Opal-Free, Live | 0 | 1 | 0.0053 | 0.9853 |
| 3 | Opal-Free, Live | 1.00E+10 | 1 | 0.0144 | 0.9826 |
| 4 | Opal-Free, Live | 1.00E+10 | 1 | 0.0150 | 0.9836 |
| | | | | | |
| 5 | Opal-Free, Live | 0 | 2 | 0.0066 | 0.9842 |
| 6 | Opal-Free, Live | 0 | 2 | 0.0065 | 0.9827 |
| 7 | Opal-Free, Live | 1.00E+10 | 2 | 0.0147 | 0.9859 |
| 8 | Opal-Free, Live | 1.00E+10 | 2 | 0.0149 | 0.9726 |

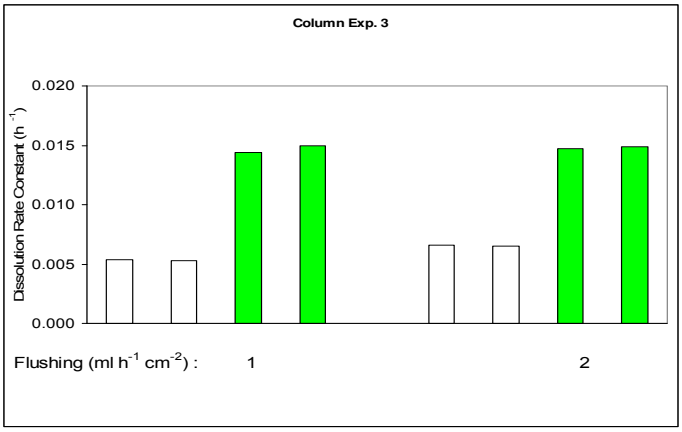


Figure 3.7. Dissolution-rate constant calculated for column experiment III.

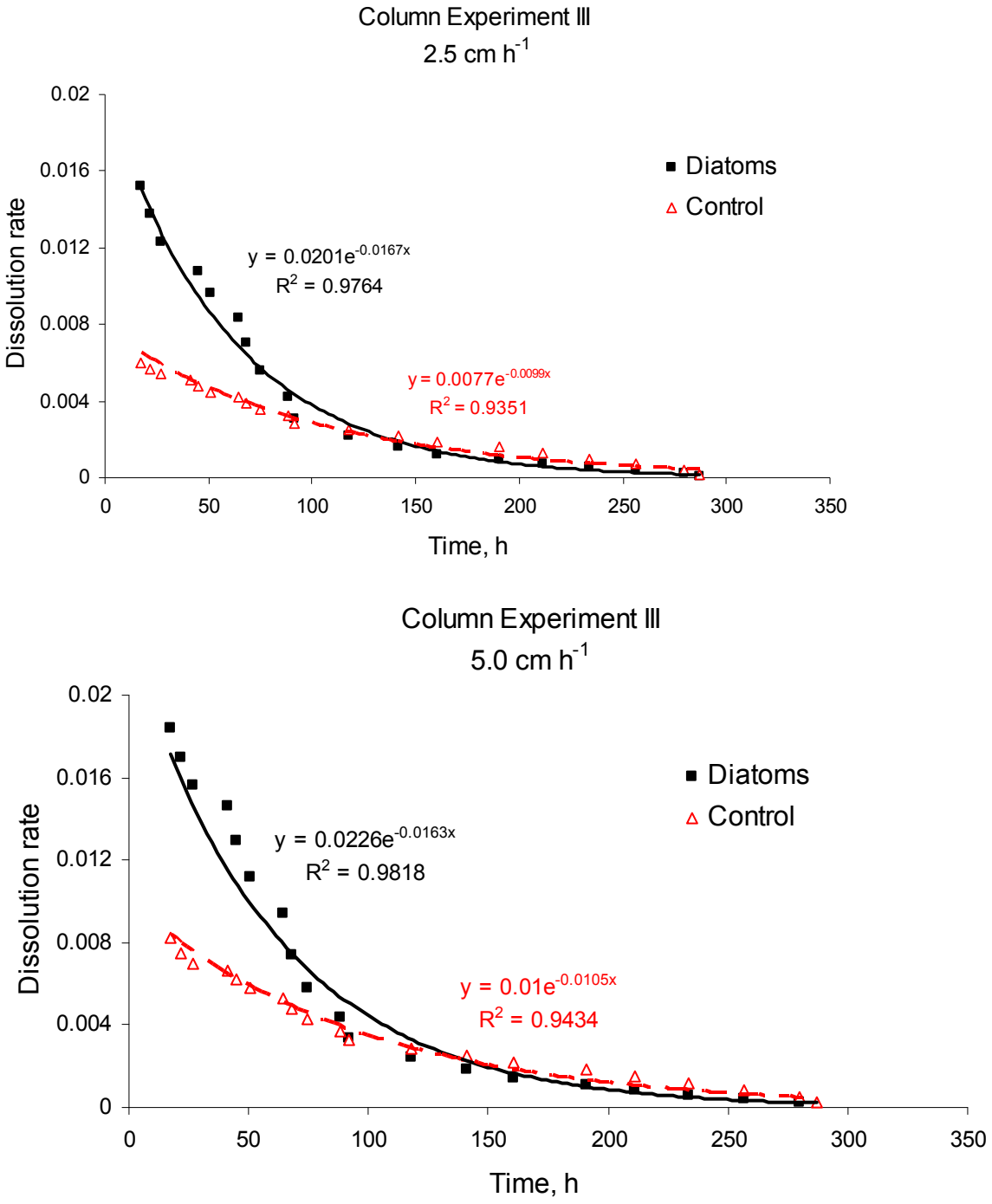


Figure 3.8. Dissolution rates of opal in the columns of experiment III. The curves from the amended columns (black squares) indicate the two different dissolution rate constants before and after approximately 100 h. The curves shown model the entire data series and do not take into account of the change in slope.

**Reaction-rate experiment IV.** In both flow regimes—2.5 cm $h^{-1}$ and 5.0 cm $h^{-1}$—the dissolution rate constants were significantly ($\alpha$=0.05) greater for the experimental columns than the control columns (Table 3.10 and Figure 3.9 and 3.11). Flushing velocity had no significant effect as was found in column experiment III, on the rate constants.

Table 3.10. Column experiment IV dissolution rate constants and $R^2$ values.

| Column Experiment IV | | | | | |
|---|---|---|---|---|---|
| Initial Rates | Sediment Characteristics | (Diatom Cells $l^{-1}$ Pore Water) | Flow Rate (ml $h^{-1}$ $cm^{-2}$) | *k* | $r^2$ |
| Column No. | | | | | |
| 1 | Opal-Free, Live | 0 | 1 | 0.0038 | 0.9912 |
| 2 | Opal-Free, Live | 0 | 1 | 0.0040 | 0.9882 |
| 3 | Opal-Free, Live | 1.00E+10 | 1 | 0.0111 | 0.9862 |
| 4 | Opal-Free, Live | 1.00E+10 | 1 | 0.0111 | 0.9783 |
| | | | | | |
| 5 | Opal-Free, Live | 0 | 2 | 0.0057 | 0.9846 |
| 6 | Opal-Free, Live | 0 | 2 | 0.0033 | 0.9841 |
| 7 | Opal-Free, Live | 1.00E+10 | 2 | 0.0114 | 0.9884 |
| 8 | Opal-Free, Live | 1.00E+10 | 2 | 0.0114 | 0.9772 |

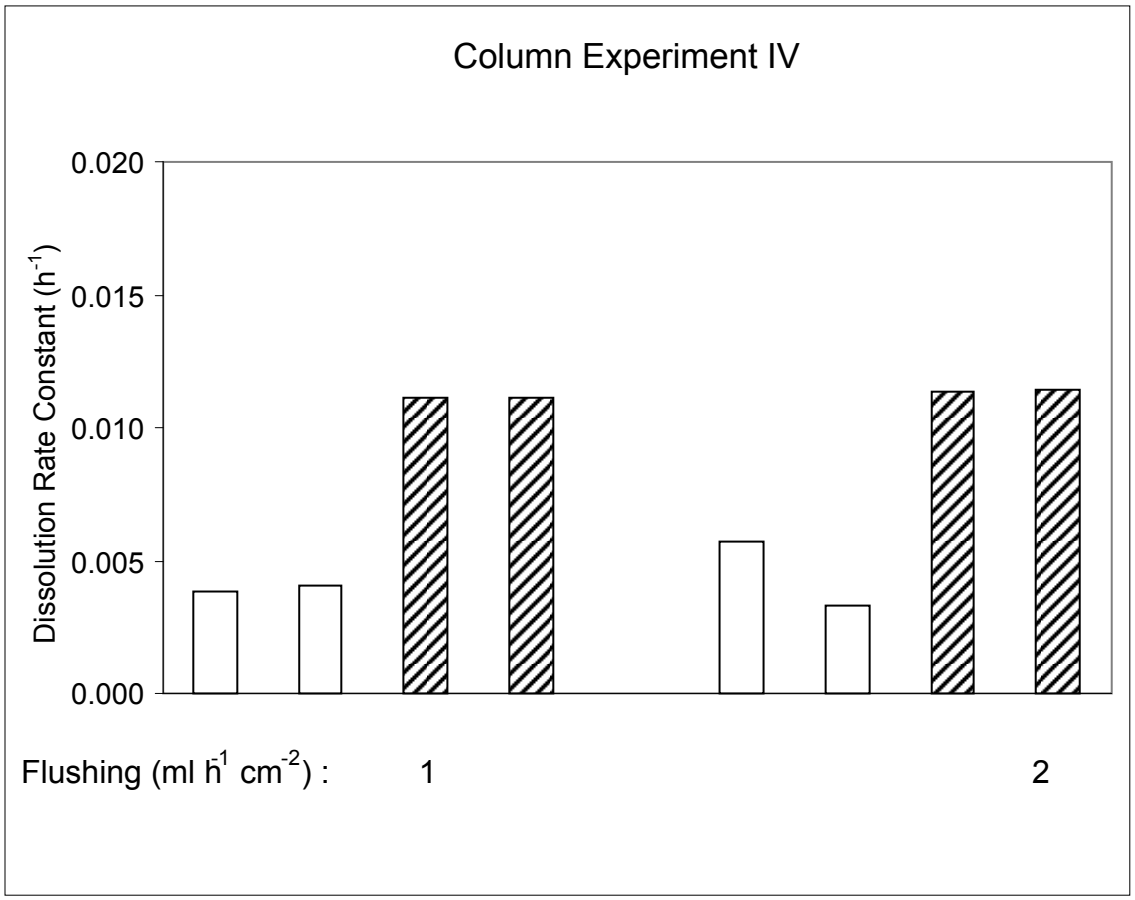

Figure 3.9. Dissolution rate constants calculated for column experiment IV with cleaned diatom frustules.

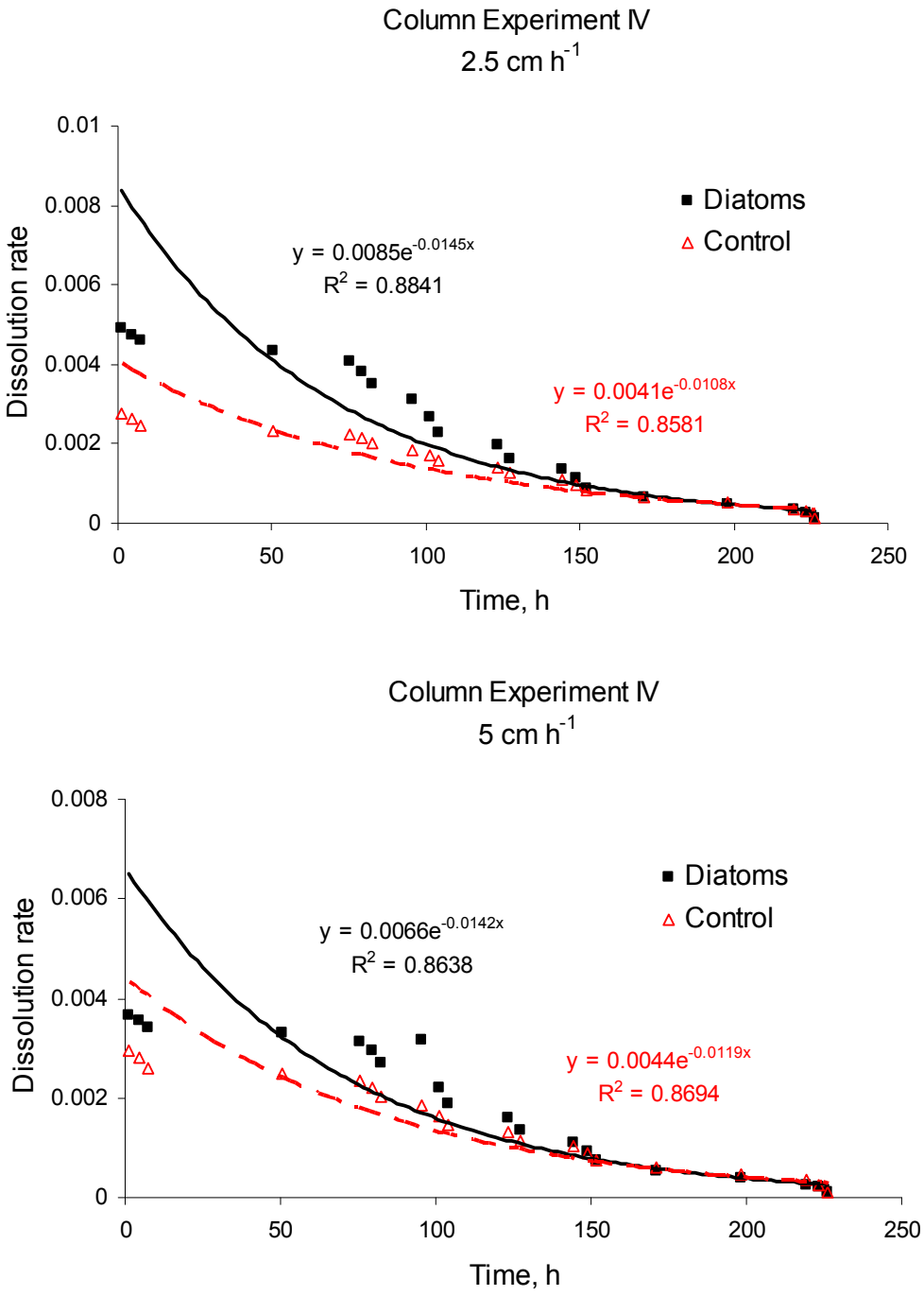


Figure 3.10. Dissolution rates of opal in column experiment IV.

**Reaction-rate experiment V.** The dissolution rate constants were the same regardless of flow regime or diatom concentration (Table 3.11 and Figure 3.11, 3.12, and 3.13).

Table 3.11. Coil experiment (reaction-rate experiment V) dissolution rate over time**.**

| Coil Experiment Initial Rates | | | | | |
|---|---|---|---|---|---|
| Coil No. | Sediment Characteristics | (Diatom Frustules $l^{-1}$ water) | Flow Rate | *k* | $r^2$ |
| 1 | Water | 0 | 1 | 0.0054 | 0.9690 |
| 2 | Water | 0 | 1 | 0.0058 | 0.9759 |
| 3 | Water | 1.00E+10 | 1 | 0.0070 | 0.9292 |
| 4 | Water | 1.00E+10 | 1 | 0.0086 | 0.9022 |
| | | | | | |
| 5 | Water | 0 | 2 | 0.0054 | 0.9723 |
| 6 | Water | 0 | 2 | 0.0052 | 0.9791 |
| 7 | Water | 1.00E+10 | 2 | 0.0088 | 0.9456 |
| 8 | Water | 1.00E+10 | 2 | 0.0082 | 0.9707 |

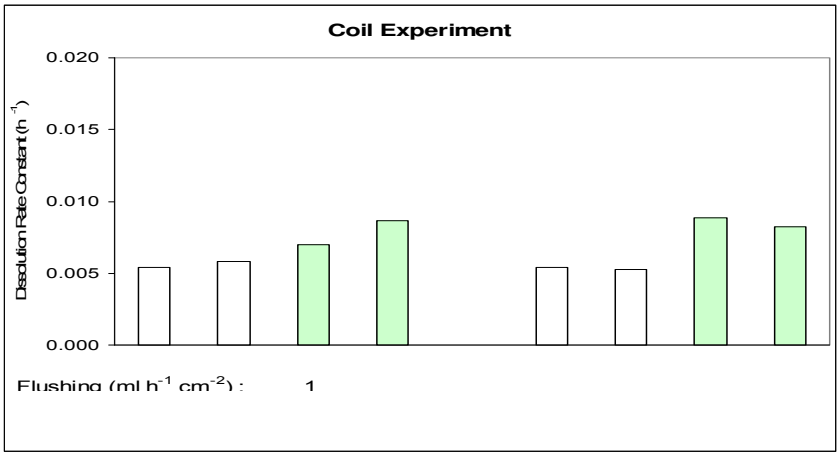


Figure 3.11. Dissolution rate constants calculated for the coil experiment (reaction-rate experiment V) with digested diatoms.

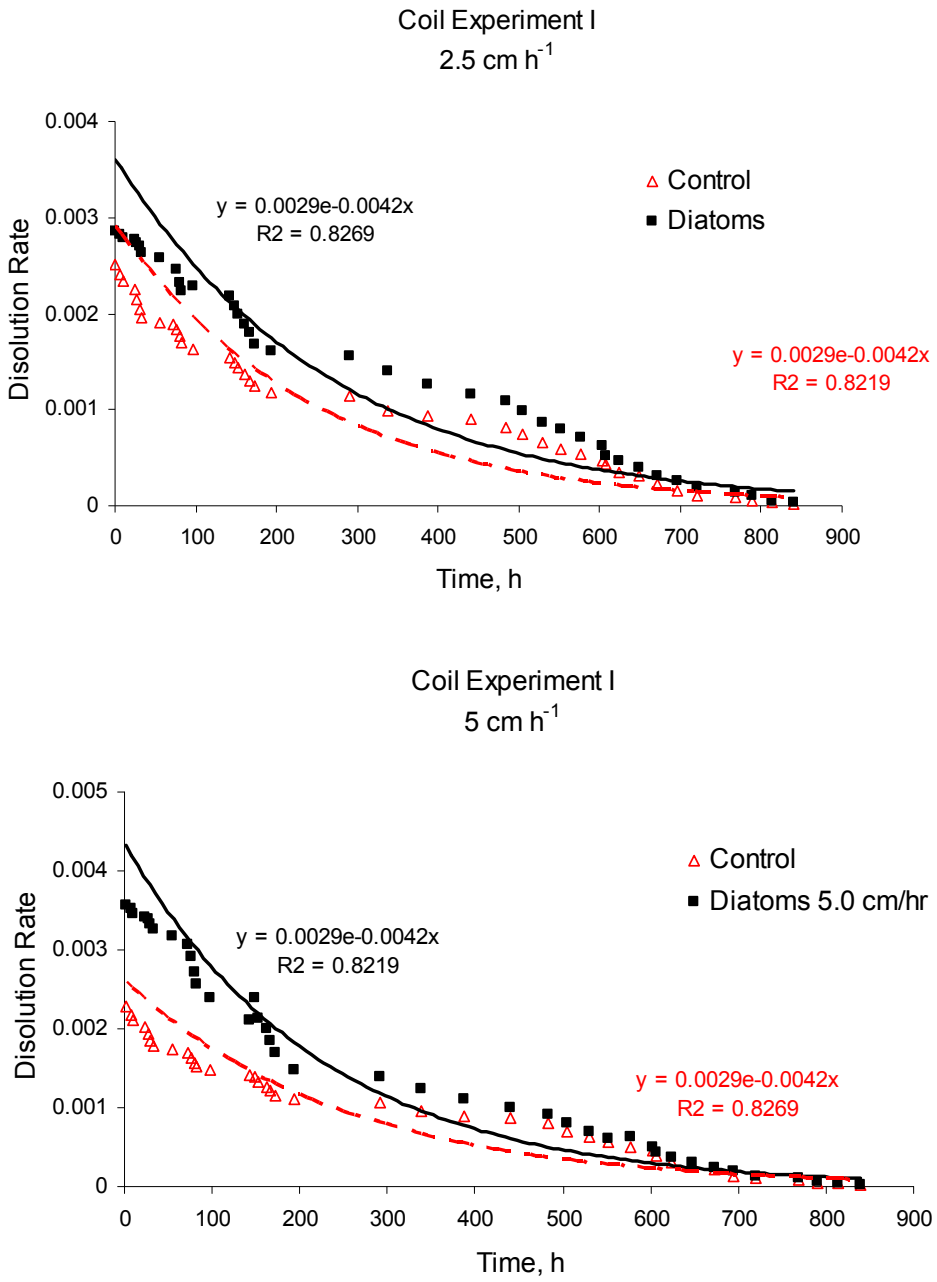


Figure 3.12. Coil experiment 1 dissolution rate over time.

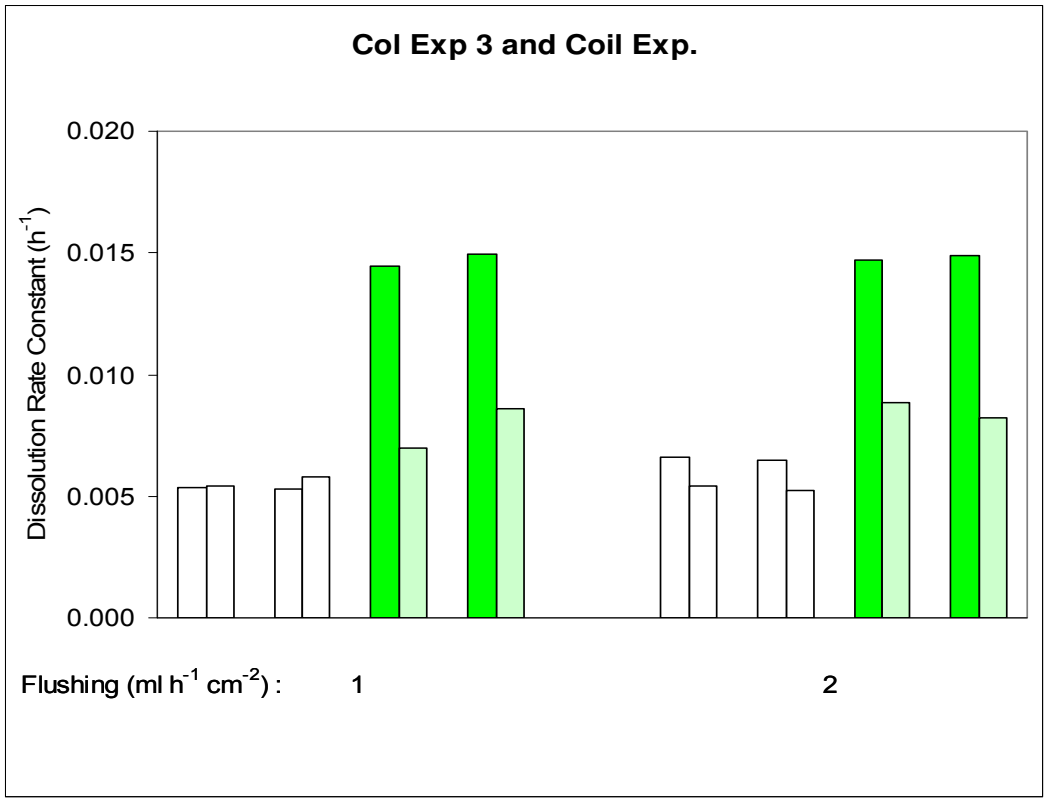

Figure 3.13. Dissolution rate constants from column experiment III (left columns) and the coil experiment (right columns).

## Discussion

### $BSiO_2$ Dissolution Kinetics

The most frequently used rate expression for $bSiO_2$ dissolution is a first-order kinetic law. According to this law, the rate depends linearly on the degree of undersaturation of the solution (Van Cappellen and Qiu, 1997b). The linear rate law has been reported to fit the $Si(OH)_4$ versus time measured in batch dissolution experiments (Hurd, 1973; Kamatani and Riley, 1979). Most dissolution-rate experiments have been based on batch experiments, and few studies have been conducted using flow-through reactors (Van Cappellen and Qui 1997 a, b). The first-order kinetic rate law, however, cannot explain results produced in the mixed-flow through reactors (Rickert et al., 2002). Studies using flow-through reactors have revealed that under very high degrees of undersaturation the dissolution kinetics switch from a linear dependence on the degree of undersaturation to an exponential dependence (Van Cappellen and Qiu, 1997b; Rickert, 2000).

**Effect of Flow Rates on $BSiO_2$ Dissolution**

Van Cappellen and Qiu (1997 a, b) were the first to conduct flow-through experiments to study the thermodynamics of $bSiO_2$ dissolution in deep-sea sediments from the Southern Ocean. Gallinari et al. (2002) used flow-through reactors to study other deep-sea settings. Dixit et al. (2001) also used flow-through reactors. In fact, the reaction-rate experiments conducted in this study were similar to those conducted in Dixit et al.'s work. However, the speeds used in Dixit et al.'s work were slower than those used in this study. They pumped solutions of a known composition through reactors using a peristaltic pump with controlled flow rates ranging from 1 to 10 ml $h^{-1}$, whereas speeds of 25 ml $h^{-1}$ and 50 ml $h^{-1}$ were used in this study.

According to Rickert et al. (2002), flow rates play a significant role in determining reaction rates in flow-through studies, and the reaction rate is directly proportional to the flow rate. The experimental columns in the third and fourth reaction-rate experiments showed larger rate constants than those seen in the bottle experiments. These larger rate constants may be attributed to the fact that the columns were exposed to speeds of 2.5 cm $h^{-1}$ and 5.0 cm $h^{-1}$, while the bottles were either kept stagnant or shaken producing water velocities assumed to be less than ~0.2 cm $h^{-1}$. This finding supports the working hypothesis that pore-water flows enhance the dissolution rate of $bSiO_2$. However, the rate constants were not significantly greater in the 5.0 cm $h^{-1}$ columns than in the 2.5 cm $h^{-1}$ columns. This finding suggests that these speeds were too similar to see a significant increase in dissolution rate with increase in flow rates. The largest increase in dissolution rate is expected to occur at the transition from stagnant to low flow conditions as the onset of flow reduces the thickness of the diffusive-boundary layer (DBL) around the frustules and removes diffusive gradients.

The findings presented above disagree with Kamatani and Riley (1979), who stated that dissolution rate in sediments appeared to be slow. The rate constants for both bottle experiments, which simulated the water column, and those observed in the coil experiment were lower than those observed in column experiments III and IV. Thus, the null hypothesis that flow has no effect on diatom dissolution can be rejected, and these findings suggest that diatoms degrade in permeable sediments faster than in the water column due to higher microbial activities and flushing rates. However, this applies to the dissolution of fresh diatoms in sands. $Si(OH)_4$ frustules are biogeochemically altered in fine-grained sediment through various means such as association with clay minerals. As a result, frustule dissolution rates can decrease dramatically

resulting in preservation of diatoms in marine deposits (Dixit et al., 2001; Rickert et al., 2002; Van Cappellen et al., 2002).

The increase in dissolution rates seen in column experiment III agrees with the findings of Rickert et al. (2002). In the water column, as represented by the coil experiment, the dissolution rates showed small variation. Some opal was still present in the sediment of these two experiments of the controls as indicated by the dissolution curves. These results demonstrate that the dissolution rate in percolated sands exceeds the rates in water when the same water volume and water discharge ratios are maintained for sand-filled and water-only filled columns.

**Effect of Sediment Combustion on $BSiO_2$ Dissolution**

In the first column experiment, the background $bSiO_2$ concentration was too high to measure differences in concentration due to dissolution rate differences in treatment and control columns. However, the columns filled with combusted sand produced an interesting finding. The concentrations in these columns were much greater than the concentrations measured in both the control and experimental columns filled with natural sediment. Combustion may enhance the dissolution of $Si(OH)_4$ in the sand either by removing the organic coating from diatom frustules or by affecting the surface of the sand grains resulting in enhanced $Si(OH)_4$ dissolution. Further research should be conducted to clarify this process. Kamatani and Oku (2000) noted that $Si(OH)_4$ dissolved from non-$bSiO_2$ compounds in sediment samples complicates the determination of $bSiO_2$ in marine sediments and suspended matter.

**Effect of Organic Coating on $BSiO_2$ Dissolution**

In the third and fourth column experiments, the rate constants were higher in the experimental columns, the columns with diatoms, than in the control columns. However, flushing velocity did not have a significant effect in either experiment ($\alpha = 0.05$). Furthermore, the rate constants in the columns with the cleaned diatoms were not significantly different than the columns with the uncleaned diatoms. This finding contradicted the findings of Bidle and Azam (1999). Their study revealed that in the presence of bacterial activities, four to seven times more $Si(OH)_4$ were dissolved during a 21-day incubation with fresh diatoms compared to abiotic controls. On the other hand, these findings presented in this paper may be explained by the work of Kamatani and Oku (2000). They digested two types of diatoms—*Skeletonema costatum* and *Rhizosolenia hebetata* forma spina—thoroughly in $HNO_3$ and $H_2O_2$ to remove

organic matter as was done to the cleaned diatoms used in the experiments conducted in this paper. In their study, the uncleaned diatoms showed similar-shaped dissolution curves with those of the pre-treated diatom silica walls. Kamatani and Oku (2000) postulated that the organic-matter coating is not a protective barrier against $bSiO_2$ dissolution. Instead, it was hydrolyzed and broken down at an early stage when digested in the alkaline solution at high temperature that, in turn, enhanced the $bSiO_2$ dissolution.

While increases in flow can cause increased dissolution, the removal of the organic coating does not significantly affect dissolution rate. Rickert et al. (2002) found that organic coatings are primarily important in the water column, while inorganic, or detrital, coatings are important in sediments. This conclusion may explain the findings in this study and in Kamatani and Oku's (2000) study because in both cases the organic coatings were removed, and the $bSiO_2$ dissolution in sediments was studied. Further research may need to be conducted to determine the effects of removal of the inorganic coating on the dissolution in the sediment.

**Literature Comparison**

The dissolution rate constants calculated in this study are within the same order of magnitude as those published in Truesdale et al. (2005). Their values were 0.0042 (±0.0003) at 43 µM silica loading, 0.0041 (±0.0003) at 62 µM silica loading, and 0.0036 (±0.0001) at 120 µM silica loading. These findings also show that increased concentrations may result in lower rate constants.

**$BSiO_2$ Dissolution in Water Column versus Sediments**

With Si isotopic tracers, silica dissolution rates have been measured directly in ocean surface water. The results indicate high specific dissolution rates, typically on the order of 10-100 $yr^{-1}$. In sediments, dissolution rates have been thought of as slow because of various factors including small fluxes of interstitial water and metal ion adsorption of silica walls (Kamatani and Riley, 1979). Rates in deep-sea sediments have been derived mainly from fitting transport-reaction models to pore-water depth profiles of $Si(OH)_4$. While these rates are highly variable, they are often orders of magnitude lower than in surface waters (<0.5 $yr^{-1}$) (Van Cappellen et al., 2002). In the case of these deep-sea sediments, Kamatani and Riley's statement may be correct; however, in permeable sediments, which are characterized by rapid flushing of interstitial waters and frequent resuspension that removes organic particles and relatively fresh diatoms embedded in the surface layer, the dissolution rates are not slow. In deep-sea sediments, the temperatures

are colder and the interstitial waters are less undersaturated; therefore, dissolution rates are lower (Van Cappellen et al., 2002), which also allows reaction of metal ions and clay minerals with the frustules further reducing their dissolution.

Overall, variations in dissolution kinetics are not fully understood, and this lack of understanding is a major source of uncertainty in models of nutrient Si cycling in the world's oceans (Van Cappellen et al., 2002). Results from this study may shed light on new areas of research in order to fully understand this complicated subject.

**Factors Affecting $BSiO_2$ Dissolution Rate**

The dissolution kinetics of $bSiO_2$ are influenced by the physical-chemical conditions in the fluid immediately surrounding the frustule surface. These conditions include temperature, saturation state, pH, background electrolyte composition, and concentrations of adsorbing solutes (Van Cappellen et al., 2002). Specific surface area, impurity content, and aging of the silica also have an affect. Pressure also affects the dissolution rate via its effect on silica solubility (Dixit et al., 2001).

Passow et al. (2003) investigated $bSiO_2$ dissolution rates of aggregated diatom cells. Their findings indicated that aggregated cells have lower dissolution rates when compared to dispersed cells. They based these findings on the fact that concentration of dispersed diatoms decreased over the course of the experiment, whereas the concentration of aggregated cells remained roughly the same. Further research should be conducted to better understand the role of aggregation on $bSiO_2$ dissolution rates. In this study, single *T. weissflogii* cells were used; however, in future experiments, chain-forming diatoms may be studied. Passow et al.'s finding may also have important implications in instances of $bSiO_2$ dissolution following diatom blooms.

Dissolution rate varies from one species to another and from one portion to another of the same frustule (Kamatani and Riley, 1979). Delicate parts of frustules dissolve quickly in surface waters, where high temperature and low $Si(OH)_4$ concentrations accelerate the dissolution rate. Thicker portions dissolve slowly in deeper layers where temperature is low. Grazing may also enhance dissolution as a result of physical and chemical changes to the frustule (Greenwood et al., 2001).

Diatom incorporation of aluminum can affect the dissolution rate. During the biomineralization process, diatoms can incorporate aluminum (Al) into their silica matrices. Al can also be incorporated after the death of these organisms. Incorporation of Al can increase the

preservation efficiency of $bSiO_2$ in marine sediments (Van Cappellen et al., 2002). Open-ocean waters often have very low ambient dissolved Al levels; therefore, diatoms in these environments produce opal with very low Al/Si ratios (Van Bennekom et al., 1991).

# CHAPTER 4
# FLUX CHAMBER INVESTIGATIONS

## Introduction

Chapter 2's findings indicate that diatoms accumulate in ripple troughs and slopes, and Chapter 4's findings illustrate that $bSiO_2$ dissolution occurs faster in the sediment than in the water column. In the natural environment, settling diatoms accumulate at the sediment-water interface, and benthic diatoms add to the $bSiO_2$ concentration at the sediment surface where light reaches the seabed. This chapter investigates whether water flows through the deposited diatom layer on permeable-nearshore sand sediment, and if so, does the ensuing pore-water flow increase degradation rates in the permeable sediments? The working hypothesis was that permeable sediments permit flushing of the upper sediment layers, and this flushing enhances the degradation rate of organic matter thereby mobilizing $Si(OH)_4$. Furthermore, it was tested whether with increasing advective pore-water flows, more $Si(OH)_4$ is released from permeable sediments. To answer these questions, chamber experiments were conducted in the laboratory and in the Gulf of Mexico at the selected field sites.

## Methods

### Fluorescein Advection-Chamber Experiment

**Purpose.** This experiment was conducted to determine the rates of advective pore-water exchange in the permeable sediments from the exposed field sites for differential pressure settings that are typical for the shallow Gulf of Mexico.

**Experimental set-up.** Sediment was collected from the Gulf field site on St. George Island and allowed to equilibrate in the laboratory for approximately 30 d. This waiting period allowed labile organic matter to degrade as the degradation of dying organisms in the sediment could reduce permeability due to microbial mucus production. The sediment was sieved and homogenized. Sieving removed living macrofauna, larger shells, and large pieces of organic matter that could cause artifacts in the pore-water flow measurements. Homogenization established the same sedimentary conditions in all chambers with sediment and is similar to the

homogenization that takes place in the natural environment during periods of stormy weather that mix the upper 20 cm of the shallow seabed.

Chambers were filled with sediment to similar levels, and then artificial seawater made from sodium chloride (NaCl) and deionized water (S = 32 ppt) was added to the levels reported in Table 4.1. Twelve chambers and two polypropylene containers were used in the experimental set-up. While filling the chambers with sediment, special care was taken not to entrap any bubbles in the sediment. In the stirred chambers, stirring was set at 60 rpm to generate sub-erosion velocity and a pressure gradient of 0.7 Pa $cm^{-1}$ at the sediment-water interface. Fluorescein ($C_{20}H_{10}Na_2O_5$), an inert tracer dye, was added to the chambers to a concentration of approximately 100 μM, which produced an absorbance of ~0.500 at a wavelength (λ) of 515 nm.

Table 4.1. Fluorescein advection-chamber experiment set up.

| Chamber No. | Sediment/No Sediment | Stirred (60 rpm)/Stagnant | Average Sediment Height (cm) | Water Height (cm) |
|---|---|---|---|---|
| 1 | No Sediment | Stirred | n/a | 31.43 |
| 2 | No Sediment | Stirred | n/a | 31.11 |
| 3 | Sediment | Stirred | 20.50 | 10.64 |
| 4 | Sediment | Stirred | 20.00 | 11.43 |
| 5 | Sediment | Stirred | 19.84 | 10.95 |
| 6 | Sediment | Stirred | 19.68 | 10.95 |
| 7 | No Sediment | Bubbled (No Lid) | n/a | 34.13 |
| 8 | No Sediment | Bubbled (No Lid) | n/a | 34.77 |
| 9 | No Sediment | Stagnant (Closed) | n/a | 33.66 |
| 10 | No Sediment | Stagnant (Closed) | n/a | 33.66 |
| 11 | No Sediment | Stagnant (Closed) | n/a | 33.02 |
| 12 | No Sediment | Stagnant (Closed) | n/a | 35.56 |
| 13 | Sediment | Stagnant (Closed) | 20.96 | 12.07 |
| 14 | Sediment | Stagnant (Closed) | 20.96 | 12.70 |
| 15 | Ambient Trough | Stagnant (Closed) | n/a | 35.56 |

**Sampling procedure.** This experiment was carried out in October 2005. The first water samples were taken from the chambers immediately after addition and mixing of the dye. Samples were stored in the dark and measured as soon as possible. Samples were taken from the individual chambers and the trough at set intervals the first day and in the morning, the afternoon, and the evening on the following day. Table 4.2 shows the sampling times.

Table 4.2. Fluorescein advection-chamber experiment sample times.

| Sampling | Date | Total Time (h) |
|---|---|---|
| 0 | 10/15/2005 | 0.00 |
| 1 | 10/15/2005 | 0.25 |
| 2 | 10/15/2005 | 0.50 |
| 3 | 10/15/2005 | 0.75 |
| 4 | 10/15/2005 | 1.00 |
| 5 | 10/15/2005 | 3.42 |
| 6 | 10/15/2005 | 4.42 |
| 7 | 10/15/2005 | 5.42 |
| 8 | 10/15/2005 | 6.42 |
| 9 | 10/15/2005 | 7.42 |
| 10 | 10/15/2005 | 8.42 |
| 11 | 10/16/2005 | 18.75 |
| 12 | 10/16/2005 | 22.25 |

**Sampling analysis.** A spectrophotometer was used to measure the absorbance of the samples. The samples were kept in the dark until they were measured.

**Data analysis.** Using a calibration line, the fluorescein concentrations in the chambers were calculated. Then changes in concentration over time were calculated from the concentration measurements, and the corresponding dilution volumes were calculated (i.e., how much water without dye would have to be added to cause observed concentration decreases). Pore-water fluxes in the chambers with sediment were calculated by subtracting the corresponding dilution volume recorded in the stagnant control chambers from those of the stirred chambers.

**Field Work**

In order to assess whether the findings from the laboratory studies were applicable and relevant to natural settings, in-situ chamber experiments and time series studies of water and sedimentary nutrient dynamics were conducted at the two study sites on St. George Island.

**Chamber time series.** In February (winter), May (spring), August (summer), and December (fall) of 2006, seasonal in situ benthic chamber field experiments were conducted at both sites in order to understand the complex interactions between boundary flow, sediment filtration, and microbial mineralization. The chambers measured the nutrient fluxes between the sediment and the overlying water.

**Benthic advection chambers.** The chambers were made of acrylic cylinders of 30-cm height and 19-cm ID (Fig. 4.1). The chambers were closed on one end by a transparent lid. A rotating disc mounted in the lid of the chamber sets the water column in the chamber into a circular motion, which creates a radial pressure gradient with high pressure close to the chamber wall and low pressure in the center of the enclosed sediment surface. By adjusting the rotation of the disc, the pressure gradient can be set to a magnitude that corresponds to that outside the chamber. The pressure gradients, which typically reach 0.1 to 2 Pa $cm^{-1}$, can be calculated from the dimensions of the topographical elements and the boundary-layer flow velocity (Shum, 1992; Huettel and Rusch, 2000). The pressure gradient in the chamber causes advective pore-water exchange when the sediment is permeable (i.e., $k>10^{-11}m^2$). For the flux studies, three transparent chambers that permitted photosynthesis within the chambers, and three opaque chambers that prevented photosynthesis were deployed at the respective study sites. In each set of chambers, the first chamber was set to a low differential pressure setting (~0.1 Pa $cm^{-1}$), the second to a medium differential pressure setting (0.3-0.5 Pa $cm^{-1}$), and the third to a relatively high differential pressure setting (1.0-1.8 Pa $cm^{-1}$). With these settings, the three chambers covered most of the natural differential pressure ranges active at the study sites though occasional storms likely caused higher differential pressures at the sediment-water interface.

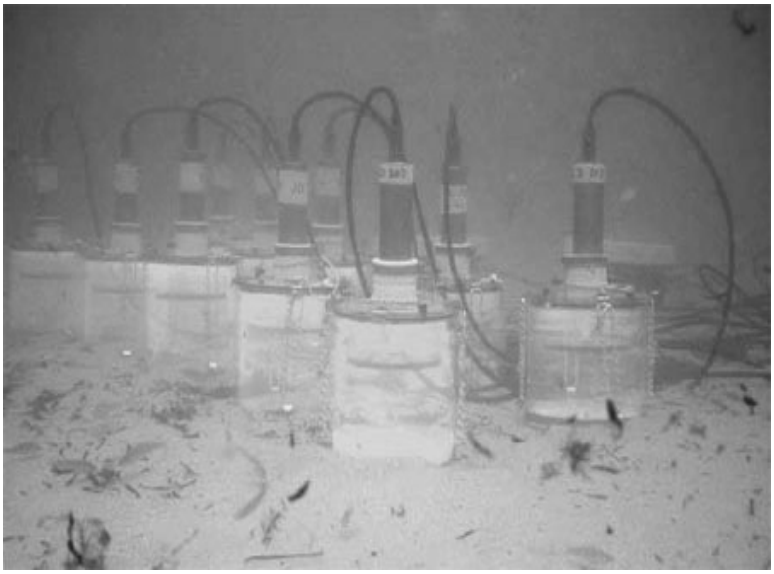

Figure 4.1. Benthic advection chambers. Photo courtesy of Dr. Markus Huettel.

**Water sampling and analysis.** Samples from the chambers and the overlying water column were collected with 140-ml syringes, filled in vials, and stored on ice or preserved with hydrochloric acid (HCl) or mercuric chloride ($HgCl_2$) until analysis. Samples for oxygen were analyzed using the Winkler titration method. Samples for inorganic nutrients nitrite ($NO_2^-$), nitrate ($NO_3^-$), ammonia ($NH_4^+$), dissolved inorganic silicate ($Si(OH)_4$ or DIS) and dissolved inorganic phosphate ($PO_4^{3-}$ or DIP) were collected and analyzed according to the methods of Grasshoff et al. (1983). For the purpose of this thesis, the $Si(OH)_4$ results will be focused on, and $NO_3^-$ will not be addressed because of uncertainty in the accuracy of the measurements. Chlorophyll samples were collected and analyzed according to Parsons et al. (1984).

## Results

### Fluorescein advection-chamber experiment

The stirred chambers without sediment showed a small decrease in fluorescein concentration over time, similar to that measured in the chambers with sediment but without stirring. To achieve the measured drop in concentration, 230-400 ml of chamber water would need to be exchanged by water without tracer in the respective chambers. In contrast, the stirred chambers with sediment showed higher changes in concentration over time corresponding to water exchange of 930 ± 180 ml. Dye concentration decreases in the stirred chambers with sediment exceeded those of the diffusion-governed chambers with sediment by a factor of 2.4

(Figure 4.2). By subtracting the dye loss in the chambers without sediment from that in the chambers with sediment and taking the experiment duration into account, the flux of unstained pore water in the stirred chambers with the sediment were determined and amounted to 457 ± 262 L $m^{-2}$ $d^{-1}$.

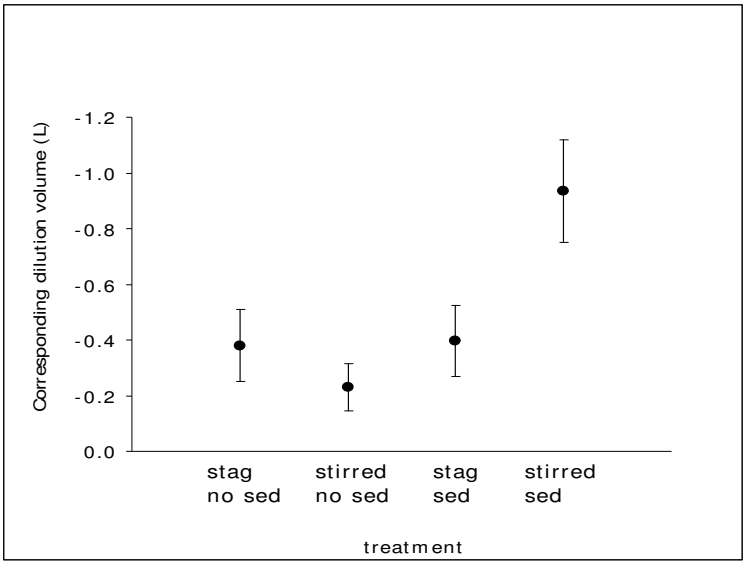

Figure 4.2. Fluorescein-advection chamber experiment results.

**Chamber Time Series**

**Gulf sediment.** $Si(OH)_4$ fluxes in the light and dark sediment chambers followed the same temporal patterns. However, in winter and spring, fluxes in the dark chambers were an order of magnitude higher than in the light chambers. The dark chamber fluxes were also higher than the light chamber fluxes for all samplings with the exception of the fall sampling, where the light chamber flux was slightly higher (0.10 mmol $m^{-2}$ $d^{-1}$ versus -0.25 mmol $m^{-2}$ $d^{-1}$). In both chambers, the fluxes were highest during the winter sampling with values of 4.91 mmol $m^{-2}$ $d^{-1}$ and 0.12 mmol $m^{-2}$ $d^{-1}$ for the dark and light chambers, respectively. The fluxes showed a downward trend winter through summer and an upward trend from summer to fall. $Si(OH)_4$, $NO_2^-$, $PO_4^{3-}$, fluxes in light and dark chambers followed similar seasonal patterns. The largest $NO_2^-$ flux in the dark chamber was in winter (0.11 mmol $m^{-2}$ $d^{-1}$), and the largest flux in the light chambers was 0.08 mmol $m^{-2}$ $d^{-1}$ in the fall. $NH_4^+$ fluxes did not follow the same seasonal patterns as $NO_2^-$, $PO_4^{3-}$, and $Si(OH)_4$. In the light chambers, $NH_4^+$ peak fluxes occurred in winter (0.65 mmol $m^{-2}$ $d^{-1}$), and the highest flux in the dark chamber was in fall (0.82 mmol $m^{-2}$ $d^{-1}$).

Unlike $NO_2^-$ and $Si(OH)_4$, $PO_4^{3-}$ fluxes were consistently higher in the light chambers with the exception of the fall sampling when the fluxes were nearly the same. In both treatments, the largest $PO_4^{3-}$ flux was in winter (0.04 mmol $m^{-2}$ $d^{-1}$ and 0.23 mmol $m^{-2}$ $d^{-1}$ for the light and dark chambers, respectively) (Figure 4.3).

**Gulf water column.** $Si(OH)_4$ fluxes in the water column, i.e., consumption or release of Si calculated for the average water column height, in both the dark and the light treatments (water only filled chamber and dark incubation bottle) increased throughout the year from winter to fall. Fluxes in both treatments increased from winter to fall, and they were of the same magnitude throughout the year, and in summer and fall, the fluxes were the same. $NO_2^-$ fluxes in the water column were orders of magnitude smaller than fluxes observed in the sediment. The seasonal fluxes in $NH_4^+$ and $PO_4^{3-}$ changes in the water column were small compared to the other measured nutrients (Figure 4.3).

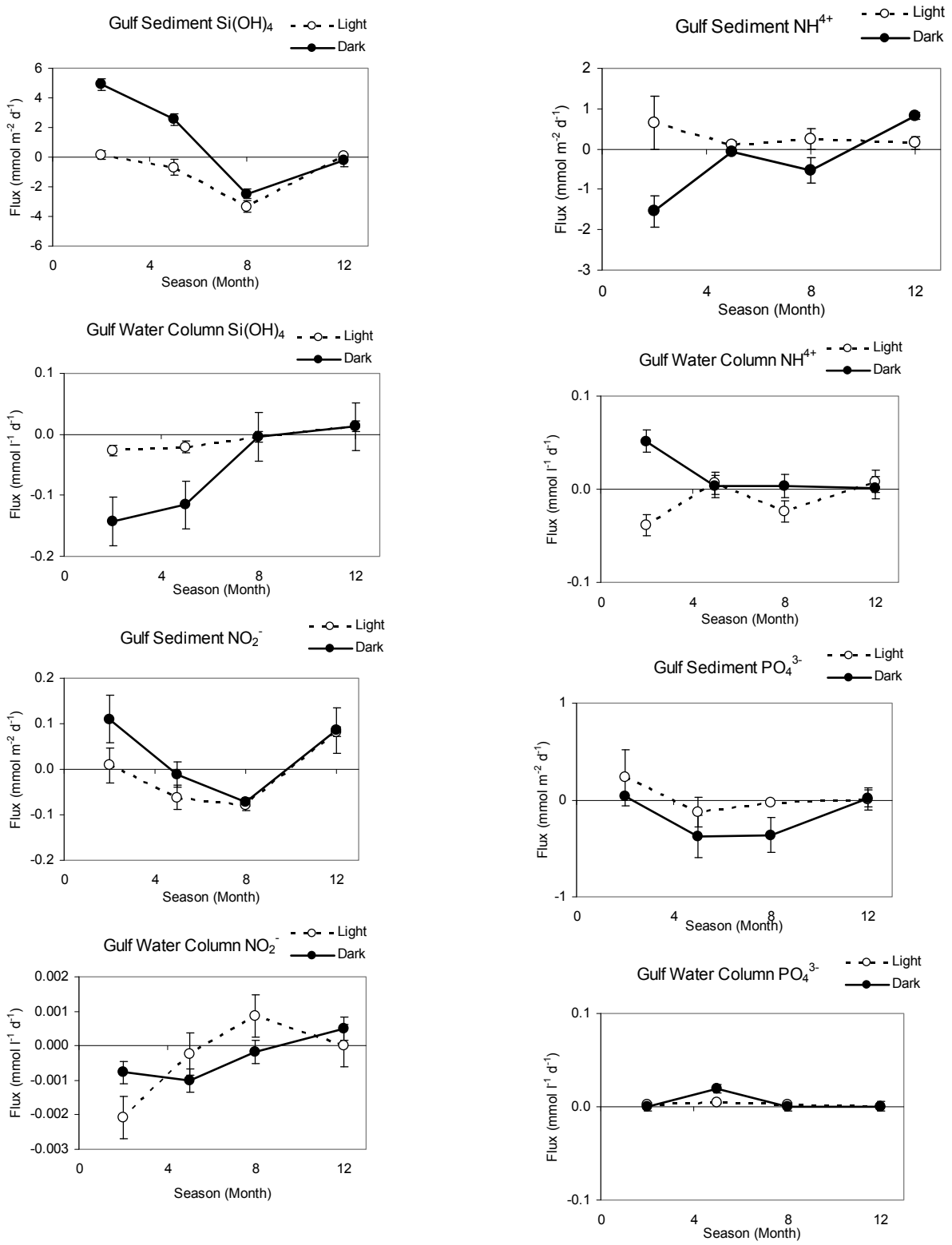


Figure 4.3. Gulf sediment and water column in-situ flux graphs.

**Bay sediment.** $Si(OH)_4$ fluxes in the light chambers followed a general downward trend throughout the year from winter to fall. At both sites, the largest flux was observed in winter, but fluxes were larger at the Bay site (24.67 mmol $m^{-2}$ $d^{-1}$ versus 0.12 mmol $m^{-2}$ $d^{-1}$). In the dark chambers, fluxes increased from winter to summer and then decreased in fall opposite the pattern seen in the dark chambers at the Gulf site. $NO_2^-$ fluxes decreased winter through fall in both treatments. $NH_4^+$ fluxes in the light and dark chambers showed similar trends. In the dark chambers, fluxes were several orders of magnitude larger in summer and fall compared to the spring. $PO_4^{3-}$ fluxes did not show a clear pattern in the light and dark chambers. Fluxes were highest in the winter and spring in the light chambers (Figure 4.4).

**Bay water column.** $Si(OH)_4$ water fluxes, i.e., consumption or release of Si calculated for the average water-column height in the water only filled light chamber and the dark bottle were similar in winter and spring. In both treatments, fluxes decreased from spring to summer. In the dark bottle, the release of $Si(OH)_4$ decreased, and in the light chamber, there was uptake of $Si(OH)_4$. The decrease was more significant in the light chambers. In the dark bottle, the fluxes decreased from spring until fall. The difference in flux between the spring (0.17 mmol $m^{-2}$ $d^{-1}$) and the fall (-0.26 mmol $m^{-2}$ $d^{-1}$) was large. In spring, the positive flux indicated that there was release of $Si(OH)_4$ in the water column, whereas in the fall, the negative flux indicate that there was uptake of $Si(OH)_4$ in the water column. In general, water-column fluxes were smaller than sediment fluxes in both directions, and flux directions, e.g., uptake or release, were not always the same in both treatments. $NO_2^-$ fluxes in both the light and dark treatments showed similar patterns. Fluxes were large in spring and fall and smaller in summer and winter. In spring and summer, the dark bottle showed release of $NO_2^-$. In the light chambers, there was release of $NO_2^-$ in spring and uptake of $NO_2^-$ in fall. In summer and winter, the dark bottle showed release of $NO_2^-$, and the light chambers showed release in summer and uptake in winter. The largest fluxes, though of the same magnitude, were observed during different seasons. They were seen in the spring in the dark treatments (0.00452 mmol $m^{-2}$ $d^{-1}$, release) and in the fall in the light treatments (0.00148 mmol $m^{-2}$ $d^{-1}$, release). $NH_4^+$ flux patterns were similar in the light and dark treatments. However, fluxes were larger in the light chambers. From spring to summer, the flux in the dark bottles decreased significantly and then increased significantly by several orders of magnitude from summer to the fall. $PO_4^{3-}$ fluxes were relatively constant over the sampling year for both the light and dark treatments. In the dark bottle, uptake of $PO_4^{3-}$ occurred in all seasons

except spring. In the light chambers, uptake of $PO_4^{3-}$ occurred during all seasons. In the light chambers, a large increase in flux was observed between winter and spring (Figure 4.4).

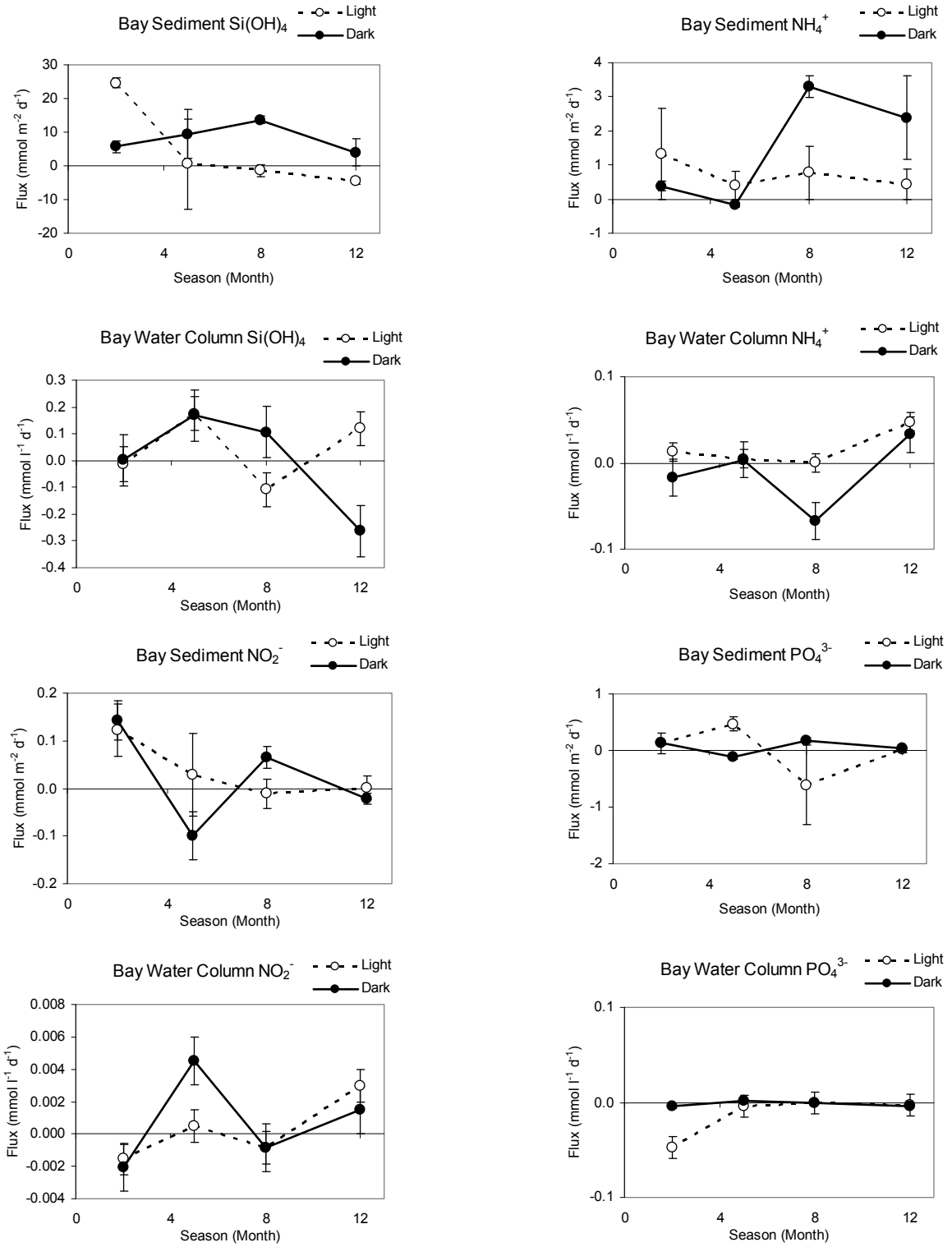


Figure 4.4. Bay sediment and water column in-situ flux graphs.

## Discussion

### Laboratory Fluxes

The fluorescein-tracer dye experiment demonstrated advective pore-water exchange caused by pressure gradients at the sediment-water interface. In the stirred chambers, the pressure gradient caused by the rotation of the water column pumped fluorescein-containing chamber water into the sediment and unstained pore water out of the sediment. The calculated flux estimate of 457 ± 262 L $m^{-2}$ $d^{-1}$ is in the range of fluxes found by various studies including Precht and Huettel (2004). In contrast, the fluorescein concentration changes in the stagnant chambers with sediment (-0.113 μM) were small and similar to those found in the chambers with water only (-0.039 μM and -0.026 μM). Fluorescein decrease in chambers without sediment may be due to some limited light exposure, which leads to the degradation of the fluorescein. All chambers were kept in the dark; however, during sampling some exposure to light could not be avoided. $Si(OH)_4$ concentrations are usually high within pore water, and flushing of these sediments moves $Si(OH)_4$ out of the sediment. Thus, the higher the advective-exchange rate, the higher the $Si(OH)_4$ flux out of the sediment.

### In-Situ Fluxes

The fluorescein experiment showed that advective pore-water exchange affects interfacial solute exchange in the Bay and Gulf sediments. In order to assess the range of the sediment-water fluxes for the range of pressure gradients active at these field sites, except under storm conditions with sediment erosion, the seasonal in-situ chamber incubation experiments were conducted.

**Gulf fluxes.** Sediment fluxes were an order of magnitude larger than the water-column fluxes for all measured nutrients. One reason for the high fluxes is the pore-water flows, as revealed by the fluorescein-tracer dye experiment, which enhance sediment-water fluid exchange and thereby, also affect Si fluxes. $Si(OH)_4$ sediment fluxes were the mirror image of the water-column fluxes. Sediment fluxes, i.e., $Si(OH)_4$, $NO_2^-$ , and $PO_4^{3-}$, were highest during the winter and then decreased in spring and summer followed by another increased in fall. $Si(OH)_4$, $NO_2^-$ , and $PO_4^{3-}$ sediment fluxes were highest in winter months and then decreased in spring and summer followed by another increase in fall. This trend reflects the growth of the phytoplankton population with increasing sunlight and nutrients (e.g., nitrogen and phosphorus) in spring. The

$Si(OH)_4$ sediment-water fluxes decreased as the benthic diatom community required more of this nutrient. Likewise, the water column $Si(OH)_4$ fluxes were negative throughout the sampling year, reflecting $Si(OH)_4$ consumption of the pelagic diatom community.

**Bay Fluxes.** Sediment $Si(OH)_4$ release in the light chambers decreased winter through fall, similar to the light chambers at the Gulf site. At both sites, winter was characterized by the largest fluxes in the light chambers. However, Bay site sediment fluxes were significantly larger (24.67 mmol $m^{-2}$ $d^{-1}$ versus 0.12 mmol $m^{-2}$ $d^{-1}$). In the dark chambers, fluxes increased winter through summer and decreased in fall opposite the dark chambers at the Gulf site. $Si(OH)_4$ fluxes in the dark and light chambers were similar in winter and spring. In both treatments, fluxes decreased from spring to summer as the growing phytoplankton population demanded more $Si(OH)_4$. Unlike the Gulf, $Si(OH)_4$ consumption and release in the sediment did not show the same pattern as $NO_2^-$ and $PO_4^{3-}$ sediment consumption and release. In the sediment, $NO_2^-$ and $PO_4^{3-}$ releases were high in winter and fall. However, in fall, the dark chambers showed consumption of $NO_2^-$. In spring, the dark chambers showed an uptake $NO_2^-$ and $PO_4^{3-}$, while the light chambers showed a release of these nutrients. In summer, the opposite was seen; $NO_2^-$ and $PO_4^{3-}$ were released in the dark chambers and uptake was shown in the light chambers.

**Comparison of $Si(OH)_4$ Fluxes**

$Si(OH)_4$ fluxes were different at the two sites. No relationship was observed between the light and dark chambers for the water-column concentration changes or the sediment fluxes. Nutrient fluxes, including $Si(OH)_4$, in the light versus the dark chambers were variable. Similar findings were reported by Marinelli et al. (1998).

Seasonal differences in nutrient concentrations were more readily observed at the Gulf site. The Gulf site is exposed to heavier wave action; therefore, organic-matter accumulation on the sediment surface does not occur at the same rate as it does at the Bay site. The Bay site's close proximity to the Apalachicola River provides a source of $NO_2^-$, $PO_4^{3-}$, and $Si(OH)_4$ (Mortazavi et al., 2000). Local river discharge can affect composition and dynamics of phytoplankton communities in the inner Northwest Florida Shelf by providing nutrients capable of supporting blooms, especially $Si(OH)_4$ (Gilbes et al., 2002).

Despite the similarities mentioned above, the findings of Marinelli et al. (1998) contrast the findings of this study. Little to no flux of nutrients took place across the sediment-water interface in chamber experiments conducted along a transect that traversed the South Atlantic

Bight (SAB) (Marinelli et al., 1998). However, Jahnke et al.'s (2003) in situ benthic-chamber incubations in the same region revealed the occurrence of highly variable but occasionally large sediment fluxes of $Si(OH)_4$, $PO_4^{3-}$, $NH_4^+$ fluxes.

Berelson et al. (1998) conducted benthic-chamber flux measurements in Port Phillip Bay, Australia in the summers of 1994 and 1995. Sediments at the study sites ranged from sandy to muds and sandy muds to pure clays. $Si(OH)_4$ fluxes at these sites ranged between 2 and 8 mmol $m^{-2}$ $d^{-1}$ except for the fluxes at the northern stations where fluxes were three to four times greater. The higher fluxes were attributed to the stations proximity to the Yarra River. These measured fluxes are larger than the summer fluxes observed at the Gulf site and smaller than those at the Bay site. In the North Sea, sediment-water exchange fluxes of $Si(OH)_4$ were determined in August 1991 and February 1992 by Gehlen et al. (1995). In August 1991, fluxes ranged from 0.18 to 8.90 mmol $m^{-2}$ $d^{-1}$, and fluxes in February 1992 decreased by a factor between two and eight (Gehlen et al., 1995). However, the upper end summer ranges of Gehlen et al. (1995) and Berelson et al. (1998) are quite similar. In this study, fluxes were higher in the winter than in the summer. This difference can be explained by plankton deposition in the North Sea, which adds substantial amounts of $bSiO_2$ to the sediment during spring and summer. At the Gulf and Bay sites in this study, high terrestrial nutrient input during winter and spring and ensuing production dominate the seasonal fluxes.

The $Si(OH)_4$ fluxes measured at the Gulf and Bay sites were relatively high, which is typical for nearshore environments that receive large volumes of Si-rich water and run-off from land. To put these numbers in perspective, they were compared to the fluxes with those reported from other coastal and off-shore environments. Hall et al. (1996) conducted benthic flux work on a basin-wide scale in the Skagerrak, a region strongly influenced by the land in the Northeastern North Sea. The fluxes reported therein are in similar ranges as those reported in this study for the Gulf site. Fluxes were reported as follows: $NH_4^+$ (-0.061 to 0.045 mmol $m^{-2}$ $d^{-1}$), $NO_2^-$ (-0.14 to 0.304 mmol $m^{-2}$ $d^{-1}$), $PO_4^{3-}$ (-0.015 to 0.1 mmol $m^{-2}$ $d^{-1}$), and $Si(OH)_4$ (0.55 to 4 mmol $m^{-2}$ $d^{-1}$). In contrast, Grandel et al. (2000) investigated benthic fluxes of $Si(OH)_4$ and $PO_4^{3-}$ for surface sediments of the abyssal Arabian Sea during four cruises (1995-1998). They reported benthic fluxes of remineralized nutrients ($Si(OH)_4$ and $PO_4^{3-}$) from the sediment to the bottom water of 0.279-0.959 mmol $m^{-2}$ $d^{-1}$ and 0.011-0.044 mmol $m^{-2}$ $d^{-1}$. The $Si(OH)_4$ fluxes reported in

their study are an order of magnitude smaller than those reported here for the Gulf sediment, while the $PO_4^{3-}$ fluxes are similar.

# CHAPTER 5
# TIME SERIES MEASUREMENTS IN WATER AND PORE WATER

## Introduction

Riverine input is one of the main sources of $Si(OH)_4$ into the coastal zone (Tréguer et al., 1995). In-situ chamber experiments suggest dependency of $Si(OH)_4$ release from shallow permeable sediment on flow. Is this effect also visible in the in-situ time series measurements of water and sediment $Si(OH)_4$ distributions? The working hypothesis for this research was that in periods of high flow after diatom deposition (e.g., spring and fall), $Si(OH)_4$ concentrations in the shallow water are highest. The objective of the experiment was to assess the seasonal patterns of $Si(OH)_4$ concentration in the water column and the sediment pore water. The approach was to conduct a time series of water-column and pore-water analyses.

## Methods

### Monthly Time Series

Monthly field samplings were conducted for fifteen months in order to monitor seasonal variations in water and sediment silica concentrations. On the Bay side, samples were taken at site I until February 2007. During this sampling, the researcher learned that the original site was no longer accessible; therefore, another site was chosen as close to the previous one as possible. Beginning in March 2006, monthly field samplings—with the exception of April 2006—were conducted at both sites (Table 5.1). Water-column samples were collected in 50-ml plastic centrifuge tubes at each site. The samples were analyzed spectrophotometrically for $NO_2^-$, $NO_3^-$, $NH_4^+$, $Si(OH)_4$, and $PO_4^{3-}$ according to the methods of Grasshoff et al. (1983). During each sampling trip, various parameters including pH, S, air temperature, and water temperature were measured in situ, and all of this information was retained in field reports (Appendix A)

Table 5.1. Nutrient time series sampling dates.

| Date |
|---|
| 2/18/2006 |
| 3/21/2006 |
| 5/6/2006 |
| 6/28/2006 |
| 7/19/2006 |
| 8/15/2006 |
| 9/22/2006 |
| 10/17/2006 |
| 11/1/2006 |
| 11/14/2006 |
| 12/11/2006 |
| 12/17/2006 |
| 1/15/2007 |
| 2/13/2007 |
| 3/20/2007 |
| 4/10/2007 |

Beginning in November 2006, sediment samples were also taken. Three 140-cc syringe sediment cores were collected at each site. In the laboratory, the cores were sliced at 2-cm depth intervals and pore water was extracted by pushing $N_2$ gas through the cores. After recording the pore-water volume, the samples were diluted to a final volume of 50.0 ml with B-pure water. With a vacuum-filtration system, the samples were filtered through a 0.8-µm membrane filter. The individual filters were air dried and then stored in separate plastic petri dishes in a refrigerator until analysis for dissolved particulate dissolvable $Si(OH)_4$ (DPS). Each filter was placed in a separate 50-ml centrifuge tube, and 25.0 ml of artificial seawater (matching measured field salinity) were added to each of the tubes. The samples were then analyzed for DPS as described in Grasshoff et al. (1983).

The diluted pore water was measured spectrophotometrically for $NO_2^-$, $NO_3^-$, $NH_4^+$, $Si(OH)_4$, and $PO_4^{3-}$ according to the methods of Grasshoff et al. (1983).

A second set of three 140-cc syringe cores was collected at each site. In the laboratory, the cores were sliced at 2-cm depth intervals, and pore water was extracted using $N_2$ gas pressure. The total silicon was determined in the pore water. The sediment was weighed and then placed in individual 50-ml plastic centrifuge tubes. Ten ml of artificial seawater of appropriate salinity were added to each of the vials, and samples were analyzed as outlined in Grasshoff et al. (1983).

For water-column DPS, two 1-L plastic bottles of water were collected from each site on each sampling occasion. The water was filtered through 0.8-µm membrane filters with a vacuum-filtration system. The exact volume of water filtered was recorded. The filters were air dried and then refrigerated in individual plastic petri dishes until analysis. DPS analysis was carried out according to the methods of Grasshoff et al. (1983).

**Data analysis.** Due to large variations in the $NO_3^-$ data caused by the column reductors, the data were not included in this thesis. Calibration lines were used to calculate the concentrations for the measured parameters. Systat v. 12 was used to create cross-correlation plots lagged at six-month intervals.

## Results

### Water Column

**Gulf water column.** $Si(OH)_4$ concentrations ranged from 1.35 µM, measured in May 2006, to 8.5 µM, measured in November 2006. No significant correlations existed between $Si(OH)_4$ concentrations and any of the other measured nutrients in the water column or Apalachicola discharge (Table 5.2).

**Bay water column.** $Si(OH)_4$ concentrations were 2 to 35-fold larger than those observed at the Gulf site, and they ranged from 5.7 µM, measured in January 2007, to 69.9 µM, measured in December 2006. The differences in $Si(OH)_4$ concentration between the Bay compared to the Gulf were significant (t-test, $\alpha = 0.05$). As with the Gulf $Si(OH)_4$ concentrations, the Bay $Si(OH)_4$ concentrations showed no significant correlations to any of the other measured nutrients in the water column or to flow (Table 5.2).

**Similarities and differences.** Overall, Bay $Si(OH)_4$ concentrations remained high throughout the entire sampling schedule, unlike the Gulf site where seasonal variations were observed. Gulf $Si(OH)_4$ was highest in the fall/winter months and lowest in the spring/summer months.

**Pore Water**

**Gulf pore water.** Pore-water $Si(OH)_4$ concentrations showed a steady decrease over the study period. A strong positive correlation between $Si(OH)_4$ concentrations in the 0-2 cm depth interval and $NO_2^-$ in the 0-2 cm and 4-10 cm depth intervals was observed (Table 5.2). At all depths, $Si(OH)_4$ showed a strong negative correlation to Apalachicola discharge (Figure 5.1). The pore-water $Si(OH)_4$ concentration lagged behind the water-column concentrations by one month (Figure 5.2). A one-month shift of the data increases the correlation significantly.

Table 5.2. Gulf water column and pore-water correlations. WC stands for water column, and PW stands for pore water.

| | Month | Flow (m/s) | GULF Nitrite WC | GULF $NH_4$ WC | GULF DIP WC | GULF DIS WC | GULF Nitrite PW | GULF $NH_4$ PW | GULF DIP PW | GULF DIS PW |
|---|---|---|---|---|---|---|---|---|---|---|
| Month | 1.00 | | | | | | | | | |
| Flow (m/s) | 0.67 | 1.00 | | | | | | | | |
| GULF Nitrite Water Column | -0.19 | 0.02 | 1.00 | | | | | | | |
| GULF $NH_4$ WC | -0.63 | -0.39 | 0.56 | 1.00 | | | | | | |
| GULF DIP WC | -0.24 | -0.06 | 0.96 | 0.48 | 1.00 | | | | | |
| GULF DIS WC | -0.78 | -0.47 | -0.26 | 0.47 | -0.31 | 1.00 | | | | |
| GULF Nitrite PW | -0.47 | -0.70 | -0.27 | -0.06 | -0.02 | 0.20 | 1.00 | | | |
| GULF $NH_4$ PW | -0.57 | -0.34 | 0.80 | 0.73 | 0.71 | 0.20 | -0.15 | 1.00 | | |
| GULF DIP PW | -0.29 | 0.04 | 0.12 | -0.27 | 0.27 | -0.09 | 0.33 | 0.19 | 1.00 | |
| GULF DIS PW | -0.77 | -0.91 | 0.32 | 0.48 | 0.43 | 0.37 | 0.67 | 0.58 | 0.20 | 1.00 |

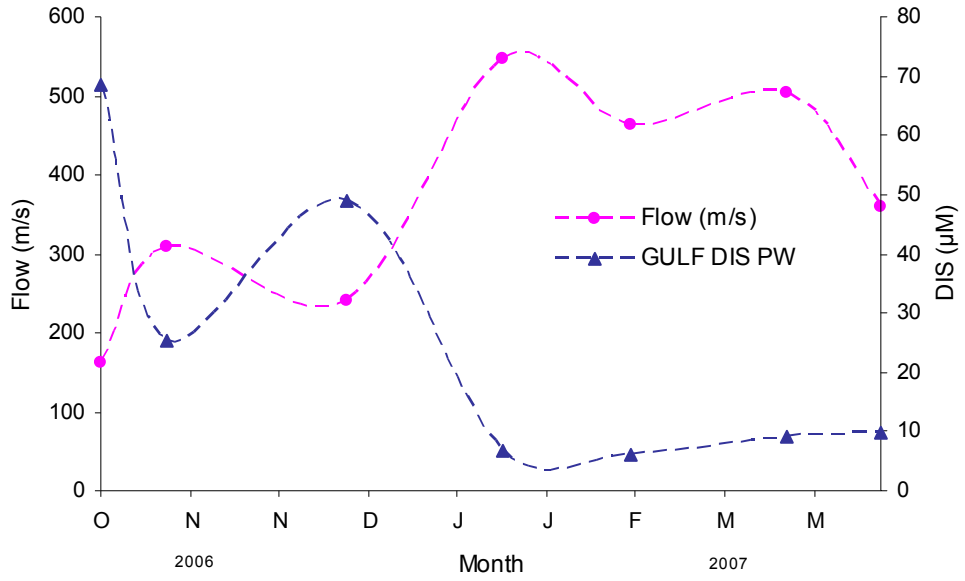


Figure 5.1. Gulf DIS pore water vs. Apalachicola discharge (flow m/s).

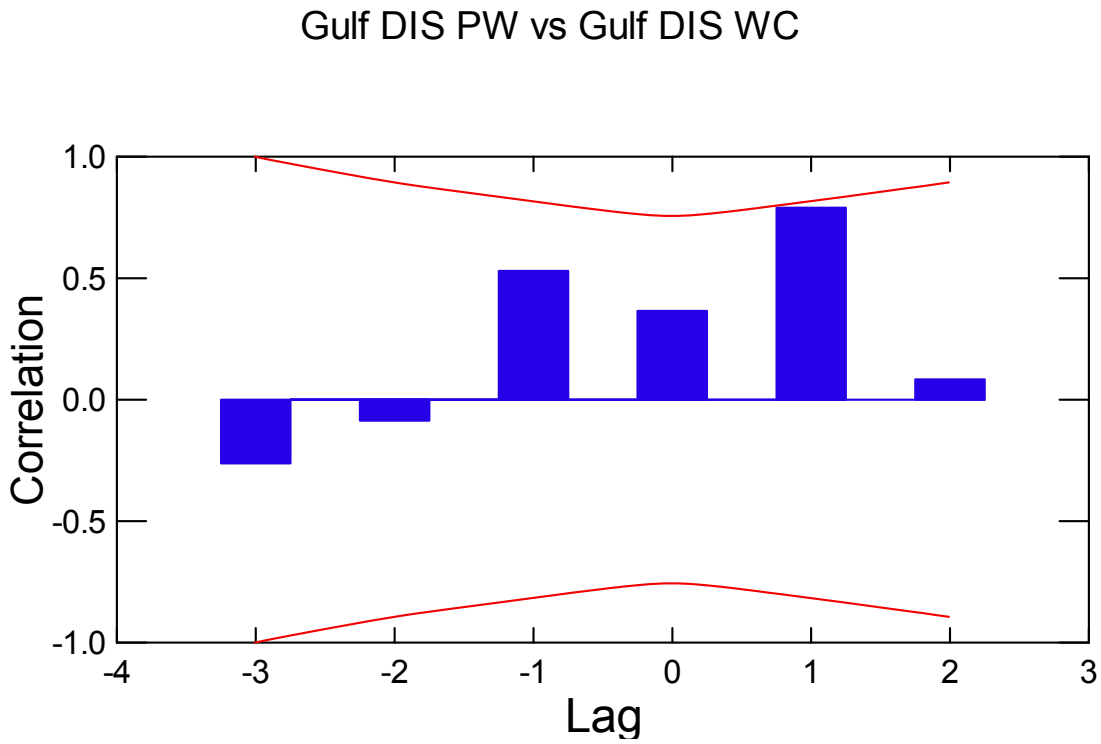


Figure 5.2. Cross correlation plot Gulf DIS pore water vs. Gulf DIS water column.

**Bay pore water.** $Si(OH)_4$ pore-water concentrations followed a similar pattern as the water column $Si(OH)_4$ (Figure 5.3). This pattern was observed in the 0-4 cm and 4-10 cm depth intervals. $Si(OH)_4$ concentrations again lagged behind the water column concentrations by one month, and a one-month shift of the data increases the correlation significantly (Figure 5.4). $Si(OH)_4$ pore-water concentrations and $PO_4^{3-}$ water-column concentrations were positive correlated suggesting $Si(OH)_4$ generation at times of high sedimentary decomposition and nutrient mobilization. $Si(OH)_4$ in the pore water showed a significant positive correlation to $NH_4^+$ in the water column when lagged one month (Table 5.3).

Table 5.3. Bay water column and pore-water correlations. WC stands for water column, and PW stands for pore water.

| | Month | Flow (m/s) | BAY Nitrite WC | BAY $NH_4$ WC | BAY DIP WC | BAY DIS WC | BAY Nitrite PW | BAY $NH_4$ PW | BAY DIP PW | BAY DIS PW |
|---|---|---|---|---|---|---|---|---|---|---|
| Month | 1.00 | | | | | | | | | |
| Flow (m/s) | 0.67 | 1.00 | | | | | | | | |
| BAY Nitrite WC | 0.53 | 0.41 | 1.00 | | | | | | | |
| BAY $NH_4$ WC | -0.36 | -0.05 | -0.20 | 1.00 | | | | | | |
| BAY DIP WC | 0.07 | -0.03 | 0.21 | -0.26 | 1.00 | | | | | |
| BAY DIS WC | 0.49 | 0.16 | 0.37 | 0.47 | -0.29 | 1.00 | | | | |
| BAY Nitrite PW | -0.34 | -0.74 | -0.19 | -0.58 | -0.04 | -0.40 | 1.00 | | | |
| BAY $NH_4$ PW | 0.02 | -0.05 | 0.33 | -0.20 | -0.64 | 0.10 | 0.34 | 1.00 | | |
| BAY DIP PW | -0.32 | -0.09 | -0.22 | -0.40 | -0.56 | -0.56 | 0.51 | 0.65 | 1.00 | |
| BAY DIS PW | -0.05 | -0.51 | 0.26 | -0.47 | 0.67 | -0.22 | 0.54 | 0.00 | -0.19 | 1.00 |

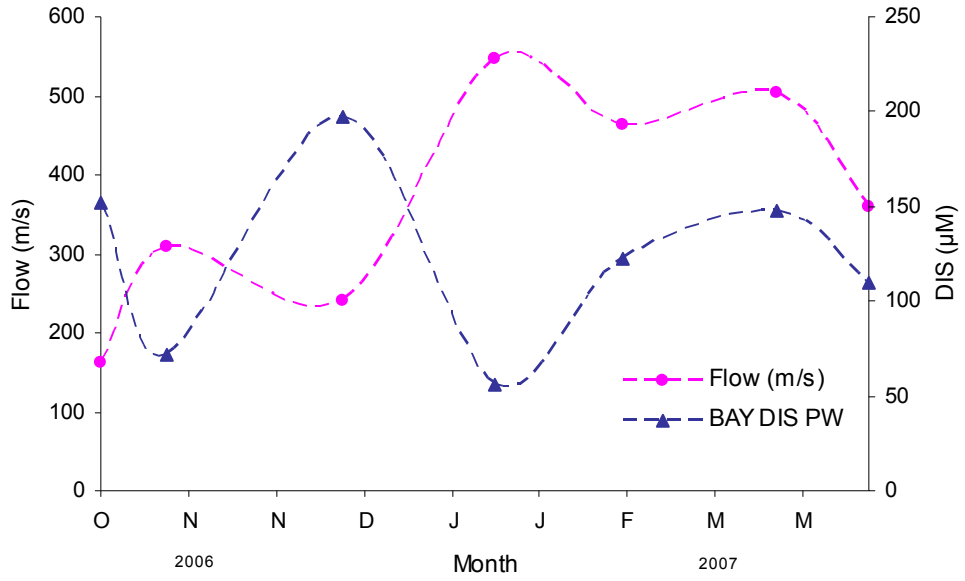


Figure 5.3. Bay DIS pore water vs. Apalachicola discharge (flow m/s).

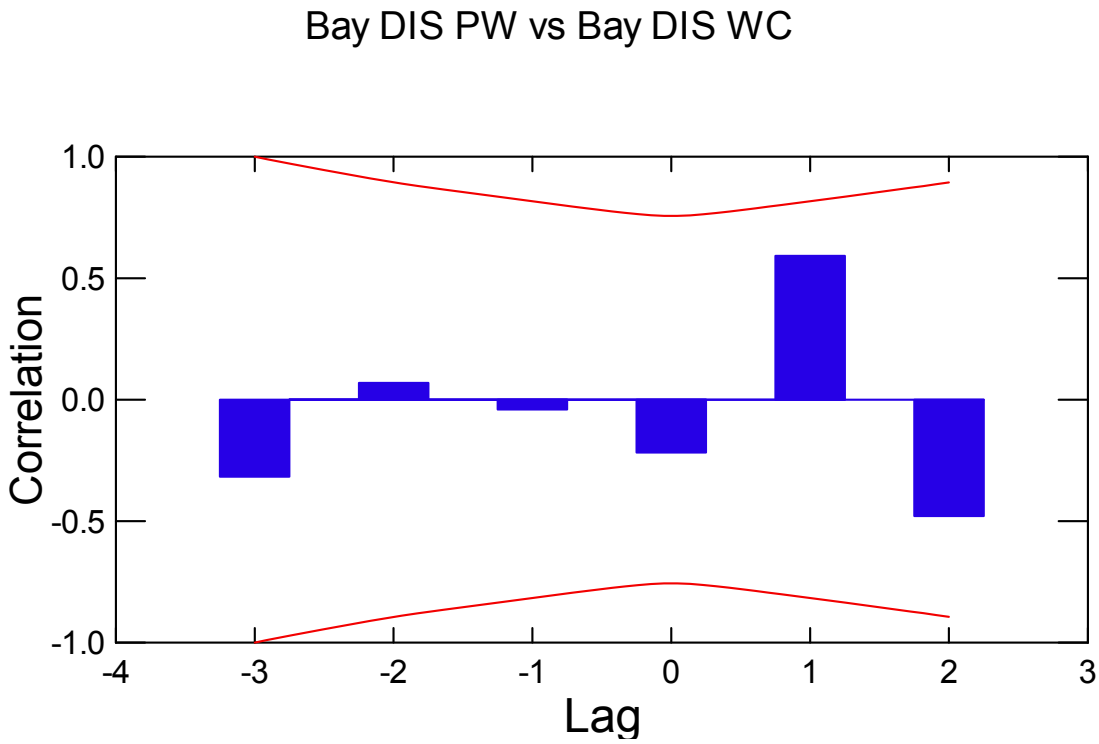


Figure 5.4. Cross correlation plot Bay DIS pore water vs. Bay DIS water column.

**Similarities and differences.** As found with the water column, $Si(OH)_4$ concentrations in the pore water were higher at the Bay site than the pore water at the Gulf site. In the Gulf sites, $Si(OH)_4$ in the pore water did not show any strong correlations with water-column nutrients (Table 5.4). The Bay $Si(OH)_4$ pore water showed correlation with $NH_4^+$ and $PO_4^{3-}$.

Table 5.4 Pore water correlations plot Gulf and Bay. WC stands for water column, and PW stands for pore water.

| | GULF Nitrite PW | GULF $NH_4$ PW | GULF DIP PW | GULF DIS PW | BAY Nitrite PW | BAY $NH_4$ PW | BAY DIP PW | BAY DIS PW |
|---|---|---|---|---|---|---|---|---|
| GULF Nitrite PW | 1.00 | | | | | | | |
| GULF $NH_4$ PW | -0.15 | 1.00 | | | | | | |
| GULF DIP PW | 0.33 | 0.19 | 1.00 | | | | | |
| GULF DIS PW | 0.67 | 0.58 | 0.20 | 1.00 | | | | |
| BAY Nitrite PW | 0.41 | 0.60 | 0.19 | 0.81 | 1.00 | | | |
| BAY $NH_4$ PW | -0.43 | 0.65 | -0.43 | 0.16 | 0.34 | 1.00 | | |
| BAY DIP PW | -0.26 | 0.91 | 0.34 | 0.33 | 0.51 | 0.65 | 1.00 | |
| BAY DIS PW | 0.72 | -0.09 | 0.03 | 0.57 | 0.54 | 0.00 | -0.19 | 1.00 |

**Gulf/Bay water column total silica (TSi) and dissolved particulate silicate (DPS).** In general, the Bay TSi concentrations were higher than those measured at the Gulf site. Gulf TSi and Gulf DPS showed a significant positive correlation (Table 5.5). No other water column measurement showed any correlation to these two parameters.

Table 5.5. TSi and DPS water column and pore water correlations. WC stands for water column, and PW stands for pore water.

| | Gulf DPS | Bay DPS | Gulf Tsi | Bay Tsi | Gulf TSI Sed | Bay TSI Sed | Gulf DPS Sed | Bay DPS Sed |
|---|---|---|---|---|---|---|---|---|
| Gulf DPS | 1.00 | | | | | | | |
| Bay DPS | 0.47 | 1.00 | | | | | | |
| Gulf Tsi | 0.82 | 0.33 | 1.00 | | | | | |
| Bay Tsi | -0.07 | 0.05 | -0.43 | 1.00 | | | | |
| Gulf TSi Sed | -0.45 | -0.31 | -0.26 | 0.06 | 1.00 | | | |
| Bay TSi Sed | 0.43 | 0.24 | 0.39 | -0.02 | 0.58 | 1.00 | | |
| Gulf DPS Sed | -0.72 | 0.02 | -0.64 | 0.50 | 0.16 | -0.48 | 1.00 | |
| Bay DPS Sed | -0.62 | 0.24 | -0.71 | 0.13 | -0.19 | -0.60 | 0.68 | 1.00 |

**Similarities and differences.** The lowest Gulf TSi concentration was measured on April 10, 2007, which was also the sampling at which the lowest Bay DPS concentration was measured.

**Gulf sediment total Si and DPS.** For the total Si in the sediment, in general, the concentrations vary throughout the depth and time intervals. DPS decreased from the first measurement (November 14, 2006) and remains low until the last measurement (April 10, 2007).

**Bay sediment total Si and DPS.** The TSi and DPS in the Bay followed the same pattern as the Gulf. Across the depth profile, Bay TSI and Bay DPS sediment shared a very strong correlation.

**Similarities and differences.** Gulf DPS sediment showed a negative correlation with both water column Gulf DPS and TSi. The Bay DPS sediment did not share this correlation with its Bay water-column measurements.

## Discussion

### Influence of River Discharge on $Si(OH)_4$ Distribution

Conley (1997) noted that amorphous silica transported from terrestrial environments to the ocean via rivers is an important source of $Si(OH)_4$ to the marine environment. At the study sites, discharge maxima occur in winter and early spring in response to increased rainfall over the ACF watershed, and periods of low river flow are typical of the summer and fall seasons (Mortazavi et al., 2000). This seasonal pattern in flow from Apalachicola River was also seen in this study. Because the Bay site is closer in proximity to the mouth of the Apalachicola River, $Si(OH)_4$ concentrations were always higher at the Bay site when compared to the Gulf site. At the Gulf site, the wave action is stronger than at the Bay site; therefore, the entire 10-cm depth interval was equally affected by boundary currents and ensuing sediment flushing. The results indicate the $Si(OH)_4$ concentrations in the water column and pore water are more closely linked than the water column and sediment $PO_4^{3-}$, $NH_4^+$, and $NO_2^-$ concentrations. As $Si(OH)_4$ is not as limited and as reactive as $PO_4^{3-}$, $NH_4^+$, and $NO_2^-$, it behaves more like a conservative tracer, and thus, the pore-water flushing can link pore water $Si(OH)_4$ concentrations more closely to the water-column concentrations as compared to the limited P and N nutrients (Appendix A).

In this study, the in-situ time series measurements of water-column and sediment $Si(OH)_4$ distributions and the in-situ chamber experiments conducted in Chapter 4 suggest a seasonal

dependency of $Si(OH)_4$ release from shallow permeable sediment. At the Gulf site, pore-water $Si(OH)_4$ concentrations showed a strong negative correlation at all depths with Apalachicola River discharge. Highest discharges coincided with lowest measured $Si(OH)_4$ concentrations in the sediment. This relationship suggests that during periods of high flow, the sediments are relatively $Si(OH)_4$ depleted , which can be explained by the flushing of $Si(OH)_4$ from the sediment and consumption during the summer season. At the Bay site, pore-water $Si(OH)_4$ concentrations were also negatively correlated to Apalachicola River discharge; however, the relationship was not as strong as the one observed at the Gulf site. The 0-2 cm depth profile showed a strong correlation (-0.71), while the 4-10 cm depth profile was not as strong (-0.51). The river influence is stronger in the enclosed Bay, thus a relative $Si(OH)_4$ depletion as observed in the Gulf does not occur in the Bay.

The seasonal inverse correlation was also observed in the TSi and DPS. Gulf DPS in the sediment showed a negative correlation with both water column Gulf DPS and TSi. When concentrations were higher in the sediment, they were lower in the water column and vice-versa. The Bay DPS in the sediment did not share this correlation with its Bay water column measurements. These results suggest that $Si(OH)_4$, TSi, and DPS show stronger benthic-pelagic coupling at the Gulf site than at the Bay site. Such results were expected due to the Gulf site's exposure to higher energy from waves and wind and the slightly higher permeability of the sediment.

While the depth profiles at both sites revealed changes in concentration with depth, the findings in this study were different than those described by McManus et al. (1995) and Ragueneau et al. (2001). These studies suggest that typical downcore profiles of $Si(OH)_4$ concentrations in pore waters exhibit an exponential increase just below the sediment-water interface before leveling off in the top 10 to 20 cm or deeper. This difference is due to the fact that in permeable sediments, advective flows allow for rapid flushing of sediments. The flushing can remove $Si(OH)_4$ from the sediment more rapidly than it can be generated by the dissolution of embedded $bSiO_2$, and only below the flushed sediment horizon, $Si(OH)_4$ concentrations can build up in the pore water. As pelagic diatoms are filtered into the uppermost layer of the bed (Ehrenhauss and Huettel, 2004) producing highest concentrations of particulate $bSiO_2$ in the surface layer, $Si(OH)_4$ regeneration here is highest causing $Si(OH)_4$ concentrations to increase towards the surface despite the flushing. The results of this process are the concave $Si(OH)_4$

profiles with a concentration maximum near the sediment surface, a concentration drop below the surface layer, and increased concentrations at the sediment depths that are not affected by the pore-water flushing.

How do the nutrient concentrations measured in this study compare to concentrations measured in similar coastal areas and areas with extreme $bSiO_2$ dissolution? Burford et al.(2008) measured water-column nutrient concentrations in three intertidal mudflat sites in Darwin Harbor, in northern Australia. In general, their $PO_4^{3-}$, $NH_4^{+,}$ and $NO^{2-}$ concentrations were not significantly different than values measured at the study sites in this chapter. Cai et al. (2004) conducted work in the Pearl River Estuary and its adjacent continental shelf in the Northern South China Sea. This estuary is characterized by high nutrient concentrations—130-140 μM $Si(OH)_4$ and 0.2-1.2 μM $PO_4^{3-}$. These $Si(OH)_4$ concentrations are at least an order of magnitude higher than the concentrations observed at the sites in this study. Meanwhile, the low end of the $PO_4^{3-}$ range is of the same magnitude as those measured in this study.

In comparison, upwelled waters off the coast of Peru (15ºS), Baja California and northwest Africa contain between 14 and 30 μM $Si(OH)_4$ and support the highest silica production rates reported in the sea (Nelson et al., 1995). These concentrations are within the same range and magnitude as those observed at the Bay site, emphasizing the high levels of $Si(OH)_4$ in the Bay due to the riverine input. These values reach values as recoded in regions were extreme $bSiO_2$ dissolution takes place. Quéguiner et al., 1997 conducted work in the Atlantic sector of the Southern Ocean during austral spring 1992. Maximum $bSiO_2$ concentrations of 11.7 μM were measured during later November at the southern border of the Polar Frontal region. Smith et al. (1996) reported $Si(OH)_4$ values ranging from 49± 7.6 to 77.7± 1.4 μM in the upper 30 m of the Ross Sea.

**Relationship of $Si(OH)_4$ to Other Parameters**

$NH_4^+$ and $PO_4^{3-}$ are mobilized from sediments when the sediment is oxygen depleted or only a thin oxic layer covers the sediment. Correlation of $Si(OH)_4$ concentrations with $NH_4^+$ and $PO_4^{3-}$ concentrations, thus, indicating $Si(OH)_4$ regeneration during mineralization in anoxic sediments. A very thin oxidized surface layer was only observed during spring and summer months at the Bay site. In contrast, $NO_3^-$ typically occurs at higher concentrations in oxidized sediment layers, and the $NO_2^-$ concentrations co-vary with the $NO_3^-$ as long as the sediment does

not become anoxic. The correlation of $Si(OH)_4$ with $NO_2^-$ concentrations at the Gulf site, thus may reflect oxic organic-matter decomposition and associated $Si(OH)_4$ regeneration.

In the Gulf and Bay water column, the seasonal patterns in $NO_2^-$ and $PO_4^{3-}$ were similar. $NO_2^-$ concentrations usually behave similar to $NO_3^-$ concentrations except during rapid or large environmental changes. Thus, the seasonal pattern of inorganic N and P reflects the seasonal demand of these nutrients by primary producers. Furthermore, $Si(OH)_4$ concentrations peaked during periods of low N and P input from the Apalachicola River. When these nutrients are less available, diatom populations decrease, and $Si(OH)_4$ concentrations increase.

# CHAPTER 6
# CONCLUSION

Riverine inputs, groundwater efflux, and terrestrial runoff enrich coastal waters with silica. Diatoms, which require silicic acid for frustule formation and cell growth, are therefore predominantly found in these waters. Less than half of the pelagic primary production is consumed in the shallow water column; the remaining fraction settles on the seafloor. Large fractions of these shelf sediments are composed of permeable relict sands, which do not accumulate organic matter. As a result, the fate of the deposited diatoms and the $bSiO_2$ is poorly understood, and little is known about the processes that control transport and decomposition of sedimented diatoms in permeable shelf beds. The research conducted in this study attempted to answer this and several related questions. The work presented here is the first study of its kind in the Apalachicola Bay.

The two laboratory flume experiments revealed that diatoms accumulate in ripple troughs and the upper slopes of sediment ripples and penetrate into the upper -sediment layer. Advective flows create concentration gradients with maximum concentrations close to the sediment ripple crests. The column-reactor and reaction-rate experiments demonstrated that $bSiO_2$ dissolution occurs faster in flushed sediment than in the water column. However, contrary to the working hypotheses, neither pore flow velocity nor removal of the organic coating significantly affected dissolution. The strongest enhancement of dissolution takes place at the interface between stagnant pore-water conditions, where diffusion is the dominant transport mechanism, and slow moving pore-water. Further increase in pore-water velocity then causes relatively little change of the dissolution rate.

In-situ benthic flux studies and time-series measurements revealed that advective flows enhance remobilization of $Si(OH)_4$ back into the water column. Furthermore, these studies showed that seasonal variations in $PO_4^{3-}$ and $NO_2^-$ are seen at both sites, and $Si(OH)_4$ concentrations were not strongly correlated to any variable other than the seasonal river discharge.

In all, the findings of this study show the importance of advective pore-water exchange on diatom dissolution in permeable sediment. Additional column-reactor experiments should be conducted to determine the minimum flow rates that will significantly increase dissolution.

Time-series measurements should be continued to obtain a better picture of seasonal changes in $Si(OH)_4$ and the relation of the water column $Si(OH)_4$ concentrations to pore water flushing. Because diatom production peaks in the coastal zone where permeable sediments are the most common sediment type, a thorough investigation of the contribution of the sedimentary flushing process to the $Si(OH)_4$ regeneration is central for understanding the Si cycle in the shelf and ocean.

# APPENDIX

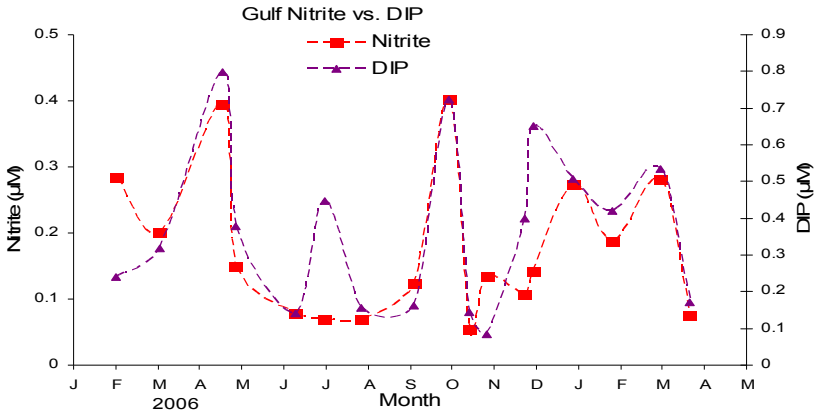


Figure A.1. Nutrient time series Gulf nitrite vs. DIP.

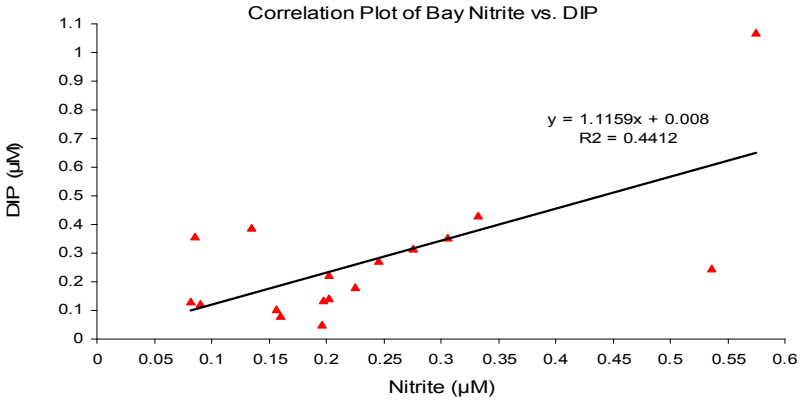


Figure A.2. Bay nitrite vs. DIP regression.

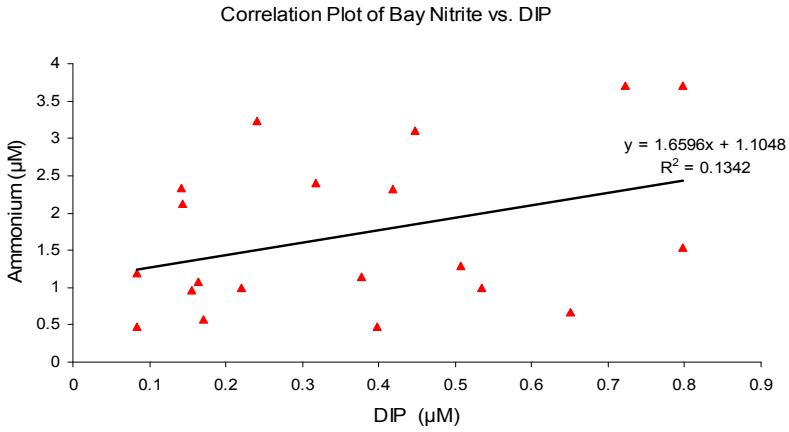


Figure A.3. Nutrient time series Gulf ammonium vs. DIP regression.

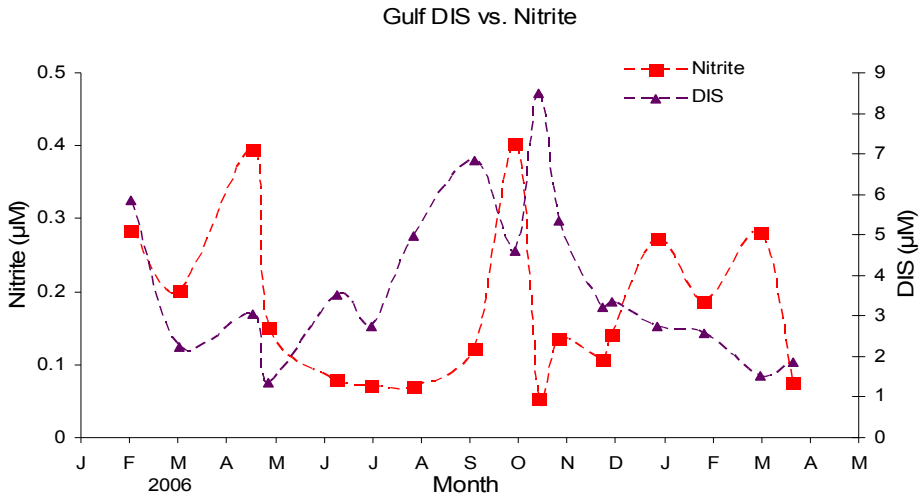


Figure A.4. Nutrient time series Gulf DIS vs. nitrite over time.

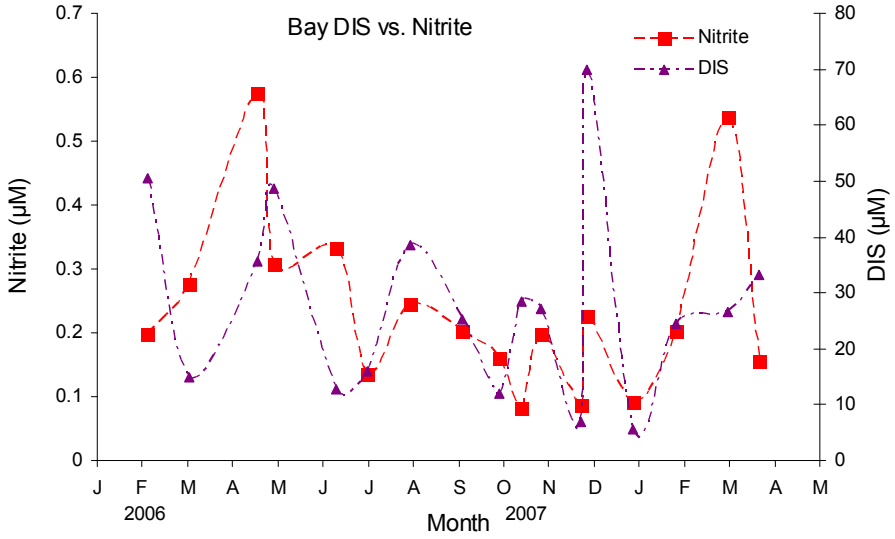


Figure A.5. Nutrient time series Bay DIS and nitrite over time.

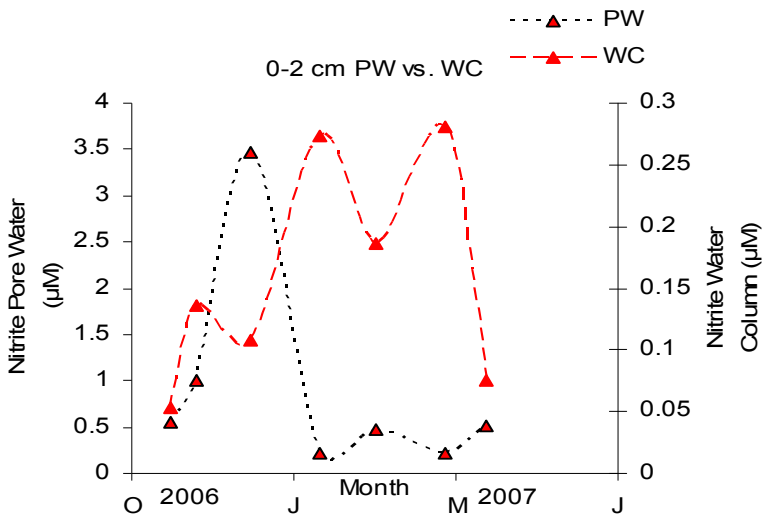


Figure A.6. Gulf nitrite pore water 0-2 cm and nitrite water column.

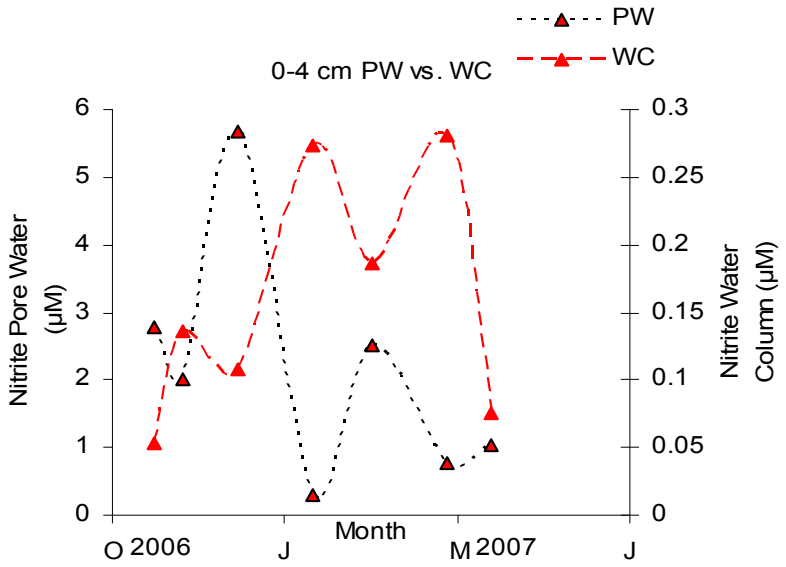


Figure A.7. Gulf nitrite pore water 0-4 cm and nitrite water column.

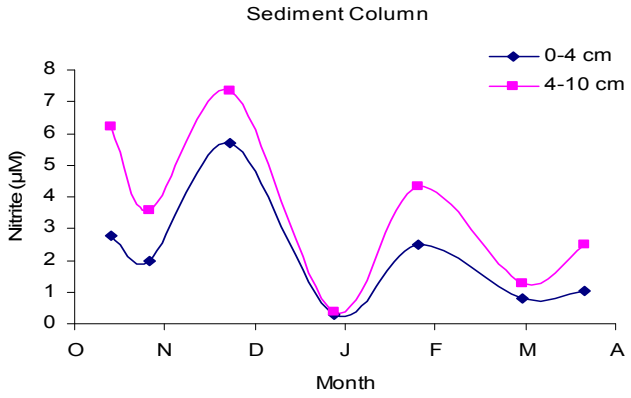


Figure A.8. Gulf nitrite 0-2 cm and 4-10 cm over time.

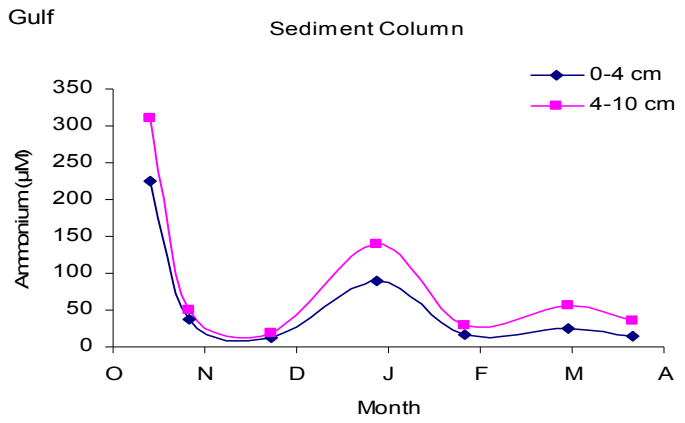


Figure A.9. Gulf ammonium 0-2 cm and 4-10 cm over time.

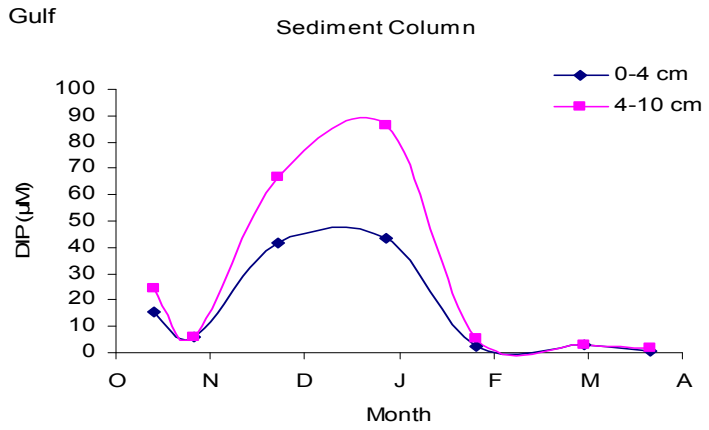


Figure A.10. Gulf DIP 0-4 cm and 4-10 cm over time.

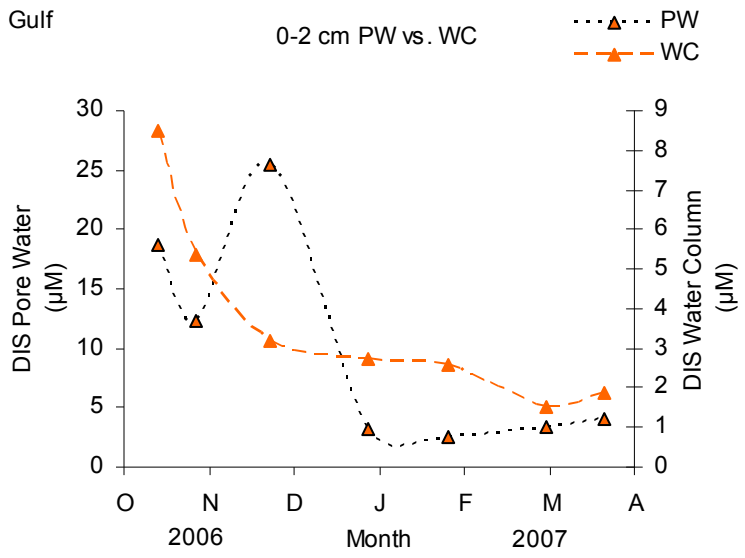


Figure A.11. Gulf DIS 0-2 cm and DIS water column.

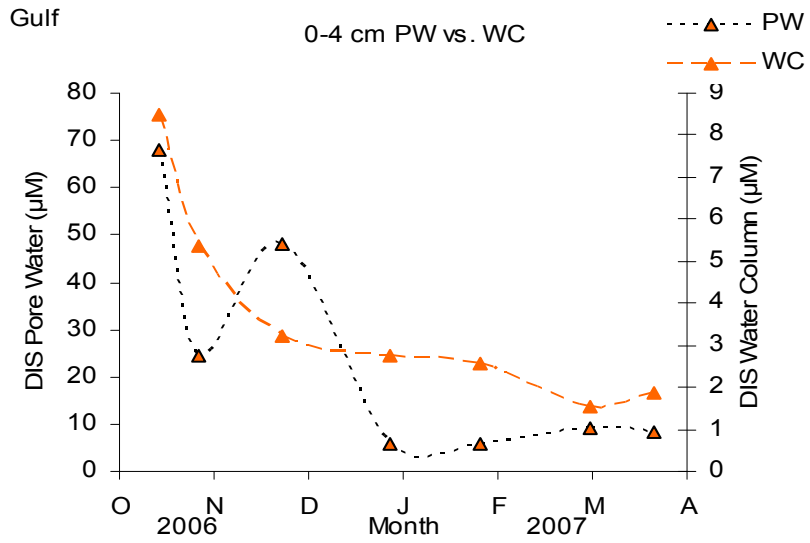


Figure A.12. Gulf DIS 0-4 cm and DIS water column.

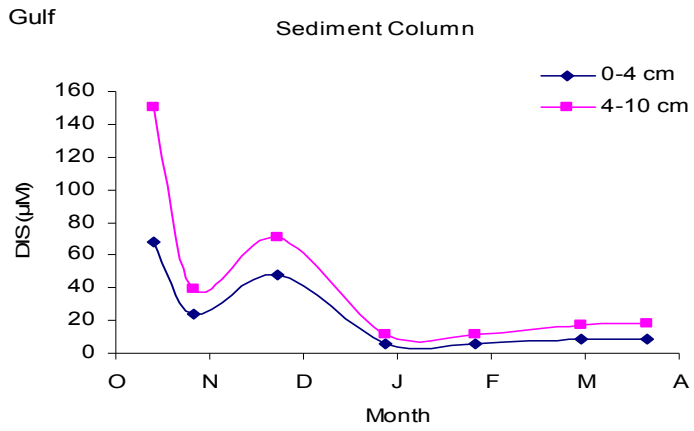


Figure A.13. Bay DIS 0-4 cm and 4-10 cm.

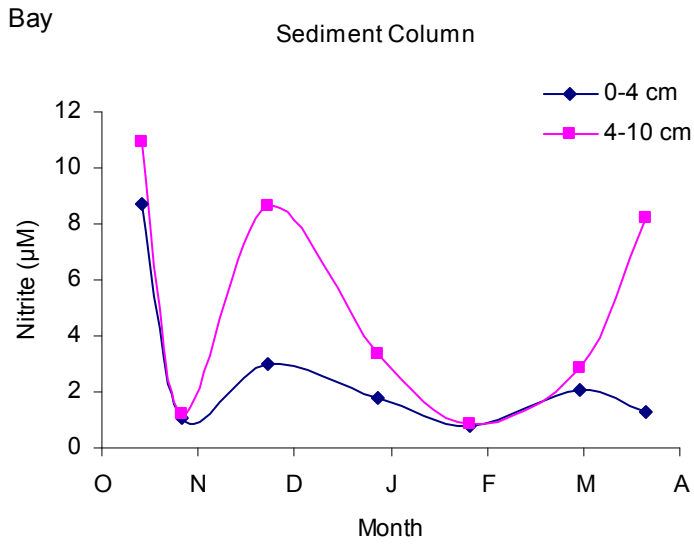


Figure A.14. Bay nitrite 0-4 cm and 4-10 cm.

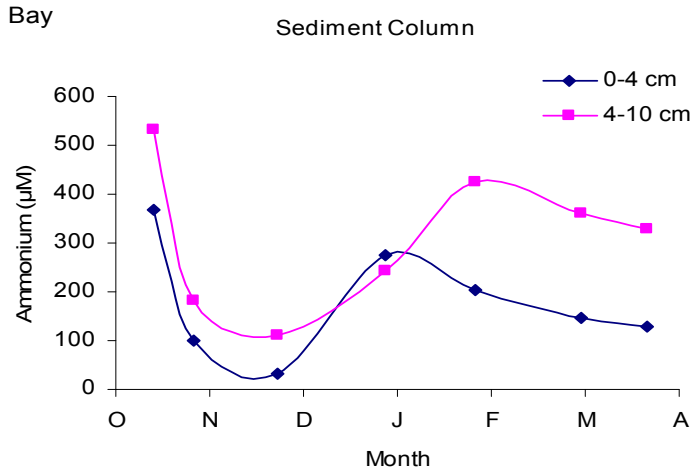


Figure A.15. Bay ammonium 0-4 cm and 4-10 cm.

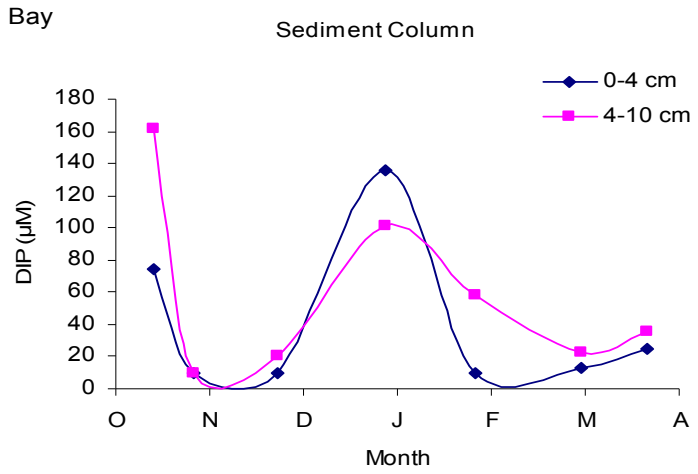


Figure A.16. Bay DIP 0-4 cm and 4-10 cm.

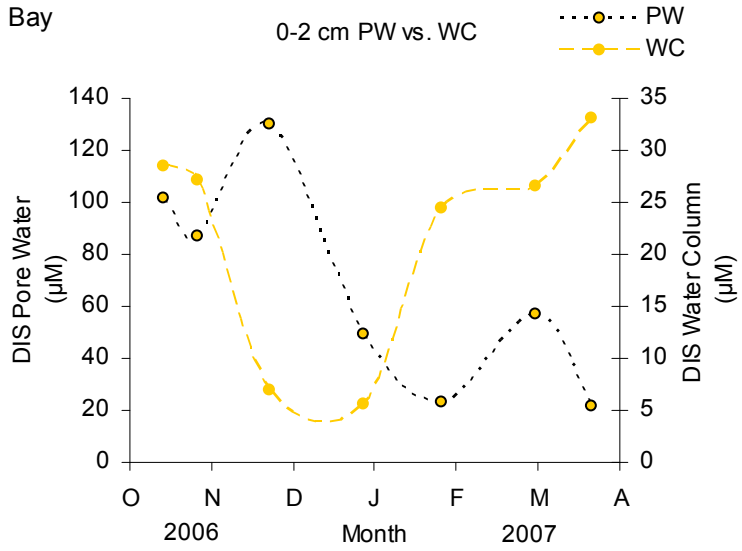


Figure A.17. DIS 0-2 cm and water column.

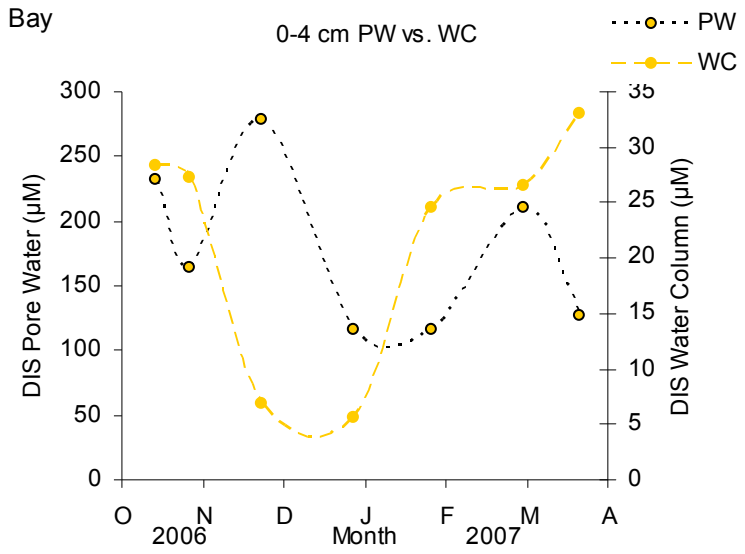


Figure A.18. DIS 0-4 cm and water column.

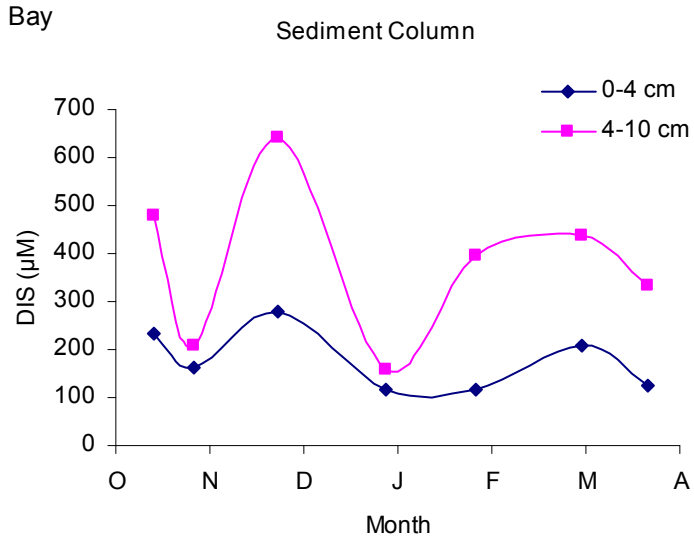


Figure A.19. DIS 0-4 cm and 4-10 cm.

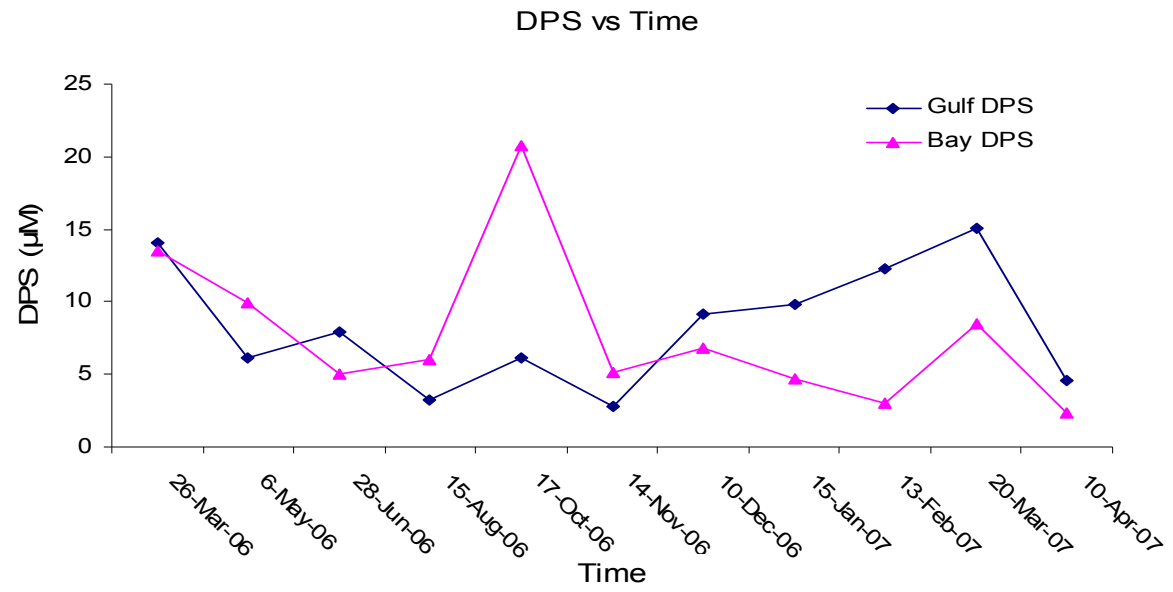


Figure A.20. Gulf and Bay DPS over time.

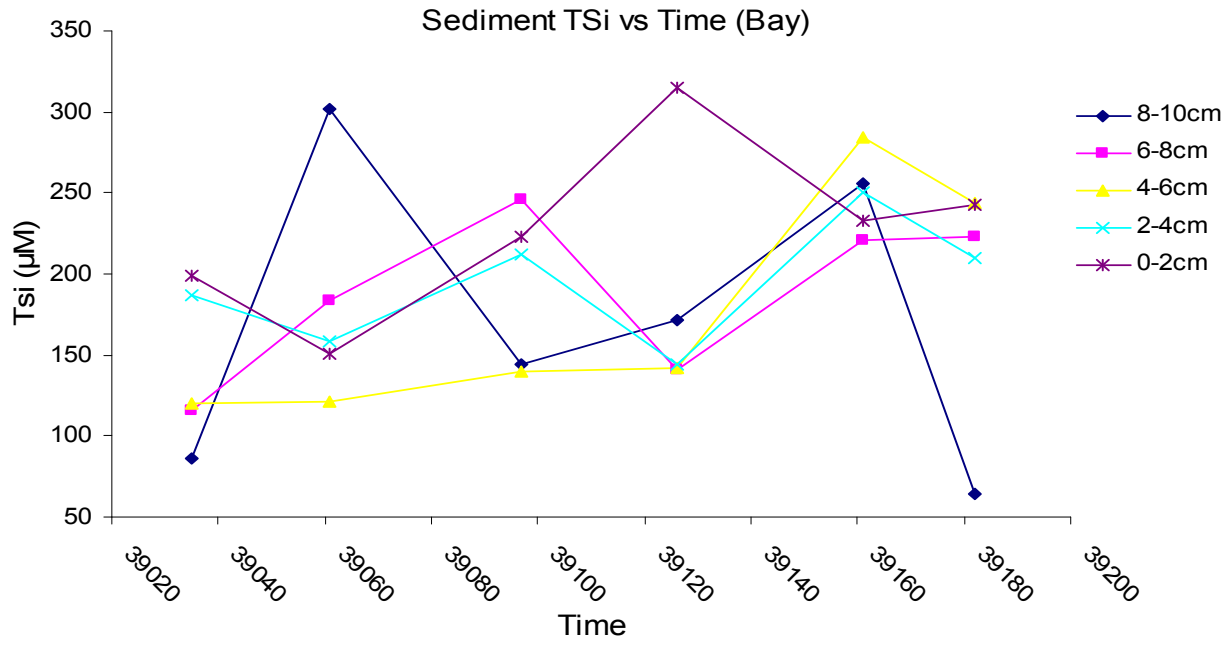


Figure A.21. Bay TSi pore water.

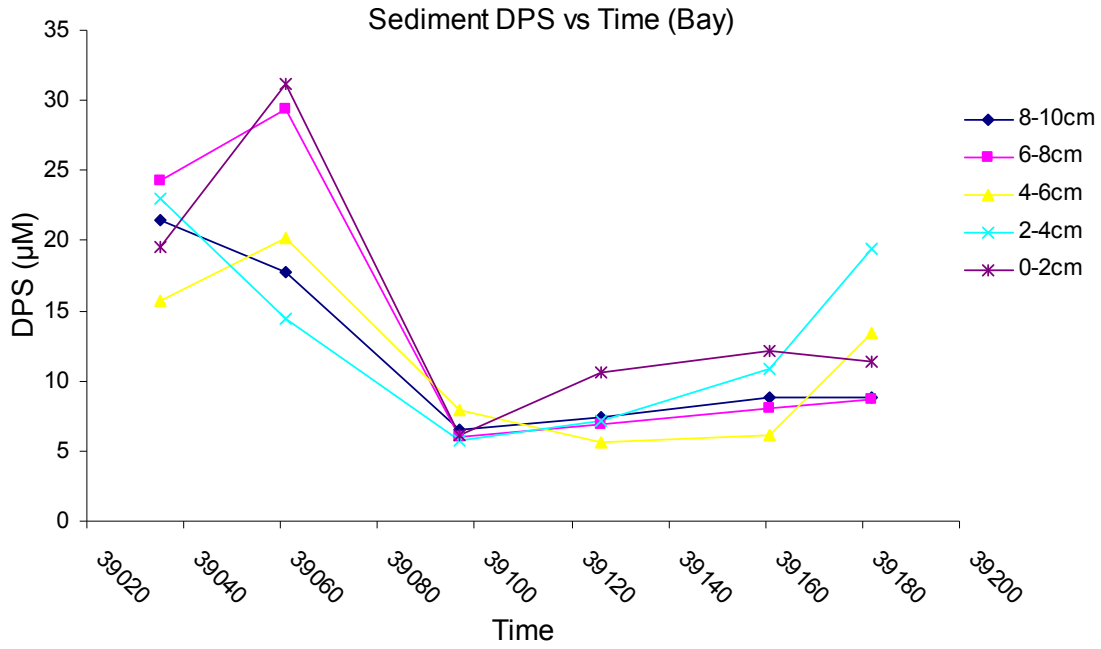


Figure A.22. Bay DPS pore water.

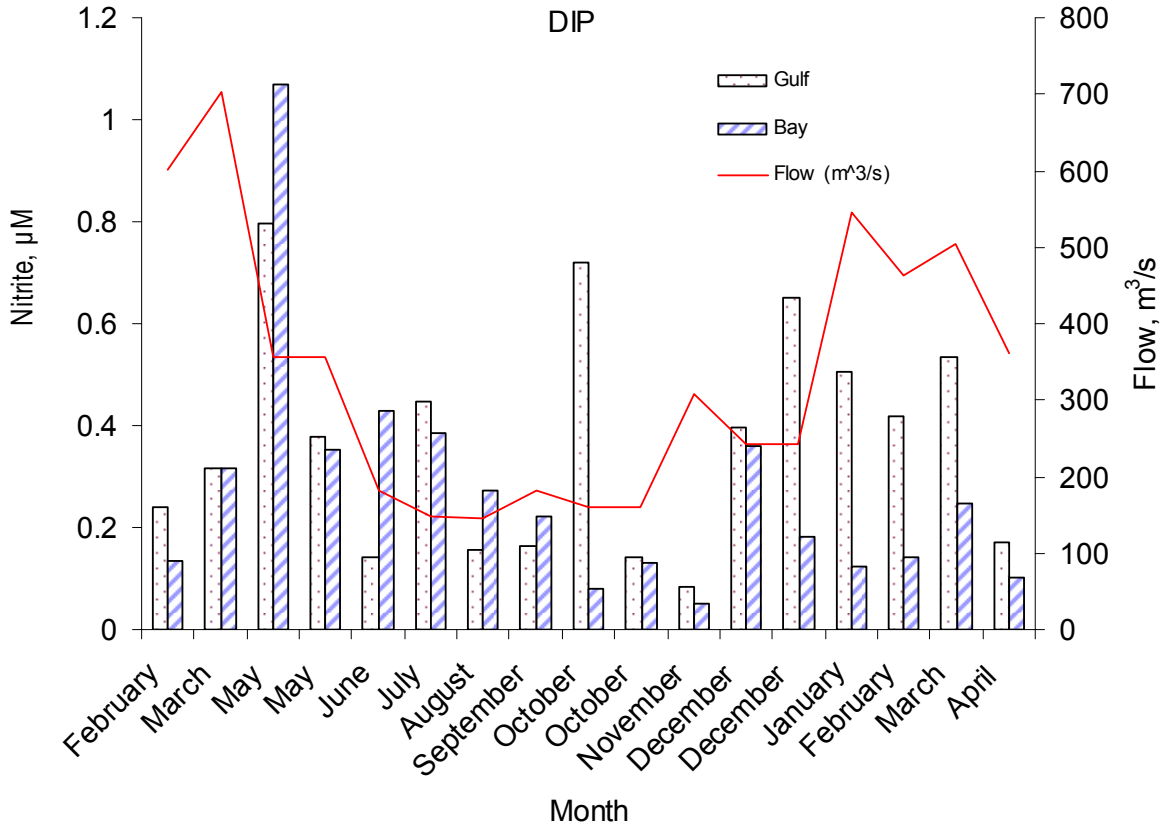


Figure A.23. Gulf and Bay DIP with flow over time.

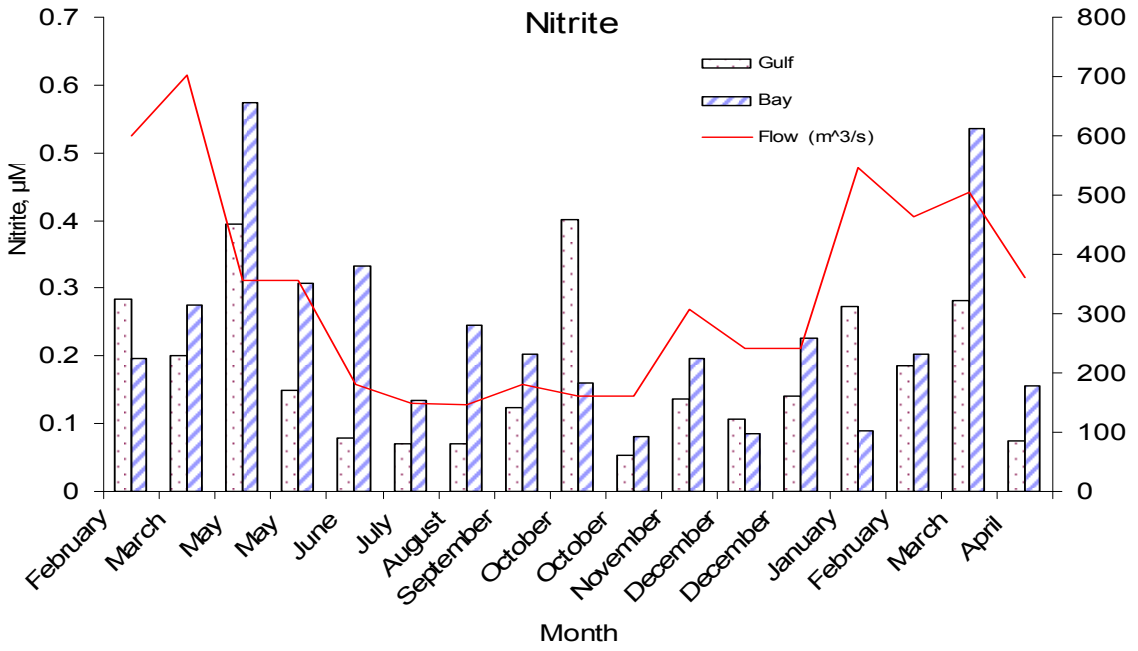


Figure A.24. Gulf and Bay nitrite with flow over time.

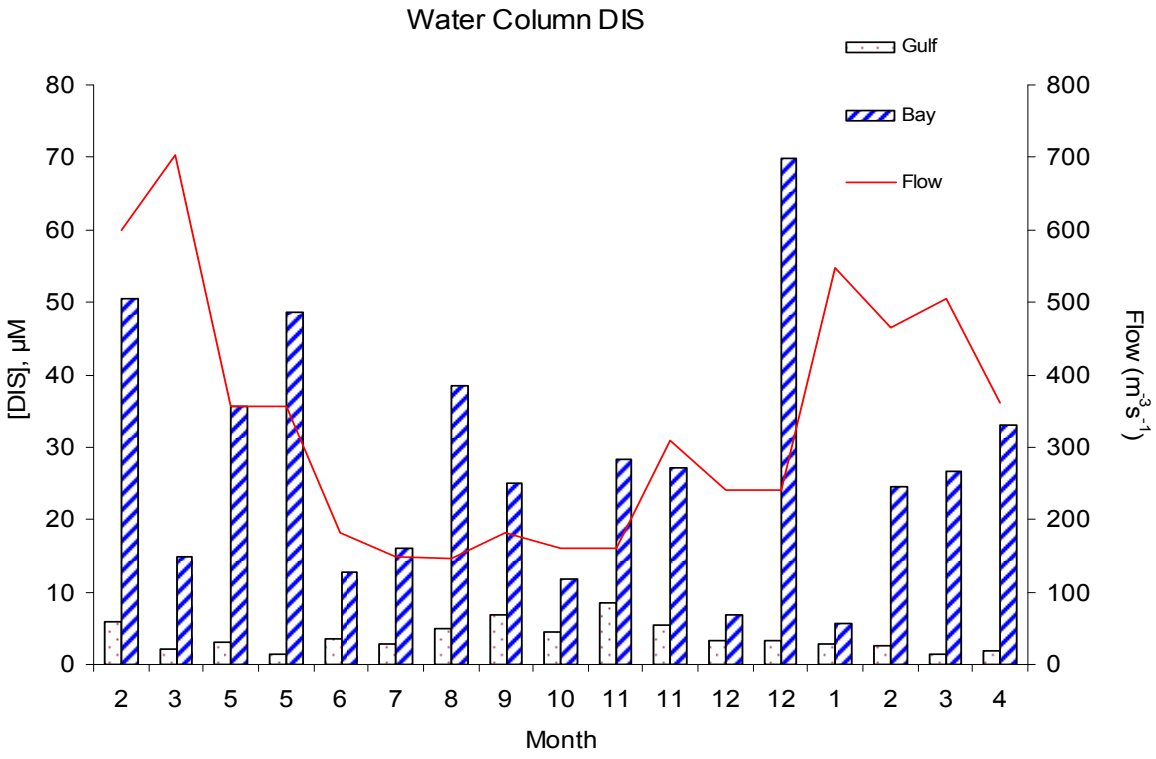


Figure A.25. Gulf and Bay DIS with flow over time.

## REFERENCES


Berelson, W.M., Heggie, D., Longmore, A., Kilgore, T., Nicholson, G., Skyring, G., 1998. Benthic Nutrient Recycling in Port Phillip Bay, Australia. Estuarine, Coastal and Shelf Science 46, 917-934.

Bidle, K.D., Azam, F., 1999. Accelerated dissolution of diatom silica by marine bacterial assemblages. Nature 397, 508-512.

Bidle, K.D., Azam, F., 2001. Bacterial control of silicon regeneration from diatom detritus: significance of bacterial ectohydrolases and species identity. Limnology and Oceanography 46, 1606–1623.

Bidle, K.D., Brzezinski, M.A., Long, R.A., Jones, J.L., Azam, F., 2003. Diminished efficiency in the oceanic silica pump caused by bacteria-mediated silica dissolution. Limnology and Oceanography 48, 1855-1868.

Brzezinski, M.A., Alldredge, A.L., O'Bryan, L.M., 1997. Silica cycling within marine snow. Limnology and Oceanography 42, 1706-1713.

Buesseler, K.O., 1998. The decoupling of production and particulate export in the surface ocean. Global Biogeochemical Cycles 12, 297-310.

Burford, M.A., Alongi, D.M., McKinnon, A.D., Trott, L.A., 2008. Primary production and nutrients in a tropical macrotidal estuary, Darwin Harbour, Australia. Estuarine, Coastal and Shelf Science 79, 440-448.

Cai, W.J., Dai, M., Wang, Y., Zhai, W., Huang, T., Chen, S., Zhang, F., Chen, Z., Wang, Z., 2004. The biogeochemistry of inorganic carbon and nutrients in the Pearl River estuary and the adjacent Northern South China Sea. Continental Shelf Research 24, 1301-1319.

Canfield, D.E., Thamdrup, B., Kristensen, E., 2005. Aquatic Geomicrobiology. Elsevier Academic Press, 441-463.

Conley, D.J., 1997. Riverine contribution of biogenic silica to the oceanic silica budget. Limnology and Oceanography 42, 774-777.

Danovaro, R., Armeni, M., Dell-Anno, A., Fabiano, M., Manini, E., Marrale, D., Pusceddu, A., Vanucci, S., 2001. Small-scale distribution of bacteria, enzymatic activities, and organic matter in sediments. Microbial Ecology 42, 177-185.

DeMaster, D.J., 1981. The supply and accumulation of silica in the marine environment. Geochemica et Cosmochimica Acta 45, 1715-1732.

DeMaster, D.J., 2002. The accumulation and cycling of biogenic silica in the Southern Ocean: revisiting the marine silica budget. Deep-Sea Research II 49, 3155-3167.

Denis, L., Grenz, C., 2003. Spatial variability in oxygen and nutrient fluxes at the sediment-water interface on the continental shelf in the Gulf of Lions (NW Mediterranean). Oceanologica Acta 26, 373-389.

Dittmar, T., Kattner, G., 2003. The biogeochemistry of the river and shelf ecosystem of the Arctic Ocean: a review. Marine Chemistry 83, 103-120.

Dixit, S., Van Cappellen, P., van Bennekom, A.J., 2001. Processes controlling solubility of biogenic silica and pore water build-up of silicic acid in marine sediments. Marine Chemistry 73, 333-352.

Dugdale, R.C., Wilkerson, F.P., Minas, H.J., 1995. The role of a silicate pump in driving new production. Deep-Sea Research I 42, 697-719.

Ehrenhauss, S., Huettel, M., 2004. Advective transport and decomposition of chain-forming planktonic diatoms in permeable sediments. Journal of Sea Research 52, 179-197.

Engel, A., Goldthwait, S., Passow, U., Alldredge, A., 2002. Temporal decoupling of carbon and nitrogen dynamics in a mesocosm diatom bloom. Limnology and Oceanography 47, 753-761.

Froelich, P., Bender, M., Luedtke, N., Heath, G., Devries, T., 1982. The marine phosphorus cycle. American Journal of Science 282, 474-511.

Fujii, M., Chai, F., 2005. Effects of biogenic silica dissolution on silicon cycling and export production. Geophysical Research Letters 32, 5617-5620.

Gallinari, M., Ragueneau, O., Corrin, L., DeMaster, D.J., Tréguer, P., 2002. The importance of water column processes on the dissolution properties of biogenic silica in deep-sea sediments I. Solubility. Geochimica et Cosmochimica Acta 66, 2701-2717.

Gehlen, M., Malschaert, H., Van Raaphorst, W.R., 1995. Spatial and temporal variability of benthic silica fluxes in the southeastern North Sea. Continental Shelf Research 15, 1675-1696.

Gilbes, F., Müller-Karger, F.E., Del Castillo, C.E., 2002. New evidence for the West Florida Shelf plume. Continental Shelf Research 22, 2479-2496.

Grandel, S., Rickert, D., Schlüter, M., Wallmann, K., 2000. Pore-water distribution and quantification of diffusive benthic fluxes of silicic acid, nitrate and phosphate in surface sediments of the deep Arabian Sea. Deep-Sea Research II 47, 2707-2734.

Grasshoff, K., Ehrhardt, M., Kremling, K., 1983. Methods of Seawater Analysis, 2nd Edition. Verlag Chemie, Weinheim.

Greenwood, J.E., Truesdale, V.W., Rendell, A.R., 2001. Biogenic silica dissolution in seawater—in vitro chemical kinetics. Progress in Oceanography 48, 1-23.

Hall, O.J., Hulth, S., Hulthe, G., Landén, A., Tengberg, A., 1996. Benthic nutrient fluxes on a basin-wide scale in the Skagerrak (North-eastern North Sea). Journal of Sea Research 35, 123-137.

Hecky, R.E., Mopper, K., Kilham, P., Degens, E.T., 1973. The amino acid and sugar composition of diatom cell-walls. Marine Biology 19, 323-331.

Hubbard, M.L., Riley, J.P., 1984. Kinetic studies of the rate of dissolution of silica and diatom tests in sea water. Jounral of Oceanographic Society of Japan, 148-154.

Huettel, M., Gust, G., 1992. Impact of bioroughness on interfacial solute exchange in permeable sediments. Marine Ecology Progress Series 89, 253-267.

Huettel, M., Røy, H., Precht, E., Ehrenhauss, S., 2003. Hydrodynamical impact on biogeochemical processes in aquatic sediments. Hydrobiologia 494, 231-236.

Huettel, M., Rusch, A., 2000. Transport and degradation of phytoplankton in permeable sediment. Limnology and Oceanography 45, 534-549.

Huettel, M., Ziebis, W., Forster, S., 1996. Flow-induced uptake of particulate matter in permeable sediments. Limnology and Oceanography 41, 309-322.

Huettel, M., Ziebis, W., Forster, S., Luther, G.W., 1998. Advective transport affecting metal and nutrient distributions and interfacial fluxes in permeable sediments. Geochemica Cosmica Act 62, 613-631.

Hurd, D.C., 1973. Interactions of biogenic opal, sediment and seawater in the Central Equatorial Pacific. Geochemica et Cosmochimica Act 37, 2257-2282.

Jahnke, R.A., Alexander, C.R., Kostka, J.E., 2003. Advective pore water input of nutrients to the Satilla River Estuary, Georgia, USA. Estuarine, Coastal and Shelf Science 56, 641-653.

Jahnke, R.A., Nelson, J.R., Marinelli, R.L., J.E. Eckman, 2000. Benthic flux of biogenic elements on the Southeastern US continental shelf: influence of pore water advective transport and benthic microalgae. Contintental Shelf Research 20, 109-127.

Jenness, M. I., Duineveld, G. C. A., 1985. Effects of tidal currents on chlorophyll a content of sandy sediments in the southern North Sea. Marine Ecology Progress Series 21**,** 283-287.

Jørgensen, B.B., 1996. Material flux in the sediment. In: Jørgensen, B.B., Richardson, K. (Eds.), Coastal and Estuarine Studies. Eutrophication in Coastal Marine Ecosystems. American Geophysical Union, Washington, DC, pp. 115-135.

Kamatani, A., 1982. Dissolution rates of silica from diatoms decomposing at various temperatures. Marine Biology 68, 91-96.

Kamatani, A., Oku, O., 2000. Measuring biogenic silica in marine sediments. Marine Chemistry 68, 219-229.

Kamatani, A., Riley, J.P., 1979. Rate of dissolution of diatom silica walls in seawater. Marine Biology 55, 29-35.

Kamatani, A., Riley, J.P., Skirrow, G., 1980. The dissolution of opaline silica of diatom tests in sea water. Journal of Oceanographic Society of Japan 36, 201-208.

Khalil, K., Rabouille, C., Gallinari, M., Soetaert, K., DeMaster, D.J., Ragueneau, O., 2007. Constraining biogenic silica dissolution in marine sediments: A comparison between diagenetic models and experimental dissolution rates.

Klute, A., Dirksen, C., 1986. Hydraulic conductivity and diffusivity: Laboratory methods, p. 687–734. *In* A. Klute [ed.], Methods of soil analysis—part 1—physical and mineralogical methods, second edition. American Society of Agronomy. Madison, WI.

Lewin, J.C., 1961. The dissolution of silica from diatom walls. Geochemica Cosmochmica Acta 21,182-198.

Marinelli, R.L., Jahnke, R.A., Craven, D.B., Nelson, J.R., Eckman, J.E., 1998. Sediment nutrient dynamics on the South Atlantic Bight continental shelf. Limnology and Oceanography 43, 1305-1320.

McManus, J., Hammond, D.E., Berelson, W.M., Kilgore, T.E., DeMaster, D.J., Ragueneau, O.G., Collier, R.W., 1995. Early diagenesis of biogenic opal: Dissolution rates, kinetics and paleooceanographic implication. Deep Sea Research, Part II 38, 1481-1516.

Mortazavi, B., Iverson, R.L., Landing, W.M., Huang, W., 2000. Phosphorus budget of Apalachicola Bay: a river-dominated estuary in the northeastern Gulf Of Mexico. Marine Ecology Progress Series 198, 33-42.

Nelson, D.M., Tréguer, P., Brzezinski, M.A., Leynaert, A., Quéguiner, B., 1995. Production and dissolution of biogenic silica in the ocean: Revised global estimates, comparison with regional data and relationship to biogenic sedimentation. Global Biogeochemical Cycle 9, 359-372.

Parsons, T.R., Maita, Y., Lalli, C.M., 1984. A Manual of Chemical and Biological Methods for Seawater Analysis. Pergamon Press, Oxford.

Passow, U., Engel, A., Ploug, H., 2003. The role of aggregation for the dissolution of diatom frustules. FEMS Microbiology Ecology 46, 247-255.

Pilditch, C.A., Miller, D.C., 2006. Phytoplankton deposition to permeable sediments under oscillatory flow: Effects of ripple geometry and resuspension. Continental Shelf Research 26, 1806-1825.

Precht, E., Huettel, M., 2003. Advective pore-water exchange driven by surface gravity waves and its ecological implications. Limnology and Oceanography 48, 1674-1684.

Precht, E., Huettel, M., 2004. Rapid wave-driven advective pore water exchange in a permeable coastal sediment. Journal of Sea Research 51, 93-107.

Quéguiner, B., Tréguer, P., Peeken, I., Scharek, R., 1997. Biogeochemical dynamics and the silicon cycle in the Atlantic sector of the Southern Ocean during austral spring 1992. Deep Sea Research Part II: Topical Studies in Oceanography 44, 69-89.

Ragueneau, O., Tréguer, P., Leynaert, A., Anderson, R.F., Brzezinski, M.A., DeMaster, D.J., Dugdale, R.C., Dymond, J., Fischer, G., Francois, R., Heinze, C., Maier-Reimer, E., Martin-Jézéquel, V., Nelson, D.M., Quéguiner, B., 2000. A review of the Si cycle in the modern ocean: recent progress and missing gaps in the application of biogenic opal as a paleoproductivity proxy. Global and Planetary Change 26, 317-365.

Reimers, C.E., Stecher H.A. III, Taghon, G.L., Fuller, C.M., Huettel, M., Rusch, A., Ryckelynck, N., Wild, C., 2004. In situ measurements of advective solute transport in permeable shelf sands. Continental Shelf Research 24, 183-201.

Rickert, D., 2000. Dissolution kinetics of biogenic silica in marine environments. In Reports on Polar Research 351, 211.

Rickert, D., Schlüter, M., Wallmann, K., 2002. Dissolution kinetics of biogenic silica from the water column to the sediments. Geochimica et Cosmochimica Act 66, 439-455.

Riggs, S.R., Snyder, S.W., Hine, C., Mearns, D.L., 1996. Hardbottom morphology and relationship to the geologic framework-Mid Atlantic continental shelf. Journal of Sedimentary Research 66, 830-846.

Rusch, A., Huettel, M., 2000. Advective particle transport into permeable sediments-evidence from experiments in an intertidal sandflat. Limnology and Oceanography 45, 525-533.

Sarthou, G., Timmermans, K.R., Blain, S., Tréguer, P., 2005. Growth physiology and fate of diatoms in the ocean: a review. Journal of Sea Research 53, 25-42.

Sayles, F.L., Deuser, W.G., Goudreau, J.E., Dickinson, W.H., Jickells, T.D., King, P., 1996. The benthic cycle of biogenic opal at the Bermuda Atlantic time series site. Deep-Sea Research, Part II 43, 383-409.

Shemesh, A., Burckle, L.H., Froelich, P.N., 1989. Dissolution and preservation of Antarctic diatoms and the effect on sediment *Thanatocenoses.* Quaternary Research 31, 288-308.

Shum, K.T., 1992. Wave-induced advective transport below a rippled water-sediment interface. Journal of Geophysical Research 97, 789-808.

Shum, K.T., 1993. The effects of wave induced pore water circulation on the distribution and flux of pore water constituents in a rippled sediment bed. Journal of Geophysical Research 98, 10,289-10,301.

Smetacek, V.S., 1985. Role of sinking in diatom life-history cycles: ecological, evolutionary and geological significance. Marine Biology 84, 239-251.

Smith, W.O. Jr., Shields, A.R., Peloquin, J.A., Catalano, G., Tozzi, S., Dinniman, M.S., Asper, V.A., 2006. Interannual variations in nutrients, net community production, and biogeochemical cycles in the Ross Sea. Deep-Sea Research II 53, 815-833.

Tréguer, P., Kamatani, A., Gueneley, S., Quéguiner, B., 1989. Kinetics of dissolution of Antarctic diatom frustules and the biogeochemical cycle of silicon in the southern ocean. Polar Biology 9, 397-403.

Tréguer, P., Nelson, D.M., Van Bennekom, A.J., DeMaster, D.J., Leynaert, A., Quéguiner, B., 1995. The silica balance in the world ocean: a reestimate. Science 268, 375-379.

Truesedale, V.W., Greenwood, J.E., Rendell, A., 2005 a. The rate-equation for biogenic silica dissolution in seawater –new hypotheses. Aquatic Geochemistry 11, 319-343.

Truesdale, V.W., Greenwood, J.E., Rendell, A., 2005 b. In vitro, batch-dissolution of biogenic silica in seawater – the application of recent modeling to real data. Progress in Oceanography 66, 1-24.

Van Bennekom, A.J., Buma, A.G.J., Nolting, R.F., 1991. Dissolved aluminum in the Weddell-Scotia Confluence and effect of Al on the dissolution kinetics of biogenic silica. Marine Chemistry 35, 423-434.

Van Cappellen, P., Dixit, S., van Beusekom, J., 2002. Biogenic silica dissolution in the oceans: Reconciling experimental and field-based dissolution rates. Global Biogeochemical Cycle 16, 1075-1084.

Van Cappellen, P., Qiu, L., 1997a. Biogenic silica dissolution in sediments of the Southern Ocean: I. Solubility. Deep-Sea Research Part II 44, 1109-1128.

Van Cappellen, P., Qiu, L.Q., 1997b. Biogenic silica dissolution in sediments of the Southern Ocean. II. Kinetics. Deep-Sea Research Part II 44, 1129-1149.

Wischmeyer, A.G. Del Amo, Y., Brzezinski, M., Wolf-Gladrow, D.A., 2003. Theoretical constraints on the uptake of silicic acid species by marine diatoms. Marine Chemistry 82, 13-29.

Yool, A., Tyrrell, T., 2003. Role of diatoms in regulating the ocean's silicon cycle. Global Biogeochemical Cycle 17, 1103-1123.

## BIOGRAPHICAL SKETCH

EDUCATION

| | |
|---|---|
| *2004-2008* | Florida State University, Tallahassee, Florida<br>Master of Science, Biological Oceanography<br>Advisor: Markus Huettel<br>Thesis: Dissolution of biogenic silica in permeable coastal sands |
| *2000-2004* | Mississippi State University, Starkville, Mississippi<br>Bachelors of Science, Animal and Dairy Science |

RESEARCH

| | |
|---|---|
| *2004-2008* | Department of Oceanography, Florida State University, Tallahassee, Florida<br>Research Assistant: Biogeochemical processes in permeable sediments |
| *Summer 2004* | College of Veterinary Medicine, Mississippi State University, Starkville, Mississippi<br>National Institutes of Health (NIH) Research Fellow: Vaccine effectiveness against *Edwardsiella ictaluri* |

TEACHING

| | |
|---|---|
| *Spring-Summer2007* | Saturday-at-the Sea, Florida State University, Tallahassee, Florida<br>Instructor |
| *2004-2005* | Department of Oceanography, Florida State University, Tallahassee, Florida<br>Graduate Teaching Assistant |

PRESENTATIONS

| | |
|---|---|
| *2008* | Higgs, M., Huettel, M. (2008). Dissolution of biogenic silica in permeable coastal sands. Presented at the 2008 American Society of Limnology and Oceanography Conference, Orlando, Florida. |